EVIDENCE FOR FAULT ASPERITIES FROM SYSTEMATIC TIME-DOMAIN MODELING OF TELESEISMIC WAVEFORMS

Thesis by

John Edward Ebel

In Partial Fulfillment of the Requirements

For the Degree of

Doctor of Philosophy

California Institute of Technology

Pasadena, California

1981

(Submitted October 1, 1980)

To my Father

who provided the means

that made my education possible

ACKNOWLEDGEMENTS

It is my pleasure to thank the faculty, staff and students of the Seismolab for all of the happy days I have shared with them during my tenure as a graduate student. The faculty, especially my official thesis advisor, Don Helmberger, and my unofficial thesis advisor, Hiroo Kanamori, provided me with stimulating instruction, direction and ideas on topics both inside and outside my area of active research. I am also grateful to Larry Burdick, Chuck Langston and George Mellman who helped answer many questions during my early days here as "John Ebel, boy seismologist."

I want to also thank at this time the many people who helped with the production of this thesis. Gladys Engen was responsible for finding the excellent fit to the strong motion data in Chapter 3. John Cipar, Don Helmberger, Hiroo Kanamori, Thorne Lay, Vicky Le Fevre, George Mellman, Kerry Sieh and Terry Wallace provided comments and suggestions to improve the text. Joe Galvan and Laszlo Lenches aided with the production of the figures. Dee Page patiently assisted with problems which cropped up during the typing of the thesis, and Martha Bouey stayed up late one Saturday night to number the pages and to help me assemble the final text.

This research was supported by the National Science Foundation in grants Nos. EAR78-14786, EAR78-11973 and PFR-7921769, and by the U. S. Geological Survey in grant No. 14-080-001-17631.

ABSTRACT

A simple method for determining which events prior to a main shock may be "true" foreshocks, events which are caused by the same failure process as that which triggers the main shock, is proposed. An event is regarded as a "true" foreshock if it takes place within a certain time period of, is at least half a magnitude unit smaller than and occurs within the aftershock zone of a main shock. The time periods of potential foreshock occurrence computed from local and regional seismicity rates for four events were calculated to range from several days to several weeks prior to the corresponding main shocks.

A detailed analysis of two foreshocks (FS-1, M = 7, and FS-2, M = 6-1/2), the main shock (M, M = 7-1/2) and two aftershocks (A-1, M = 6-3/4, and A-2, M = 7) from the August 11, 1965 New Hebrides Islands earthquake sequence is presented. Focal mechanisms, depths, moments, time function durations and directions of rupture (if they could be inferred) for the events have been found using time domain synthetic seismograms of the far-field body waves and surface waves. The focal mechanisms of all the events except A-2 are consistent with faulting on the interface between the subducting Indian plate and the overriding Pacific plate. A-2 was an event on a steeply-dipping fault which ruptured into the underthrusting plate. The observed radiation patterns for the Rayleigh and Love waves from these events are consistent with the results of the body-wave analysis. The theoretical static vertical surface displacements computed from the teleseismic source model for M

are much smaller than the observed coastal uplift indicating that very long-period deformations accompanied the earthquake. The seismicity during the sequence migrated first from northwest to southeast and then toward the southwest and northeast.

A detailed source study of the short-period P waves from the Borrego Mountain earthquake in Southern California is reported. The short-period waveforms at different stations show good coherence, indicating that the seismograms contain reliable information from the source region. From simultaneous long-period-short-period deconvolutions the sP phase was found to consist of two separate pulses. Synthetic seismograms computed from the long-period source model of Burdick and Mellman (1976) did not match the data very well while synthetics with two high-frequency point sources did. The results of a waveform inversion analysis indicate that both sources were located at a depth of 8 km, had similar focal mechanisms, had time function durations of approximately 2 seconds and occurred about 2.2 seconds apart. Synthetic displacement, velocity and acceleration records, computed from a smoothed version of the teleseismic, short-period source model, fit both the amplitudes and waveforms of the SH wavetrain from the strong-motion data from El Centro, California.

The existence of asperities on the fault zones in the two source regions is inferred. In the New Hebrides three asperities are proposed--one at the northern end of the 1965 seismic zone, one between the islands of Santo and Mallikolo, and one near the southern end of the main shock fault plane. The sequence of events reflects a pattern of

the loading and breaking of asperities on the fault. For the Borrego Mountain earthquake the short-period sources represent the breaking of two asperities. The stress drops of the two events were several hundred bars each while the average stress drop for the entire event was about 20 bars. For both the New Hebrides events and the Borrego Mountain earthquake, the area of the asperities which ruptured during the main event was no more than 15% of the total fault area.

TABLE OF CONTENTS

INTRODUCTION

One important goal of present seismological research is the understanding and modeling of the shocks which lead up to and accompany a large seismic failure in the earth. Achieving this goal is a difficult task because observations of earthquakes can only be made on or just below the surface of the earth and are usually made at distances far removed from earthquake source regions. Interwoven in the observations of a seismic event is information not only about the earthquake source but also about the interaction of the seismic energy with the earth as the energy travels from source region to each receiver. Thus, the goal of a seismologist becomes one of first trying to untangle the source and propagation effects from recordings of the seismic waves from an earthquake and only then using what is discovered about the source to describe the failure process that accompanied the event.

This problem of separating source and propagation effects especially plagues studies of shallow seismic sources because of the free surface and other strongly-reflecting interfaces in the crust (Langston and Helmberger, 1975; Langston, 1978b). This is unfortunate because it is only for shallow events that it is possible to make non-seismographic as well as seismographic local observations (i.e. detailed aftershock locations, surface fault offsets and strain measurements) which can be used to complement the far-field waveform observations. Fortunately, source and propagation effects in the

far-field body-wave phases of shallow earthquakes can be individually isolated using the method of synthetic seismograms (Helmberger and Burdick, 1979). This time-domain modeling technique includes both the interaction of the earthquake signal with the near source seismic structure and a set of source parameters in the computation of the synthetic seismogram and thus allows one to distinguish between the two effects in interpreting recorded body waveforms. This method has proven to be useful for isolating seimsic source parameters of many earthquakes (Burdick and Mellman, 1976; Langston, 1978a; Rial, 1978). Surface waves are also important data in earthquake source studies because they contain information about the very long period deformations associated with seismic events. Unfortunately, as with body waves, the source information in surface waveforms is hidden by propagation effects. But, again as with body waves, a time domain modeling method for surface waves has been successfully developed to isolate source information from seismic events (Kanamori, 1970a,b). The results from time domain studies of surface waves have been found to be compatible with those from body waves and have been used to investigate seismic source excitations over a broad frequency band (Kanamori and Stewart, 1976, 1978; Ebel et al., 1978).

The ability to make meaningful measurements of parameters of earthquake sources leads one to want to use these determinations to explain the occurrence of particular earthquakes and hopefully to come to some understanding of how these earthquakes fit into the general seismicity and tectonic patterns of a region. Since there are many

different kinds of earthquake classifications (foreshocks, mainshocks, aftershocks, swarm events and "background" seismicity) and several different types of earthquake mechanisms (strike-slip, thrust and normal), a study and comparison of all these different kinds of events would be a Herculean project. The purpose of this thesis is to perform just a small part of this job. It is to model some foreshocks, mainshocks and aftershocks using synthetic seismograms, discuss how the events reflect the tectonics of the source region in light of these source models and compare the source models to infer similarities and differences between the failure histories of the events.

Since one of the aims of this thesis is to investigate the source models of some foreshocks and to compare them to those found for other kinds of events in the same epicentral region, it was felt that some clarification of what is meant by the term "foreshock" as used in this thesis was necessary. In Chapter 1 the meaning of the word "foreshock" is discussed and a quantitative criterion for defining a "true" foreshock is proposed. This definition is meant to provide some means for deciding what events in other areas or at other times might be considered "true" foreshocks and which can then be studied and compared to the foreshocks presented in this work.

Chapter 2 presents a detailed discussion of the synthetic modeling of the waveforms from several events from the 1965 New Hebrides Islands earthquake swarm. This particular sequence of events was chosen for study for several reasons: two large foreshocks occurred within a day of the main shock, the foreshocks were well-recorded teleseismically on

long-period WWSSN instruments, mainshock body-wave phases were on scale at a few WWSSN stations and two aftershocks were also large enough that they could be easily modeled. Both body waves and surface waves were synthesized, and source parameters determined in the analysis for all of the events are presented and compared. Static uplift data and the time history of the earthquake sequence were also studied. The contents of this chapter appear in Ebel (1980).

Chapter 3 is a study of the short-period, far-field P waves from the 1968 Borrego Mountain earthquake in southern California. The purpose of this study is to determine how well this set of short-period records can be modeled, how compatible the short-period source model is with the long-period and strong-motion data from the event, and what additional details of the source can be found from the short-period records which were not evident in the Burdick and Mellman (1976) source model which was found from an analysis of just the long-period body-wave records. The source model found from the teleseismic short-period waveforms is then used to synthesize the displacement, velocity and acceleration records of the SH motion taken at El Centro, California.

Chapter 4 is a discussion of the observational evidence for the existence of heterogeneities of the breaking strength in the fault zones of the New Hebrides Islands earthquakes and the Borrego Mountain earthquake. Two models of fault heterogeneity, the barrier model and the asperity model, are presented and compared. The results of the anaylsis in the preceding two chapters is used to demonstrate the locations, sizes and Breaking strengths of possible asperities for each

of these two fault zones. The evolution of the seismic failure in each fault zone is discussed in light of the asperity model.

Chapter 1

A Simple Method for Identifying "True" Foreshocks of Large Earthquakes

INTRODUCTION

It has long been recognized that smaller earthquakes often precede by days, months or even years the occurrence of a large earthquake in a given region (Richter, 1958; Rikitake, 1976). Since it was believed that these small events in some way represented premonitions of the later large event, they were given the name "foreshocks". In recent years foreshocks have been studied with increasing interest because of their potential value as indicators of the imminence of large earthquakes (Rikitake, 1976). An impetus for understanding foreshocks was provided by the successful forewarning of a large earthquake which took place near Haicheng, China, in 1975. The existence of anomalous seismicity was correctly identified as a foreshock sequence by Chinese scientists and was used as one criterion for the decision to issue the prediction of a large shock (Haicheng Earthquake Study Delegation, 1977). Most recent studies of foreshocks have attempted to understand the temporal and spatial occurrence of the seismicity preceding main shocks in the hope that systematic patterns may eventually be recognized (e.g. Berg, 1968; Yamakawa et al., 1969; Mogi, 1969; Suyehiro and Sekiya, 1972; Wesson and Ellsworth, 1973; Papazachos, 1975; Jones and

Molnar, 1976; Evison, 1977a,b; Brady, 1977).

One drawback to the studies of the premonitory seismicity of large shocks is that there is no agreed upon definition of the word "foreshock". Strictly speaking, a "foreshock" is an earthquake which precedes another event in time. However most seismologists put a more restrictive definition on the term. They regard earthquakes as being foreshocks if they occur within some distance from and some time before a larger event (the main shock). The particular distances, time periods and event sizes assumed in defining a foreshock are generally stated or left implicit by the particular user of the word (Rikitake, 1976). The conjecture that a "foreshock" should be distinct from routine "background" seismicity (Richter, 1958) suggests that there is a deeper connotation of the word. This hidden meaning, which follows from the idea that a foreshock is an event which foreshadows a main shock, is that a foreshock is caused by the same failure process or processes which trigger the main shock. Unfortunately, since the triggering mechanism of earthquakes is not well understood at present, it is not possible to give a precise definition of a foreshock which would explicitly include this connotation. This means that there is an inherent ambiguity in the term "foreshock" and that the identification of "true foreshocks" (Richter, 1958), or events which definitely participate in the same failure process as the main shock, is extremely difficult.

One of the purposes of this thesis is to study the details of the

fault failure histories associated with some moderate and large earthquakes. In order to understand the total failure process of a seismic event, one must analyze not only the main shock but also any smaller events which immediately precede and take place in the same general area as the main shock. These premonitory events, which are "true" foreshocks in the sense discussed above, contain valuable information about the initiation of the failure process. It is very important to be able to identify these foreshocks so that they can be thoroughly studied.

IDENTIFICATION OF A "TRUE" FORESHOCK

Since it is not possible at present to prove that any two events are caused by a common failure process, it is not possible to give a deterministic method for identifying a "true" foreshock. However, it is possible to find earthquake sequences where there was an anomalously high rate of seismicity just prior to a main event and to tag these sequences as foreshock activities. It is also possible to extrapolate this idea to areas of lower seismicity or with less complete seismic catalogs to identify possible "true" foreshocks in these areas. This suggests that one way that "true" foreshocks can be differentiated from background seismicity is by showing that the former are events which had a low probability of occurring given the average background seismicity. This idea does not eliminate the inherent ambiguity in defining a foreshock, but rather it reduces it to a question of determining a probability level below which an event can be considered non-random.

It has been found from several studies that the distribution with time of the occurrence of earthquakes is approximately random and follows a Poisson point process (Gardner and Knopoff, 1974; McNally, 1976). The fit of the occurrence of seismicity to a Poisson distribution is found to be improved by carefully deleting aftershocks and swarms from the earthquake data set (Utsu, 1969; Shlien and Toksoz, 1970, 1974). Thus, by assuming a Poisson distribution to model the seismicity of an area, one can determine a time period prior to a main shock where there is a very low probability that a random event should take place.

For a given area on the earth the probability P(n) that n earthquakes will occur in a certain time interval t with an average rate of earthquake occurrence λ is

$$P(n) = \frac{(\lambda t)^n e^{-\lambda t}}{n!} \qquad (1\text{-}1)$$

if the seismicity follows a point Poisson process. From (1-1) it follows that the probability P(0) that no earthquakes will occur is

$$P(0) = e^{-\lambda t} \qquad (1\text{-}2)$$

and consequently the probability P(n>0) that there will be one or more earthquakes is

$$P(n>0) = 1 - e^{-\lambda t} \qquad (1\text{-}3)$$

This expression was derived for earthquake distributions by Keilis-Borok et al. (1972). From expression (1-3) the relation for the time period during which the probability P for an earthquake to occur for a given seismicity rate is

$$t = \frac{\ln (1 - P)}{-\lambda} \qquad (1\text{-}4).$$

The analysis presented in expressions (1-1) through (1-4) has been used by other investigators to look for non-random clusters of seismicity (Shimazaki, 1973; McNally, 1976). However, equation (1-4) can also be used to determine the time interval prior to a large earthquake in which there is a strong likelihood that no events should have occurred. Any events which did take place during that time period can be considered unusual events and therefore can be identified as "true" foreshocks.

Some estimate of the average seismicity rate λ is needed if (1-4) is to be used in the definition of a foreshock. For a given region the number of earthquakes N of magnitude greater than or equal to some value M that occur in some unit time period follows the relation

$$\log N = a + bM \qquad (1\text{-}5)$$

(Gutenberg and Richter, 1954). This expression, called a cumulative recurrence curve, means that the number of earthquakes in some magnitude range $M_1 \leq M \leq M_2$ during some time period T is

$$N = 10^a \, (10^{-bM_1} - 10^{-bM_2}) \qquad (1\text{-}6).$$

Thus the average seismicity rate of a region can be defined using (1-6) as

$$\lambda = \frac{10^a \, (10^{-bM_1} - 10^{-bM_2})}{T} \qquad (1\text{-}7).$$

The area within which an event to be considered a foreshock must occur is usually taken to be the aftershock area (Rikitake, 1976) and that convention will be followed in this thesis. This assumption makes it difficult to estimate λ because recurrence curves are generally found for regions which are many times larger than the aftershock zone for any particular earthquake (Everndon, 1970, has many examples of this). However, this problem can be circumvented if the easily determined average regional seismicity rate is taken to be the same as that in any small part of the region. Kagan and Knopoff (1976, 1978) have shown that this assumption is approximately true for regions with diameters ranging from about 2 to 2000 km. For the purposes stated in this

thesis, it is adequate to determine λ for any particular fault zone from the regional seismicity statistics.

The preceding discussion presents a simple method for identifying events prior to a main shock which are probably "true" foreshocks. In order for an event to be considered a "true" foreshock as defined in this thesis it must occur within a certain time period which is given by equation (1-4) and within the aftershock zone of a large event. The advantages of this simple definition are that it gives some quantitative means for defining a "true" foreshock and that it can be applied (with an increased chance of error) to data sets where the number of earthquakes is not large. It provides a criterion for other investigators to identify foreshocks to study and compare to those analyzed in this thesis.

EXAMPLES OF FORESHOCK DEFINITION

The seismicity rates and time intervals for foreshock activity for 4 events are summarized in Table 1-1 in order to demonstrate the workability of this definition. Two seismicity rates are given for each event--one calculated from the statistics of earthquake occurrence for the entire region (Central America trench and two areas in southern California) and the other is computed by merely finding the average number of events per unit time in the aftershock zones of each event. The time interval given by equation (1-4) within which a foreshock would occur is calculated assuming that the probability of a random event occurring is less than 5%. While this value is somewhat arbitrarily

TABLE 1-1

	Oaxaca	Acapulco	Borrego Mountain	San Fernando
Regional rate (Eq/fault area/yr)	.480	.430	4.89	1.29
Local rate (Eq/fault area/yr)	.667	.185	10.4	1.45
Regional foreshock time (days)	40.0	43.3	3.85	14.5
Local foreshock time (days)	28.2	101.3	1.2	12.9

chosen, it does set a threshold which is strong enough so as to eliminate most background events without being so severe that it rejects "true" foreshocks as well. Two of the events chosen for this study took place in southern California--the Borrego Mountain earthquake of April 9, 1968 (M_L = 6.8) and the San Fernando earthquake of February 9, 1971 (M_L = 6.4). The other two events occurred in the Middle America subduction zone under Mexico--the Oaxaca earthquake of November 29, 1978 (M_s = 7.8) and the Acapulco earthquake of February 14, 1979 (M_s = 7.6). The two California events were studied because the catalog of seismicity in the two epicentral regions is reasonably complete after 1932 and because the results are of interest in analyzing other California events. The Oaxaca event was chosen because it was preceded by a recognized seismic quiescence (Ohtake et al., 1977). The Acapulco event was included because it took place in the same tectonic region as the Oaxaca earthquake but was not preceded by any obviously unusual seismic quiescence. The results from these latter two earthquakes are useful for determining the limitations of this foreshock definition in regions with suspected seismic gaps.

The seismicity rates given in Table 1-1 for the Mexico and California events were calculated from the NOAA and CIT catalogs respectively. The regional seismicity rate for the Mexico trench area was found using the cumulative recurrence relation $\log N = 5.84 - .73\ M$, where N is the number of shallow (depth $\leq$100 km) events greater than or equal in magnitude to M which occurred in the time period from 1950 to 1977. This relation was computed by fitting a least-squares line

through the log N versus M data in the magnitude range $4.5 \leq M \leq 7.5$ extracted from the NOAA catalog. No attempt was made to remove aftershock sequences from the data set which was used to determine the recurrence curve. For the Imperial Valley in California the recurrence relation is $\log N = 5.13 - .75\ M$ for events in the magnitude range $2 \leq M \leq 4.5$ in the time period from 1933 to 1967. No aftershock sequences or swarms were removed from the data set used for finding this recurrence curve. For the Los Angeles basin area $\log N = 6.04 - 1.23\ M$ for events with $2.5 \leq M \leq 4.5$ from 1934 to 1970 was determined. No events from the year 1933 were used in an effort to exclude the aftershocks from the 1933 Long Beach earthquake in the statistics. For each of the earthquakes the fault zone average seismicity rate was calculated by finding the number of earthquakes which occurred in an area defined by the aftershocks of each event in the time periods mentioned above and then dividing this number by the time interval. An attempt was made to define the fault area of the Oaxaca event in such a way that the local seismicity rate was not biased by the aftershocks from the 1968 and 1965 earthquakes which took place in areas adjacent to the Oaxaca aftershock zone. It was found that some aftershocks from the 1942 and 1954 events in southern California occurred in the aftershock zone of the 1968 Borrego Mountain earthquake. A subjective determination of which events in these sequences were aftershocks was made and all of these events were removed from the data set before the local seismicity rate was computed.

As can be seen in Table 1-1 the agreement between the local and

regional seismicity rates for the Oaxaca and San Fernando events is quite good, while for the Acapulco and Borrego Mountain earthquakes the local rates are .33 and 2.0 times the regional rates respectively. It is perhaps surprising that the local and regional seismicity rates for San Fernando and Oaxaca are so close. Both events were preceded by periods of seismic quiescence (Ishida and Kanamori, 1978; Ohtake et al., 1977) which could have been expected to cause a low local seismicity rate but which evidently did not. The local seismicity rate for the Borrego Mountain aftershock zone is higher than the regional rate due to a large number of swarms which were recorded in that area. The low local seismicity rate for the Acapulco event is difficult to explain although that earthquake took place at a depth of about 60 km while the regional cumulative recurrence relation was calculated from events which occurred predominantly at depths of 33 km or less.

Of these four events, only two--the Oaxaca and Borrego Mountain events--were preceded by what would be defined here as foreshocks. The foreshock for the Borrego Mountain earthquake took place just 85 seconds before and in the same hypocentral location as the main shock. It had a local magnitude of 3.7 and was obviously a foreshock as defined above. Abundant seismicity in the magnitude range of $2 \leq M \leq 4$ was recorded in the Oaxaca fault zone in the month prior to the main shock (McNally et al., 1979). In order to demonstrate that these events were foreshocks, the average number of events per unit time in the Oaxaca fault zone is needed. In this case, that number must be extrapolated from the regional recurrence curve which had been determined from a data set

which only included earthquakes with magnitudes larger than 4. It was found that the average number of events of this magnitude range greater than magnitude 2 expected in that area for any 30 day period is about 6, which is much less than the 43 events actually observed (E. Chael, personal communication, 1980). In fact, the probability of observing 43 events in a 30 day span is only about 10^{-23} which means that these events can be considered "true" foreshocks according to the definition given in this chapter.

DISCUSSION AND CONCLUSIONS

From the four examples given above it appears that the regional seismicity rate is a reasonable number to use for defining a foreshock, although for some events the local seismicity rate may vary by as much as a factor of three from the regional rate. While this variation is large, it is probably much smaller for most events if the analysis of Kagan and Knopoff (1976, 1978) is correct. It appears that many large events do have foreshocks as defined in this thesis. Jones and Molnar (1976) reported that at least 44% of the events of magnitude 7 or greater which occurred anywhere in the world between 1950 and 1973 had seismic activity within 40 days of the main shock, and of these premonitory events, 43% took place within 24 hours of the main shocks while 81% were within two weeks of them. The average world-wide earthquake rate in the seismically active areas is about 1.56 events greater than magnitude 4 per year in a circular area of radius 100 km. This value used in equation (1-4) yields a time of 11.7 days before a

main shock within which events considered "true" foreshocks would occur. Thus a significant number of the events listed by Jones and Molnar (1976) would be considered "true" foreshocks by the definition in this thesis.

The magnitude difference between a "true" foreshock and a mainshock is another number which should be stated. There is a semantic problem here because if too many large "true" foreshocks take place in an area, the sequence of events may be considered a swarm rather a foreshock-mainshock sequence. It is the opinion of this author that if the largest event in premonitory seismic activity is no less than .5 magnitude units smaller than the largest earthquake then that seismicity can be considered a "true" foreshock sequence. This definition is based on personal preference rather than on any rigorous analysis and so it should not be taken literally by other investigators.

In this chapter it is proposed that for an event to be considered a "true" foreshock it is one that participated in the same failure process as the main shock. A "true" foreshock is defined as an event which occurs within a certain time of and within the aftershock zone of a larger main event. The time interval for "true" foreshock occurrence is computed from an expression which assumes that any event which takes place in that time span has a very low probability of occurring randomly. Time intervals within which "true" foreshocks could have occurred are given for several earthquakes and these values range from a few days to several weeks. It is noted that many large events throughout the world have been preceded by "true" foreshocks.

Chapter 2

Source Processes of the 1965 New Hebrides Islands Earthquakes Inferred from Teleseismic Waveforms

INTRODUCTION

On August 11-13, 1965, the New Hebrides Islands were shaken by a series of earthquakes that included five large events with $M_s \geq 6\ 1/2$ and numerous smaller foreshocks and aftershocks. Two of the large earthquakes were precursory to the very powerful main shock which was felt several hundred kilometers away from the epicenter. The sequence of earthquakes caused serious damage on the islands of Esperitu Santo (hereafter also called Santo) and Mallikolo (also known as Malekula) from shaking as well as from a tsunami generated by an aftershock on August 13. Deformation associated with the earthquakes uplifted the northern end of the island of Mallikolo by more than a meter and the southern end of the island of Santo by more than a third of a meter. These earthquakes occurred in a tectonically complex area where only small and moderately large shallow seismic events had been recorded since 1904.

The sequence of earthquakes began on August 11 at 3:20:05 GMT with an event (m_b = 4 3/4) located under central Santo. At 3:40:55 GMT the first large foreshock (M_s = 7) took place in the same area. This event (here called FS-1) caused extensive damage on Santo. The second large foreshock (FS-2) occurred at 19:52:28 GMT and had M_s of 6 1/2. It was followed at 22:31:46 GMT by the main event M (M_s = 7 1/2) which did most

of the damage on Mallikolo and contributed to the damage on Santo. Over 100 teleseismically-located aftershocks took place during the following week, with the largest occurring on August 12 at 8:01:44 GMT (M_s = 6 3/4), called A-1 in this study, and on August 13 at 2:40:08 GMT (M_s = 7), here called A-2. The latter raised a 2 meter tsunami at Santo and Mallikolo (Benoit and Dubois, 1971). A reference map of the New Hebrides and the time of occurrence and locations of the events events are shown in Figure 2-1 (a) and Figure 2-1 (b) respectively.

These earthquakes are well-suited for a detailed source study because the WWSSN provided a wide azimuthal coverage of stations that were at teleseimic distances appropriate for both body-wave and surface-wave analysis. The sizes of the three moderately large events (FS-1, FS-2 and A-1) were such that the teleseismic body waves were fairly simple in form and could be easily modeled. The larger events (M and A-2), while having more complicated sources, could be understood once their waveforms were compared to the other, simpler events. Also, since the earthquakes all occurred within 100 km of each other, the body-wave and surface-wave paths for the different events to a given station were very similar except for the parts of the paths in the source region itself. This meant that differences in the waveforms for different events recorded at the same station could be attributed to effects from the sources and near-source seismic velocity structure. For all the events it was found that satisfactory synthetic seismograms could be computed by using the same near-source velocity structure and by changing only the earthquake focal mechanisms and depths. The

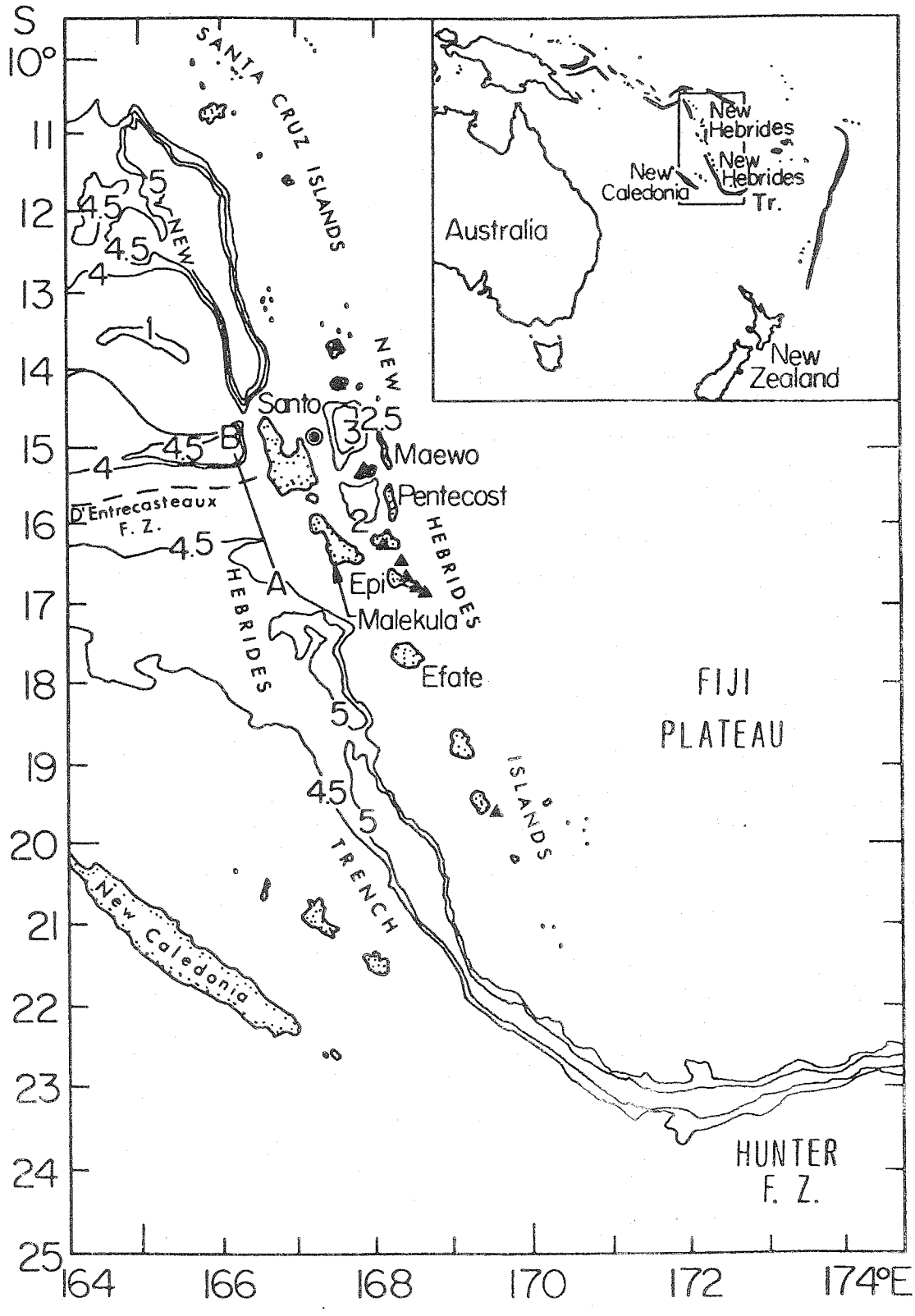

Figure 2-1(a). Regional map of the New Hebrides Islands area from Chung and Kanamori (1978). Bathymetric contours are in kilometers and triangles denote active volcanoes.

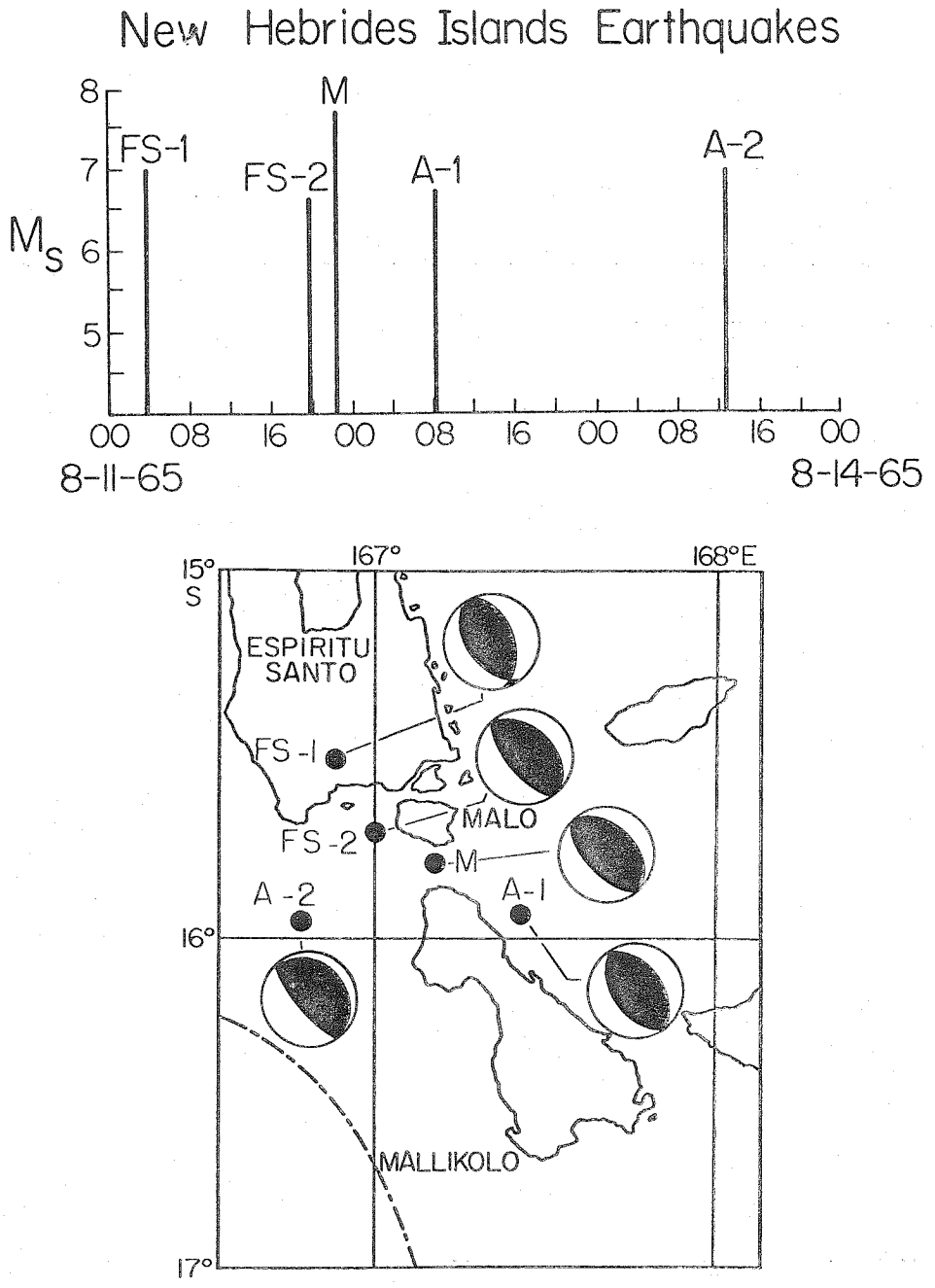

Figure 2-1(b). Times of occurrence, magnitudes and locations of the five largest New Hebrides Islands earthquakes from the 1965 sequence. The dashed line on the map represents the approximate position of the trench. The map is an adaption of a figure from Benoit and Dubois (1971).

results of the synthetic seismogram analysis combined with a study of the aftershock patterns and the coseismic uplift of Mallikolo give the deformation history of the earthquake sequence.

TECTONICS OF THE NEW HEBRIDES

The New Hebrides island-arc chain is located between 11° S, 165° E and 22° S, 170° E, in the southwest Pacific Ocean. These islands were formed as a result of the collision between the Pacific plate on the east and the Indian plate on the west (Coleman and Packham, 1976). The rate of plate convergence is very high, of the order of 9 or 10 cm/yr (Bernard Minster, personal communication, 1978). The New Hebrides are characterized by a Benioff zone which dips to the ENE at an angle of 70° (Santo, 1970; Dubois, 1971), by frequent earthquakes (Santo, 1970), and by active volcanism (Karig and Mammerickx, 1972). While the level of seismicity is high, generally the largest earthquakes in the region are only moderately large in size. There have been but two events with magnitude 8 or greater recorded in this region: one at 20° S, 168° E in 1920 (M = 8) and one at 11 3/4° S, 166 1/2° E in 1934 (M = 8.2) (Gutenberg and Richter, 1954). All other large events from this area have been no larger than M = 7 1/2.

An unusual feature of the New Hebrides is that the trench is not continuous at the center of the arc. The islands of Santo and Mallikolo, the two largest of the chain, lie where the trench should be. The trench is, in fact, non-existent at the latitude of these islands; instead, a submarine ridge called the D'Entrecasteaux fracture zone is

found to their west (Mallick, 1973; Luyendyk et al., 1974). Chung and Kanamori (1978) regard this ridge as a feature which alters the mode of subduction at this part of the island arc. They argue that the buoyancy of the D'Entrecasteaux fracture zone causes different sections of the Indian plate to subduct at different rates. They cite the occurrence of intermediate depth right-lateral and left-lateral strike-slip earthquakes under the northern part of Santo as evidence of a tear in the underthrusting plate due to the differential subduction. The events studied here are tectonically significant because they occurred in this region where the trench does not exist. Since they were shallow earthquakes which occurred directly under the islands of Santo and Mallikolo, they provide further information on the behavior of subduction of the D'Entrecasteaux fracture zone.

BODY WAVE ANALYSIS

Long-period body waves from the 1965 events were recorded by stations around the world. While the earthquakes were fairly large in magnitude, only the body waves for M were so large that they were off scale on most WWSSN long-period records. Fortunately, even for this event there were several low gain stations that did manage to record the complete body-wave train. Ten stations located at distances between 30^{o} and 80^{o} from the epicentral region were chosen for the body-wave analysis. Information on these stations is given in Table 2-1.

To find the best source model for each event, synthetic seismograms in the time domain were computed for the P waves at all ten stations

TABLE 2-1

Body Waves			Surface Waves		
station	Δ	Az	station	Δ	Az
BAG	55.8°	303°	AAE	129.4°	269°
DAV	47.0°	296°	AKU	130.0°	3°
GUA	36.5°	322°	ATL	113.9°	60°
HKC	64.2°	305°	ATU	141.1°	311°
KIP	50.3°	44°	CHG	75.5°	295°
LEM	58.9°	271°	COL	87.4°	18°
MAN	54.6°	301°	COP	135.7°	340°
MUN	48.9°	241°	ESK	139.8°	351°
RAR	31.8°	105°	GSC	88.1°	53°
TAU	31.9°	208°	KOD	92.4°	280°
			LON	88.9°	41°
			LPA	113.8°	141°
			LPB	116.8°	118°
			LPS	106.7°	87°
			MUN	48.9°	241°
			NAI	128.3°	255°
			NAT	149.2°	132°
			NNA	111.0°	110°
			POO	97.9°	287°
			PRE	122.5°	225°
			QUI	113.4°	97°
			SBA	62.1°	180°
			SDB	139.9°	222°
			TAB	123.9°	305°
			TRN	132.6°	90°

assuming a given source model, compared to the observed records and recalculated using a new model until the best visual match of synthetics to data was found. In this way the focal mechanism, depth, time function and body-wave moment for each event were determined. The algorithm for generating the synthetics is that of Langston and Helmberger (1975). In this study the near source crustal model consisted of one layer of crustal material over a mantle with lower than normal body-wave velocities (Figure 2-2). The models were computed using 5 rays: direct P, pP and sP off the bottom of the crustal layer. The source time functions for the earthquakes were always assumed to be symmetric trapezoids, and the time functions for pP and sP were made the same as for the direct P. These assumptions about the shape of the time function of the direct and the surface reflected phases are not true in the earth, but unfortunately more complex time functions are not resolvable without more detailed information on the near source and near receiver structures. A Futterman Q operator (Futterman, 1962) which is a function of t^* (the ratio of the travel time to the average attenuation along the travel path of a ray) was used to take into account the effect of the earth's anelasticity upon the far-field P waves. While he did not give a measured value for the anelasticity of the mantle in this area, Dubois (1971) reported that there is a heavily attenuating zone under the New Hebrides, so a large t^* value is proper. Since changes in t^* of up to 30% were found to have only a minor effect upon the synthetic waveforms and calculated moments, a t^* of 1.3 was used for all P-wave modeling. The body-wave moments were computed for

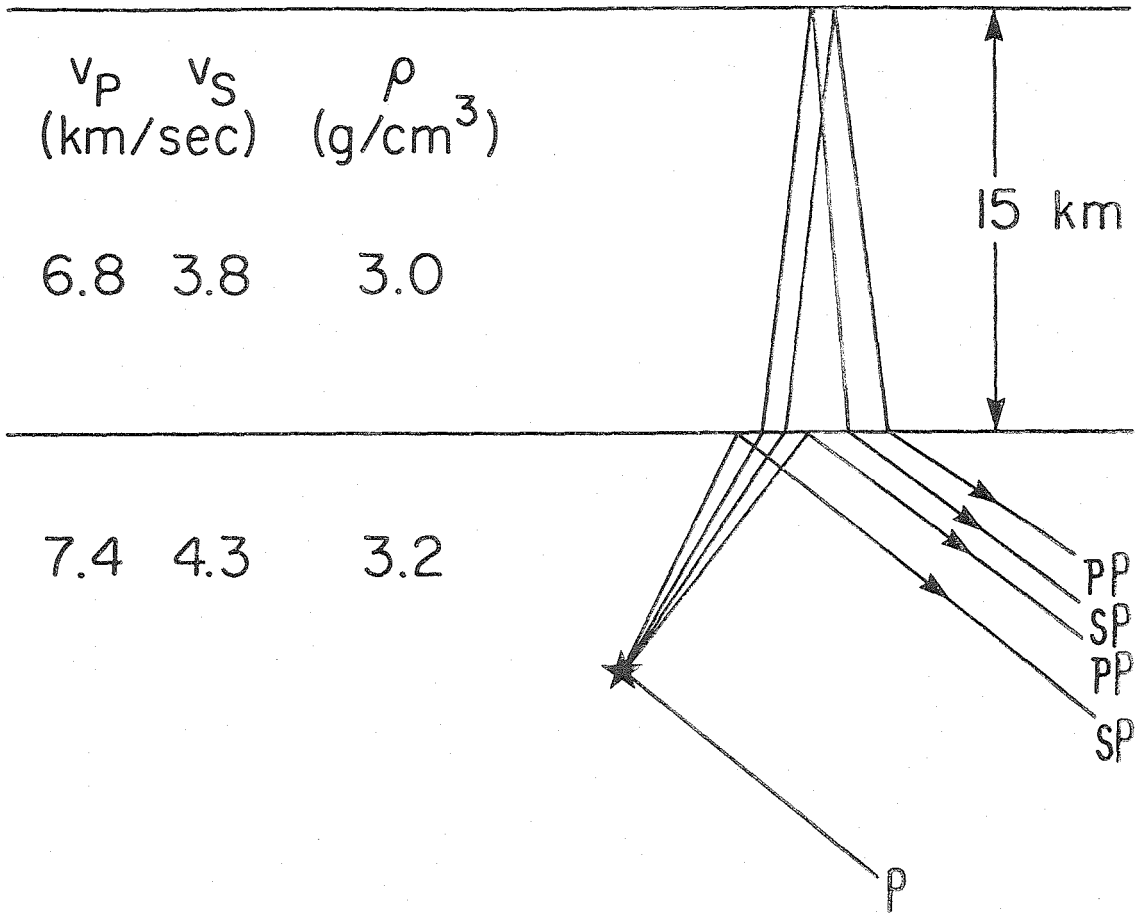

Figure 2-2. Crustal structure and cartoon of the five rays used in the body wave modeling.

each event by averaging the moment values at all the stations used in the body-wave analysis. The maximum variation in the station moments was about 50% for any one of the events. Two stations, HKC and MAN, always had higher-than-average body wave moments. No pattern was seen at the other stations.

The results of the modeling of the events are shown in Figures 2-3 through 2-7 and the source parameters for the earthquakes are given in Table 2-2. The mechanisms for the different events are similar to those of Johnson and Molnar (1972). If the east-dipping plane is taken to be the fault plane for FS-1, FS-2, M and A-1, then the mechanisms and depths of these events are consistent with those parameters that would be expected if the events took place on the contact between the two plates. A-2 is a more complicated event as can be seen by the poorer match of its synthetics to the data (Figure 2-7). It was probably associated with a different type of deformation from the shallow thrusting inferred for the other events as will be discussed later.

A number of points can be made about each of the events. FS-1 and A-1 appear to be relatively simple events and were adequately modeled with one point source. FS-2 at all stations except TAU and MUN seems to be equally simple. At these two stations, both of which have dilatational first arrivals, it was found that theoretical seismograms with one point source did not match the data very well because on the synthetic seismograms the pP arrival off the free surface causes a large negative pulse about 5 seconds after the first arrival. This large dilatational pulse clearly does not exist in the data. In an effort to

TABLE 2-2

Event	Body wave Moment	Surface wave Moment	Strike	Dip	Rake	Depth (km)	t_o (sec)	t_1 (sec)
FS-1	1.6×10^{26}	7.4×10^{26}	330°	45°	100°	23	3	1
FS-2	1.0×10^{26}	3.2×10^{26}	334°	20°	90°	15	.5	1
			334°	30°	90°	20	2.5	1
	The second source was twice the amplitude of the first and occurred 1 second after the first.							
M	1.6×10^{26}	3.0×10^{27}	334°	20°	90°	15	1	4
			330°	50°	90°	28	1	6
	The second source was three times the amplitude of the first and occurred 15 seconds after the first.							
A-1	8.0×10^{25}	2.4×10^{26}	334°	50°	90°	28	1	3
A-2		1.7×10^{27}	334°	10°	90°	10	1	10
			334°	10°	90°	30	1	10
	The second source was 5 times the amplitude of the first and occurred 20 seconds after the first.							

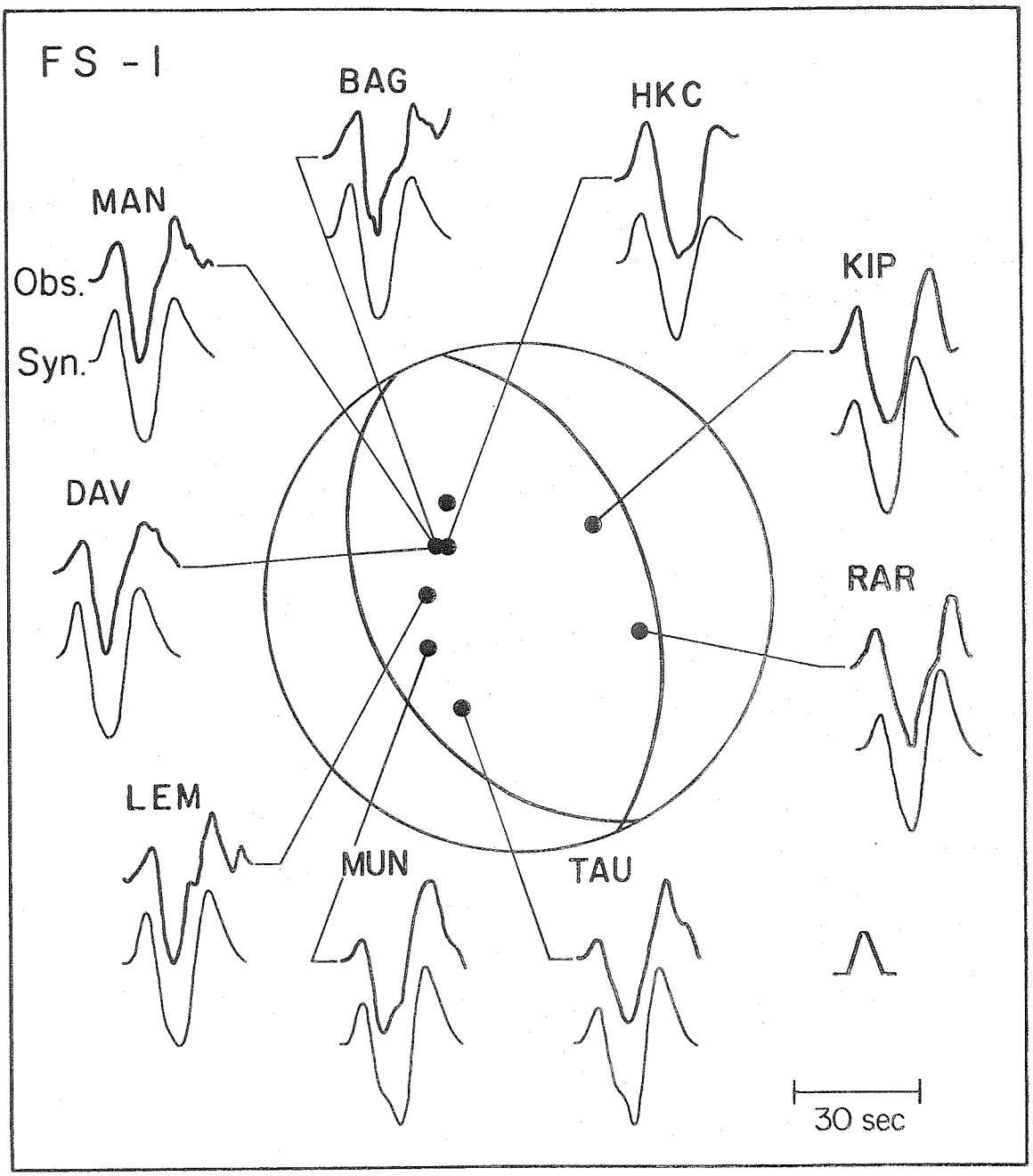

Figure 2-3. Body wave model for FS-1. The synthetic seismograms (light line) are under the observed seismograms (heavy line) for each station. The focal mechanism, the modeling procedure and the polarities of the first arrivals (open circles are dilatations, closed circles are compressions) from the observed seismograms are also given. The time function for the event is shown in the bottom right hand corner of the figure. The amplitudes of the synthetics and data are arbitrary.

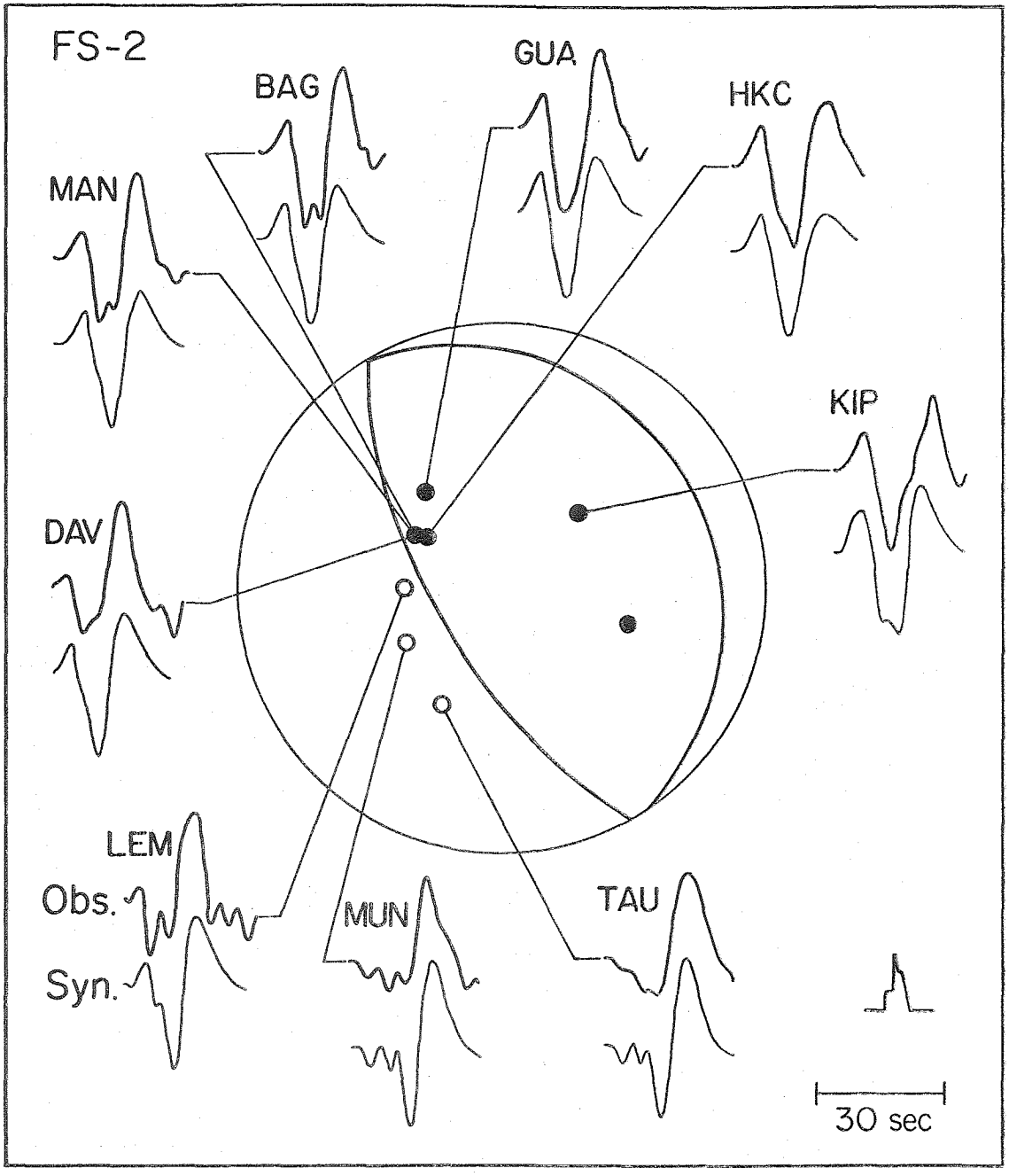

Figure 2-4. Body wave model for FS-2. Same as Figure 2-3.

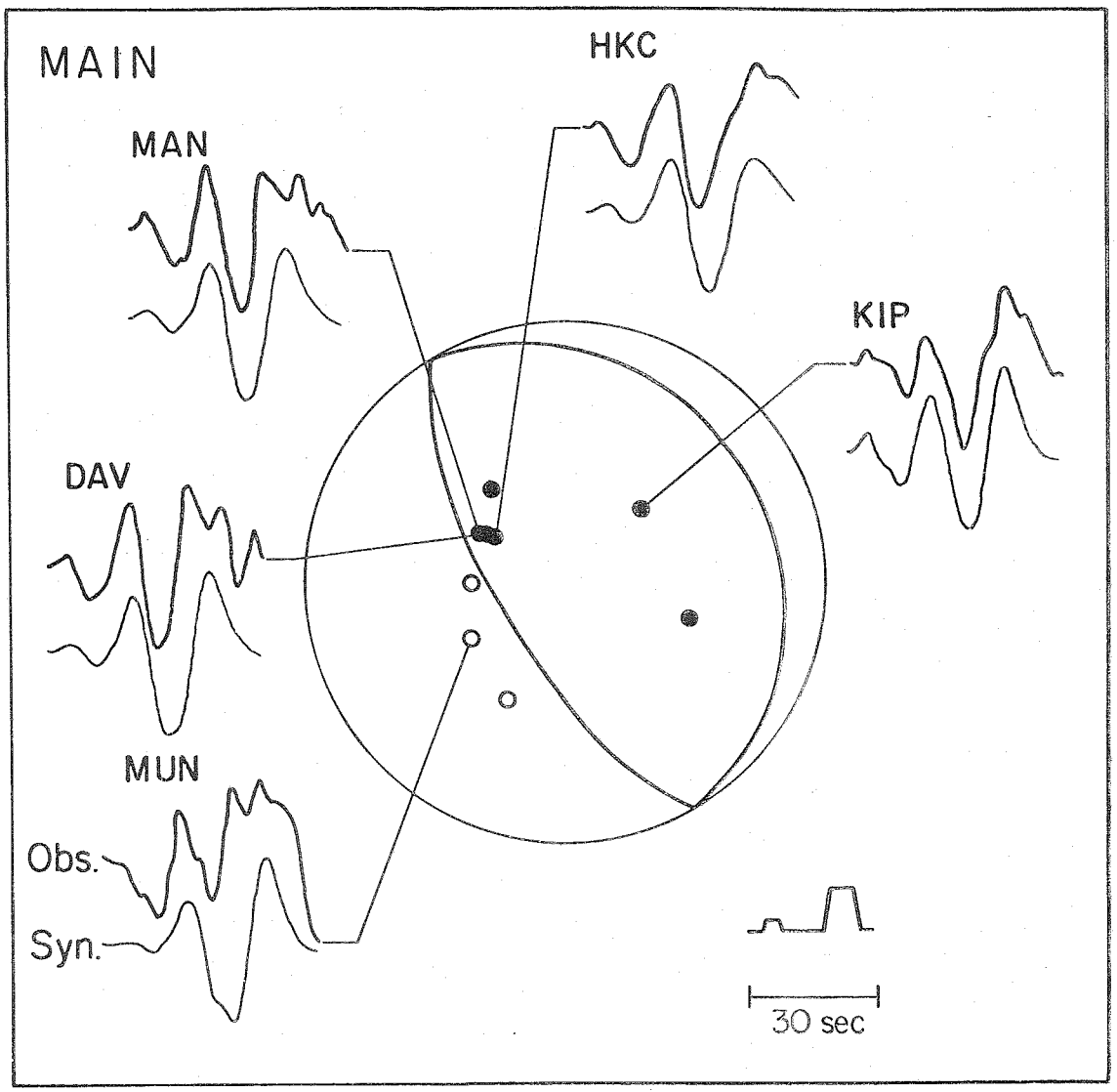

Figure 2-5. Body wave model for M. Same as Figure 2-3.

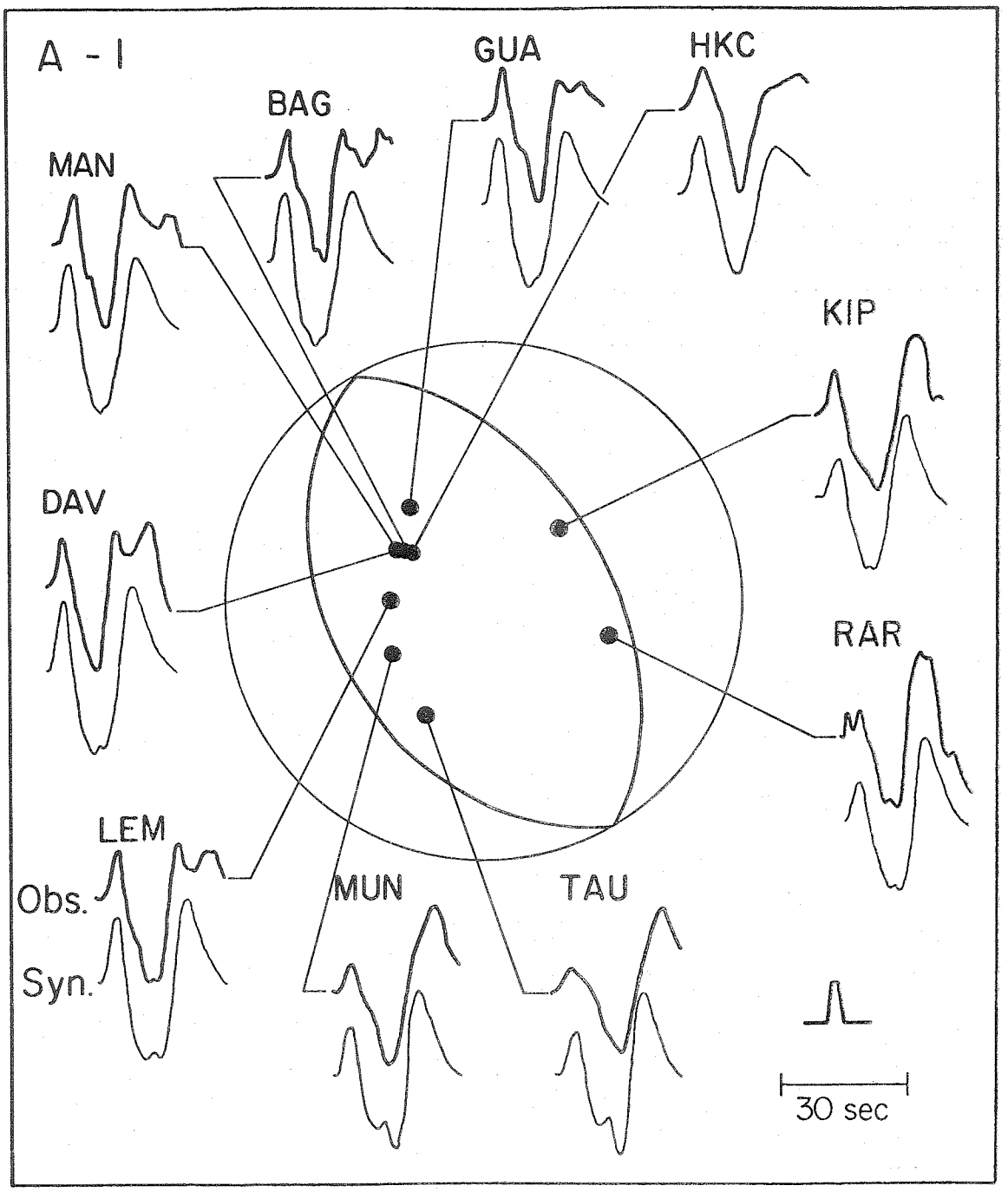

Figure 2-6. Body wave model for A-1. Same as Figure 2-3.

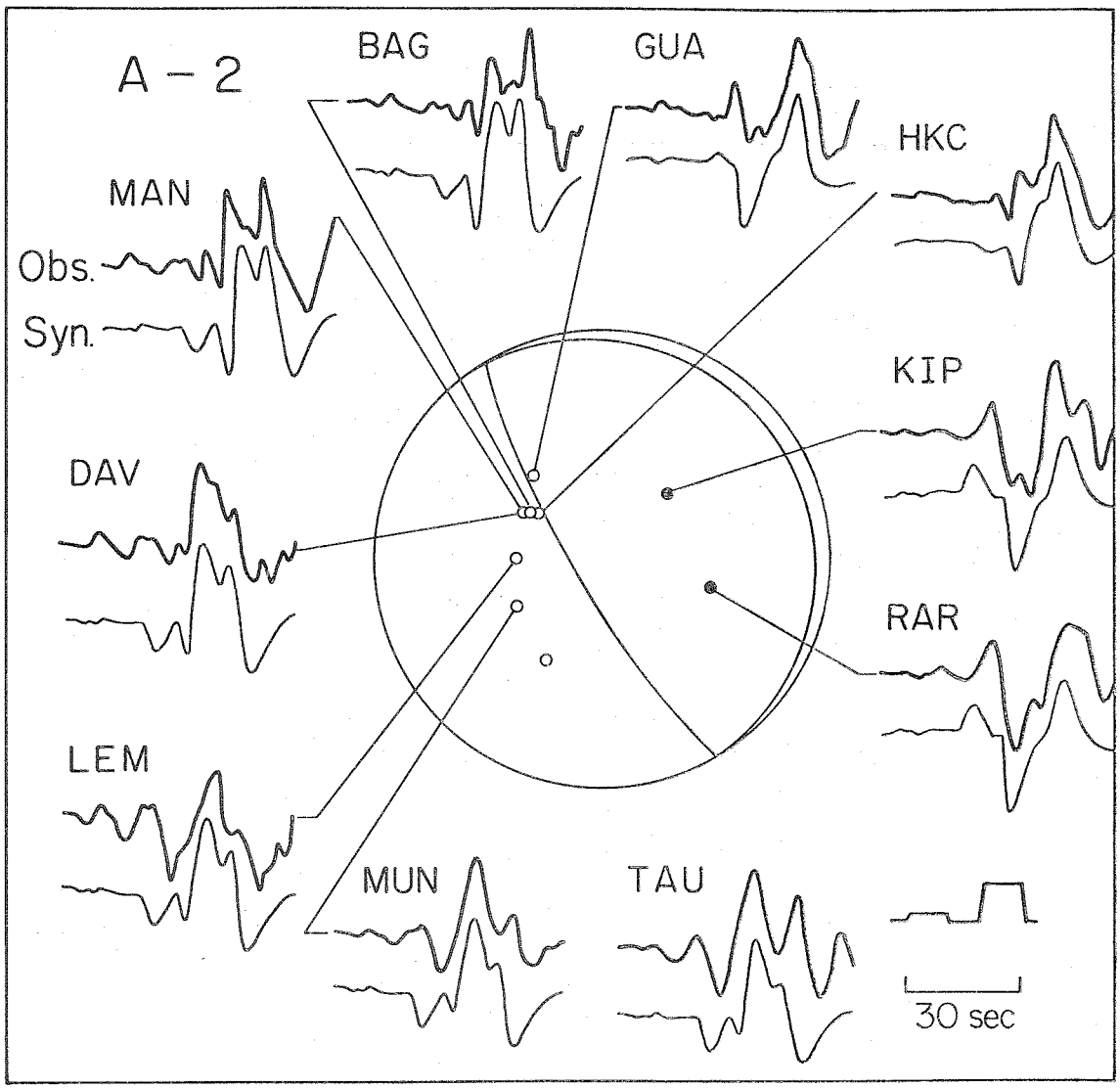

Figure 2-7. Body wave model for A-2. Same as Figure 2-3.

improve the fits, a model with two point sources was tried. It was hoped that arrivals from the two sources would destructively interfere in such a way that the pP arrival off the free surface would be a weak dilatational arrival. After several attempts in which the two sources were separated by no more than 15 km in space and 2 seconds in time, a satisfactory match to the observed seismograms was found. The best model had the first source at a depth of 15 km and had a northeast dipping plane of 20^{o} with the second source at a depth of 20 km, 7 km northeast of, 1 second later than and twice the amplitude of the first. The second source had a nodal plane that dipped 30^{o} to the northeast. While this combination of sources does not completely eliminate the large pP arrival (as can be seen by looking at the synthetics for TAU and MUN in Figure 2-4), it does reduce the pulse considerably. In fact, it reproduces the complexity of the observed seismograms at these two stations fairly well without noticeably affecting the fit of the seismograms at the other stations. The complexity of the waveforms at TAU and MUN for FS-2 and the necessity to model this event with two point sources suggest that the event had a more complex time history than FS-1 or A-1, which were satisfactorily modeled with one point source each.

The main shock waveforms are obviously more complicated than those of FS-1, FS-2 and A-1, but a model for them was surprisingly easy to find. The P waves for M were understood by comparing the waveforms of A-1 to the largest part of the mainshock waveform at each of several stations. The match was very close, as can be seen if one compares the

waveforms of Figure 2-6 to those on Figure 2-5. It was also found that the polarity of the first motions on the long period vertical records for FS-2 and M were the same at all WWSSN stations except CTA. Using these facts, a model with two point sources was tested and found to fit the data quite well. The first source has the identical focal mechanism and depth of the first source of FS-2, and the focal mechanism and depth of the second source, three times the amplitude of the first, are identical to A-1. The second source occurs 15 seconds after the first. Unfortunately, there were not enough records at different azimuths to constrain the horizontal separation of the two events using the waveform analysis. Thus, the model used in Figure 2-5 has the hypocenter of the first event, called M-1, directly above that of the second event (M-2). Actually the second source can be moved horizontally by as much as 20 km with respect to the first source without affecting the qualitative fit of the synthetic waveforms to the data. A guess at the location of the second source relative to the first can be made if it is assumed that the two events occurred on the boundary between the Pacific and Indian plates. If the northeast-dipping nodal plane is taken to be the fault plane, the second source must be located east to southeast of the first. Two consequences of this argument are that the direction of rupture of M had a component downdip on the fault and that the dip of the deeper part of the fault was steeper than that at shallower depths.

In contrast to the simplicity of the P waves for FS-1, FS-2, A-1 and even M, the P waves for A-2, shown in Figure 2-7, are extremely complicated. The first arrival from the source is so small on the

long-period records that it could not be found very easily on seismograms with even a small amount of noise. After about 20 or 30 seconds, a much stronger arrival can be seen at all stations. Models with two sources, the second five times larger than and taking place 20 seconds after the first, were tested. The strategy used in finding the focal mechanisms for the two sources was to assume that both had slip vectors at 90^{o} to a nodal plane with strike 334^{o}. The dip of the near vertical nodal plane for each source was varied separately until a good fit to the data was found. In this case the criteria for the good fit were that the relative amplitudes of the smaller first arrival and the later stronger event be approximately correct, and that the waveforms of the much larger event roughly matched those on the observed records. The best model is shown in Figure 2-7. The focal mechanism for this event was found by reading as many first arrivals from the very small P waves for the WWSSN stations as possible. Since the epicenter of this earthquake is located in a region where the trench and associated shallow subduction would be expected, since the event raised a sizeable tsunami, and since Benoit and Dubois (1971) argue from travel time data that this earthquake had a very shallow depth, the depth of the first source was assumed to be 10 km. The model in Figure 2-7 has the second source at a depth of 30 km with the same focal mechanism as the first source. The depth of the second source was determined primarily because the waveforms at KIP and RAR could only be fit with the second source being much deeper than the first. It was also found that the steeply-dipping nodal planes for each source must be within 10^{o} of

vertical. It should be noted that the durations of the synthetic P waves are shorter than those of the data and that the initial, low amplitude arrivals are not modeled well at all. Unfortunately, the complexity of the data and the simplicity of the source model prevented a better fit to the data. However it is obvious that while the model presented here lacks much of the complexity of the source for this event, it does provide a reasonable interpretation of the observed waveforms.

The results of the modeling of A-2 imply that this earthquake behaved in a very different manner from the four other large events. The two source model suggests that the event ruptured from near the earth's surface to a depth of at least 30 km. The fault plane for this event was evidently the plane which dipped steeply to the west. This event can probably best be characterized as an earthquake associated with internal deformation of the underthrusting plate, in contrast to the other events which were caused by slip on the boundary between the two plates.

The time functions found from the modeling process are simplified time histories of the dislocation processes for the different earthquakes. The time functions were assumed to be symmetric trapezoids in shape with the time duration of the first and last legs being called t_o and the time duration of the middle leg being called t_1. The trapezoid approximates the source as the convolution of two boxcar-shaped time histories: the time derivative of the particle dislocation rise time function and the fault rupture time function

(Savage, 1966). Which of t_o and t_1 represents the rise time and which represents the rupture time cannot be determined from the time function alone but must be inferred from independent data.

The resolvability of the time functions for the events can be seen by studying Figure 2-8. During the modeling it was found that the time separation between the first and second peaks of the synthetic waveforms varies with the depth of the source. A larger time separation corresponds to a deeper event. The width of the first pulse on the synthetics was determined to be sensitive to the duration of the time function. Generally, pairs of synthetics computed from time functions which had durations varying by more than one second were noticeably different. These two effects are obvious if one compares the synthetic waveforms in Figure 2-8. The effect of source depth on the waveforms is most evident by comparing the seismograms (both synthetic and observed) for FS-2 and A-1 while the difference in time functions is most easily seen by comparing the waveforms for FS-1 and A-1. In all cases the observed waveforms have details which are not modeled synthetically. These differences reflect the limitations of the simple source models used for the analysis which fit the general shape of the observations quite well but which do not fit the details of the seismograms as accurately.

One important difference was found in the time functions of the first four large events of the New Hebrides sequence. The time functions for FS-1 and FS-2 have t_o much greater than t_1, while for A-1 and M-1 t_o is much less than t_1. An examination of Figure 2-8 reveals

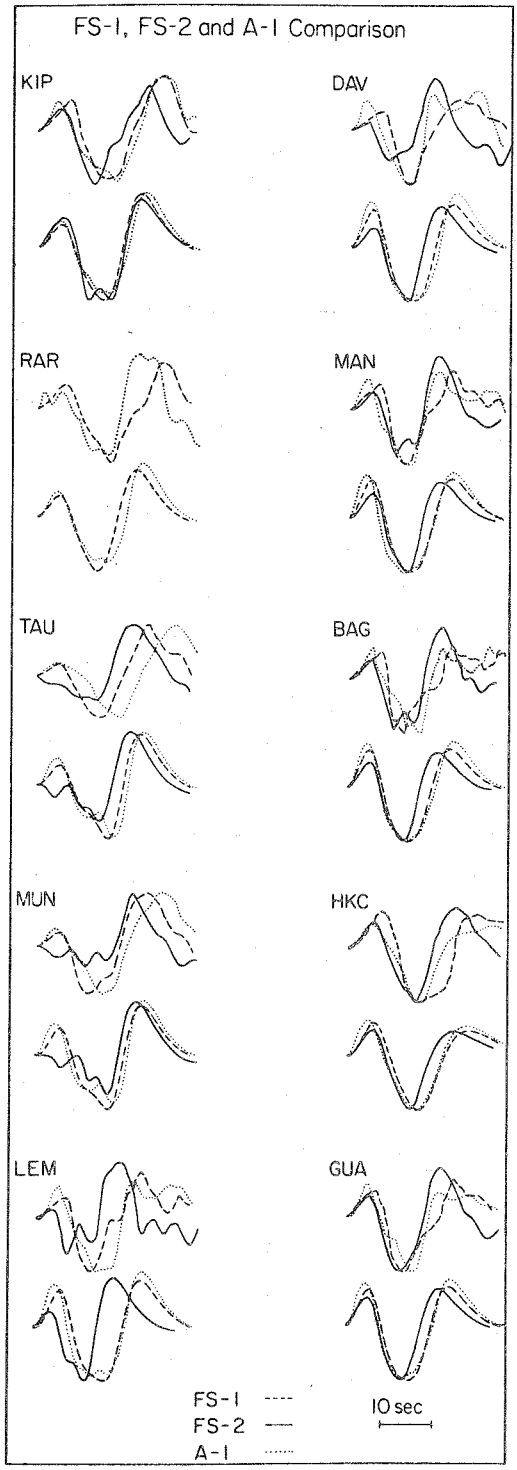

Figure 2-8. A comparison of the observed (top) and synthetic waveforms (bottom) for FS-1, FS-2 and A-1 for the 10 stations used in the body wave analysis. RAR did not record FS-2.

that the first upswings of the synthetics for the foreshocks are shorter period than the data, while that for the synthetic of A-1 is longer period than the data. This discrepancy, which can be lessened by using a more complicated time function for the synthetics, is evidence that the differences in the shapes of the time functions are greater than those found with these simple models. Except for FS-2 where it was needed for other reasons, a more complex time function was not tried because it was felt that the most important source details were already known from the simple model and that a more complicated source time function could not be resolved from the data. The difference in the shapes of the front of the time functions is resolvable because the first several seconds of the seismograms contain only the energy from the direct P wave. After about 5 seconds the reflected rays from the source region arrive and combine to obscure the details of the back of the time function. A long, low amplitude tail to the P wave time function could contain significant energy but not be detected due to its interference with the other large arrivals. Thus the shape of only the first couple of seconds of the time function is known in any detail from the modeling. The large values of t_o and small values of t_1 for FS-1 and FS-2 suggest that the rise time is comparable to the rupture time for these two events. For M-1 and A-1 the small values of t_o probably represent short rise times since, based upon guesses of their fault size made from their body wave and surface-wave moments, these events probably ruptured for several seconds. Thus, the foreshocks appear to have different source time histories than M and A-1. These differences

may be useful for identifying foreshocks to future events in the New Hebrides.

Only a small amount of additional source information could be extracted from the short-period P waves recorded at the 10 stations used for the long period analysis. No attempt at modeling the short-period P waves was made because of the lack of near-source and near-receiver seismic structure information since any meaningful modeling of the short-period records would demand a detailed knowledge of the velocity distribution and seismic discontinuities along the ray paths. However two observations can be made by examining some of the short-period waveforms shown in Figure 2-9. The first observation is that the short-period records for M and A-2 recorded at MAN reflect the more complicated sources for these events than those for FS-1, FS-2 and A-1. The largest amplitude short-period pulses for M and A-2 were recorded more than 30 seconds after the first arrivals of energy while for the other events the largest amplitudes were recorded in the first 20 seconds of the short-period coda. The second point of interest is that the short-period P wave coda for A-2 is much lower amplitude than that for FS-1 and even FS-2 at MAN. This is, in fact, true at all of the stations used in the analysis. Since the moment determined from the long-period surface waves was larger for A-2 than it was for FS-1 or FS-2, the low amplitude short-period body waves can be interpreted to mean that the spectrum of the source for A-2 was very different than those for the foreshocks. Unfortunately, this observation cannot be quantified without modeling the short-period records.

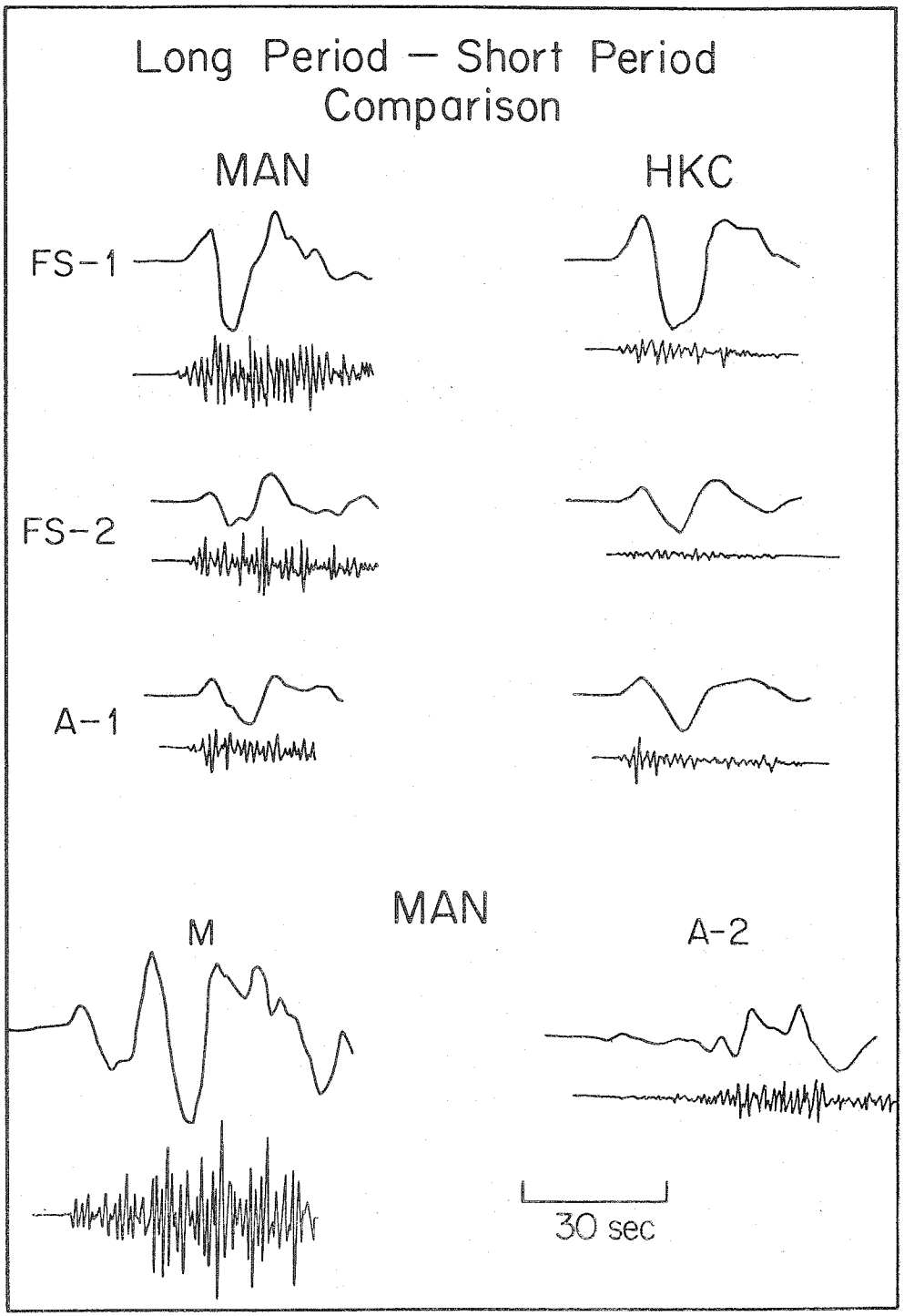

Figure 2-9. A comparison of the long period and short period P waves at MAN and HKC. The short period records have been normalized to the same gain, as have the long period waveforms. The timescale is the same for both the long period and short period records.

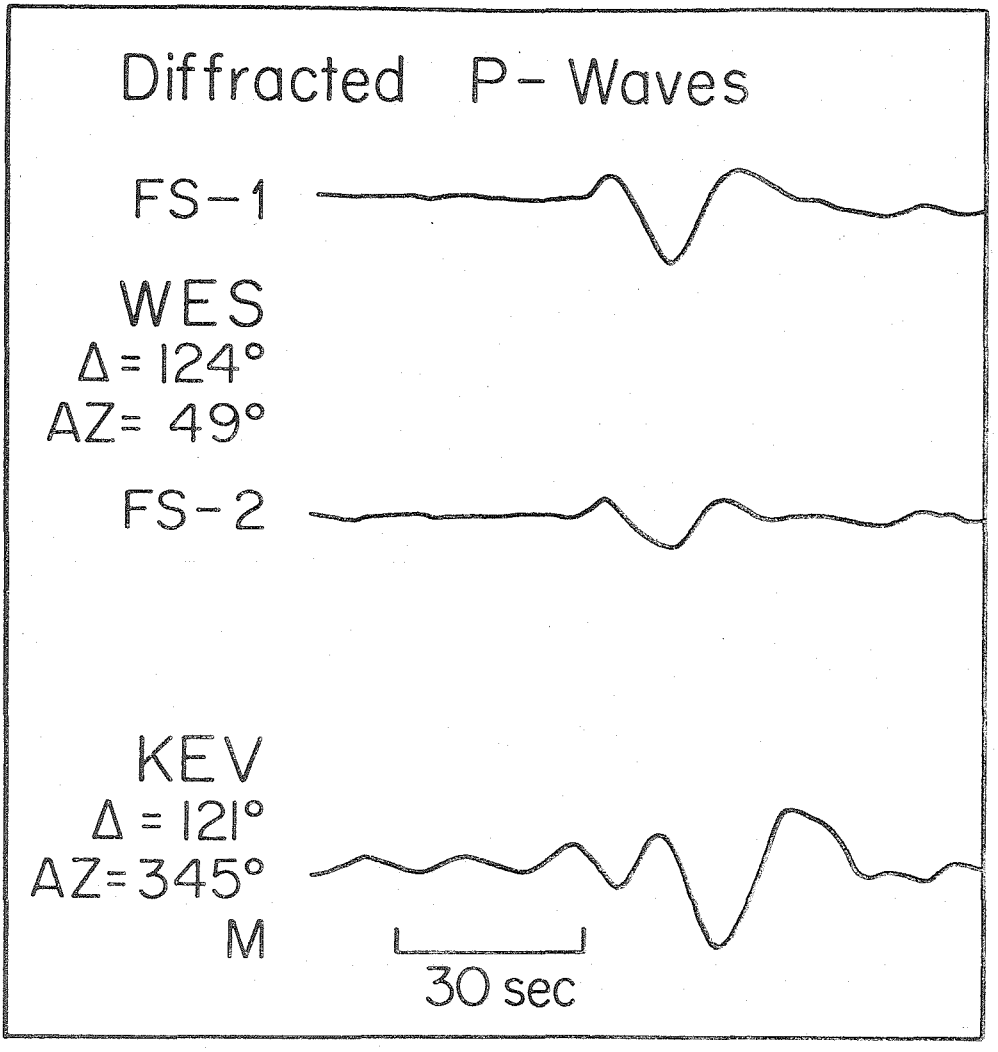

Figure 2-10. Observations of diffracted P waves for FS-1, FS-2 and M. All of the records have the same gain.

Because all of the events had thrust mechanisms, a maximum of the P wave radiation pattern was pointed in the direction of the center of the earth. This means that large PKP and diffracted P phases were observed at stations farther than 110° from the source region. Examples of diffracted P waves recorded for FS-1, FS-2 and M are shown in Figure 2-10. Since the waveforms of the diffracted arrivals appear to be filtered versions of the P waveforms shown earlier for each of these three events, the complexity of the diffracted P waves for M is additional evidence of the two source nature of that event.

The S waves from the stations in Table 2-1 were also investigated. However, when the records were digitized and rotated in order to isolate the SH components, it was found that the SH waveforms were very noisy. This was expected because the radiation patterns of the events predict that the far-field S waves should be dominated by SV energy and have only a small amount of SH energy. No attempt was made to model either the SV or SH waveforms because of the poor quality of the waveforms.

SURFACE WAVE ANALYSIS

The surface waves for these events were studied in an effort to find the details of the very long-period deformation associated with each event. For FS-1, FS-2 and A-1 Rayleigh waves R1 and Love waves G1 were used. For the main event M R3 and G3 were analyzed, while for A-2 both the pairs R1-G1 and R2-G3 were studied. The method used to reduce the data was that given in Kanamori and Stewart (1976). Essentially, the data were digitized, filtered and then corrected for attenuation and

dispersion to a propagation distance of 90^{o} for R1 and G1, and 450^{o} for R3 and G3. The filter used was a band-pass filter with cutoffs at periods of 35 and 300 seconds for R1 and G1, and periods of 60 and 400 seconds for R3 and G3. The stations used in the analysis are listed in Table 2-1, and the maximum amplitudes of the normalized and filtered surface waves for FS-2, M, A-1 and A-2 at each station are given in Table 2-3.

Radiation patterns for FS-2, A-1 and A-2 for the waves R1 and G1 and the radiation patterns for R3 and G3 for M are shown on Figures 2-11 and 2-12 together with synthetic radiation patterns for each of the waves. Because no complete radiation pattern was determined for FS-1, it is not plotted here. However its radiation pattern is essentially the same as those shown. The synthetic radiation patterns were computed from the focal mechanisms determined in the body-wave analysis, using the procedure of Kanamori and Stewart (1976). The theoretical radiation patterns were found to be virtually identical for all of the fault solutions. In general the agreement of the observed amplitudes and theoretical radiation patterns is very good, although some differences in the amplitudes of the nodal stations do exist. Some stations have observed amplitudes consistently smaller or larger than those predicted theoretically. ATL, always lower amplitude than expected, is an example of this.

Figures 2-13 and 2-14 show some theoretical and observed Rayleigh waves and Love waves respectively. The synthetic surface waves match the general features of the data although in most cases they differ in

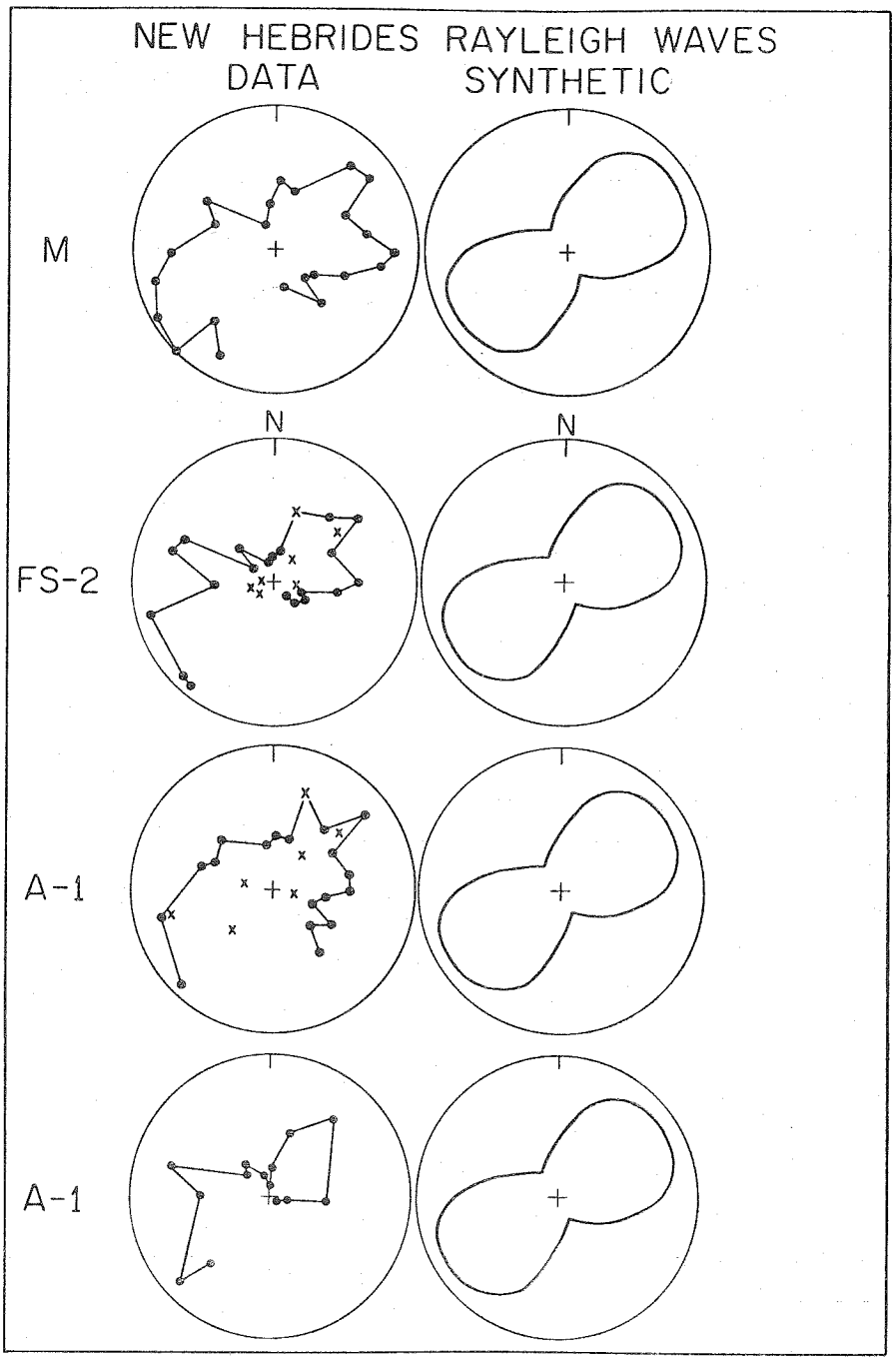

Figure 2-11. Observed Rayleigh wave radiation patterns (left) and theoretical radiation patterns (right) for the different events. The patterns are R3 for M and R1 for FS-2, A-1 and A-2. The X's represent the radiation patterns for waves of about 20 seconds durations.

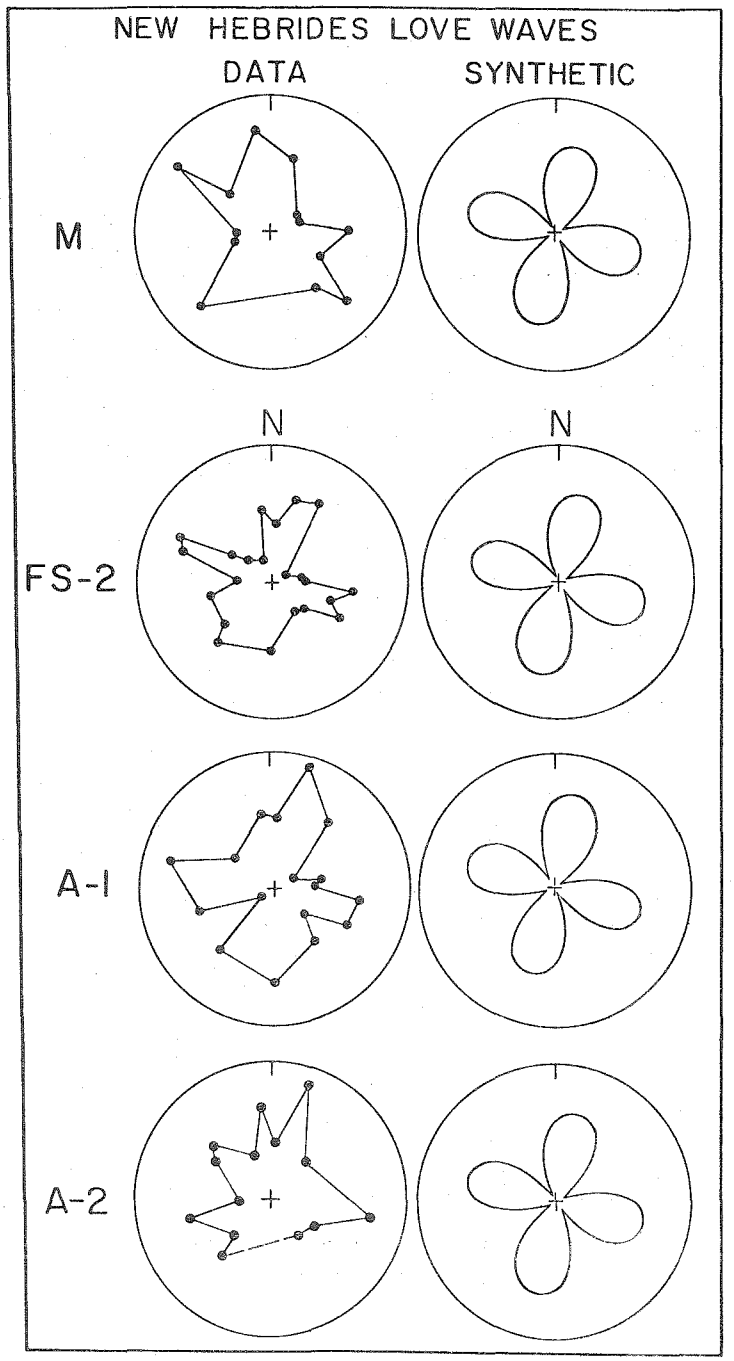

Figure 2-12. Same as Figure 2-11 for Love waves. The patterns are G3 for M and G1 for FS-2, A-1 and A-2.

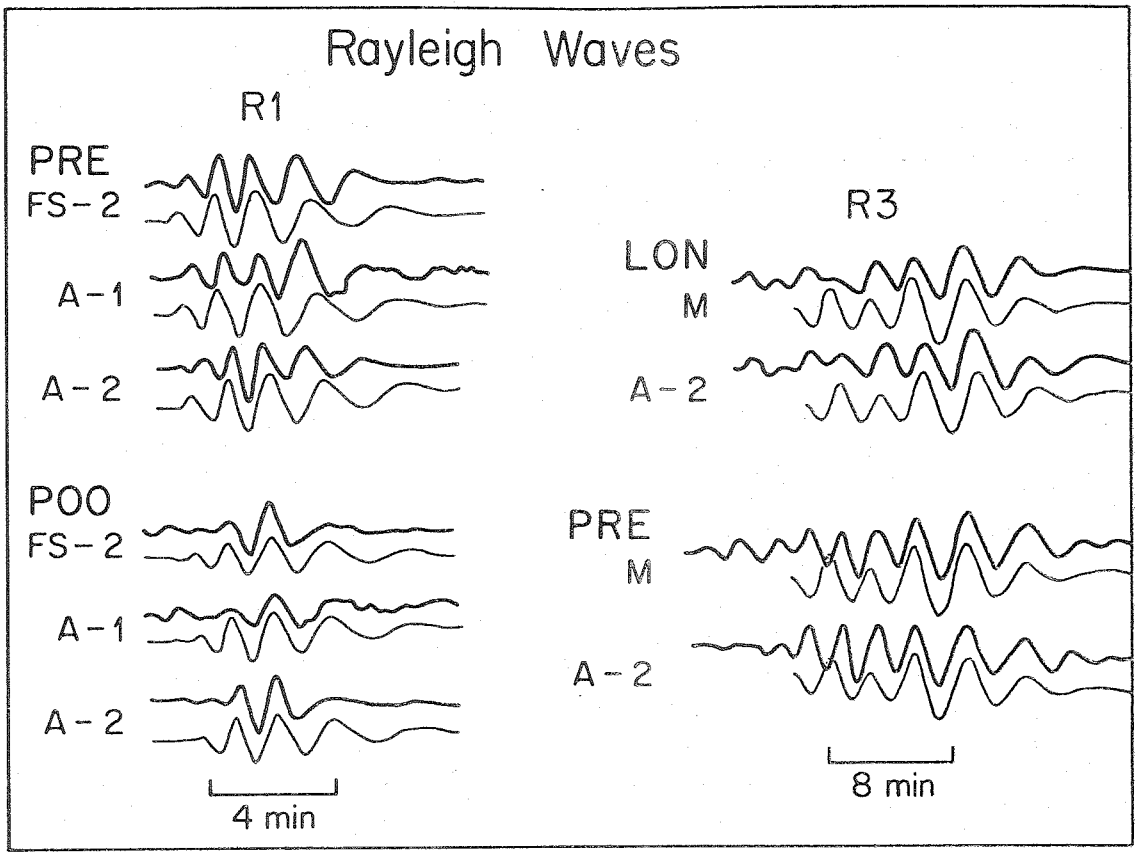

Figure 2-13. Observed Rayleigh waves (top; heavy line) and theoretical Rayleigh waves (bottom; light line). All waveforms have been filtered and equalized as described in the text and are arbitrarily normalized.

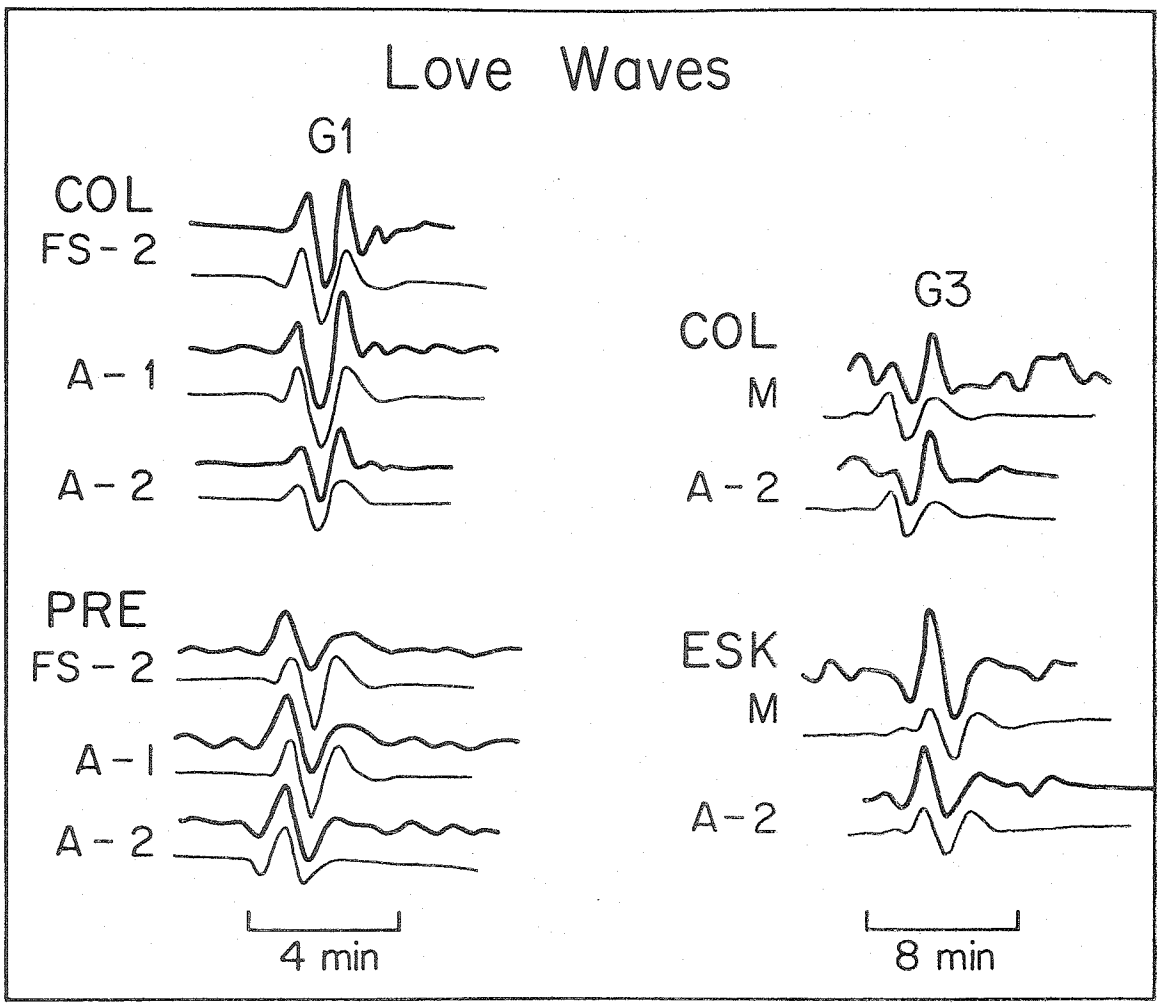

Figure 2-14. Same as Figure 2-13 for Love waves.

some details. As can be seen on these figures the same station recorded virtually identical waveforms for different events. This is even true when R1 and G1 for A-2 are compared to R1 and G1 for FS-2 and A-1. For A-2 these waves were extremely large on most of the records and they lacked the higher frequency waves present for the other events. Some of the records for A-2 had parts of the waveforms of G1 or R1 off scale. This meant that some peaks and troughs of the waveforms had to be extrapolated to positions off the records to enable digitization. The bias resulting from this procedure was small judging from the similarity of these waveforms to those from the other events. It was possible to digitize R1 and G1 for A-2 because, although the event was very large, the energy at periods of less than 30 seconds that it excited was extremely small. This made the waves clearly visible on the records.

Moments for the different earthquakes were computed by comparing the observed amplitudes to those from synthetic seismograms, and the results are shown in Table 2-3. While not reflected in the moment values calculated, the amplitudes of R1 were found to be strong functions of source depth. For example, as can be seen in Table 2-3, the G1 waves for FS-2 were only a few percent larger than those for A-1 while the R1 waves were about a factor of two larger for FS-2 than for A-1. This R1 versus G1 amplitude difference for the two earthquakes was easily modeled by computing the synthetics for FS-2 using the excitation functions for a 16 km depth source, while computing the synthetics for A-1 assuming a 33 km depth source. The difference in source depths found in the body-wave analysis was thus confirmed by the surface-wave

TABLE 2-3

Peak to peak amplitudes in centimeters on seismogram after filtering, normalizing to propagation distances of 90° (R1 and G1) and 450° (R3 and G3), and correcting to a gain of 1500.

	FS-2		A-1		A-2		M		A-2	
Station	R1	G1	R1	G1	R1	G1	R3	G3	R3	G3
AKU	.32	1.00	.25	1.01	3.12	6.56	.41			
COL	.87	1.97	.48	1.78	9.15	13.40	.31	.65	.19	.31
LON	.79	1.50	.36	1.50	13.12	5.89	.60		.29	
GSC	1.05		.57				.62			
ATL	.58	.21	.33				.41	.29	.18	
LPS	1.18	.99	.37	.25			.52	.29		
TRN	.88	.59	.39	.68			.66	.70		
QUI	.70	1.39	.26	.63			.57			.47
NNA	.58	1.08	.19	1.26	8.46	11.35	.40			.21
LPB	.37	1.45	.33		2.49		.23	.49		
NAT	.54	.78	.40	1.20	1.21	5.80	.24	.90		
LPA	.20	.77	.40	.63			.36	.66		
WEL				.87	1.67	5.01	.21			
SBA	1.09	1.77								
TAU							.66			
SDB	1.34	1.96			13.22	8.53	.52		.27	
PRE	1.33	1.08	.63	1.20	17.03	5.68	.78	.89	.31	
MUN				.26			.74			
NAI	1.33	1.22	.57	1.20		9.48	.71	.35	.30	.18
AAE	.63	.62			9.28	3.90	.59	.33		
KOD	.88									
POO	1.12	1.63	.38	1.54	13.77					
CHG	1.04	1.75	.13	.84			.37			
TAB	.28	.90			4.17	7.54	.50	1.01		
ATV	.50	.56	.39		5.03	8.52	.33	.45		
COP	.33	.41	.44		2.66	5.17	.15			.38
ESK	.26	1.32	.21	1.11	1.42	10.05	.20	.95		

study. The sensitivity of the excitation of short-period Rayleigh waves with depth and relative insensitivity of the excitation of Love waves was discussed in detail by Tsai and Aki (1970). The moment values computed from A-2 using R1 and G1 were found to be very close to those found using R3 and G3. This is good evidence that the moments computed for R1 and G1 can be directly compared to those from R3 and G3 and that there is no baseline shift involved in the different moment calculations due to the idealized earth structure assumed in the calculation of the synthetics. Also, it is apparent in Table 2-3 that the ratio of the amplitude of the surface waves from one earthquake to that for another earthquake computed at stations in the antinodal directions varied by only a few percent from that ratio at any other station. Thus, while the absolute values of the moments are somewhat uncertain due to the approximations inherent in calculating the synthetic surface waves, the moments of the events relative to each other are known very accurately.

The moments from the surface-wave analysis are consistently about a factor of three larger than those computed from the body-wave data (Table 2-2). A similar discrepancy has been noted for other earthquakes (Hart et al., 1977). Some of this discrepancy is probably due to approximations used in the computation of the body-wave and surface-wave moments, and some may be due to slower deformations which follow the initial, very high frequency source dislocations. Since the surface waves sample a much longer period than the body waves, they more accurately reflect the total dislocation processes of the events. Thus a significant portion of the earthquake moment is probably contained in

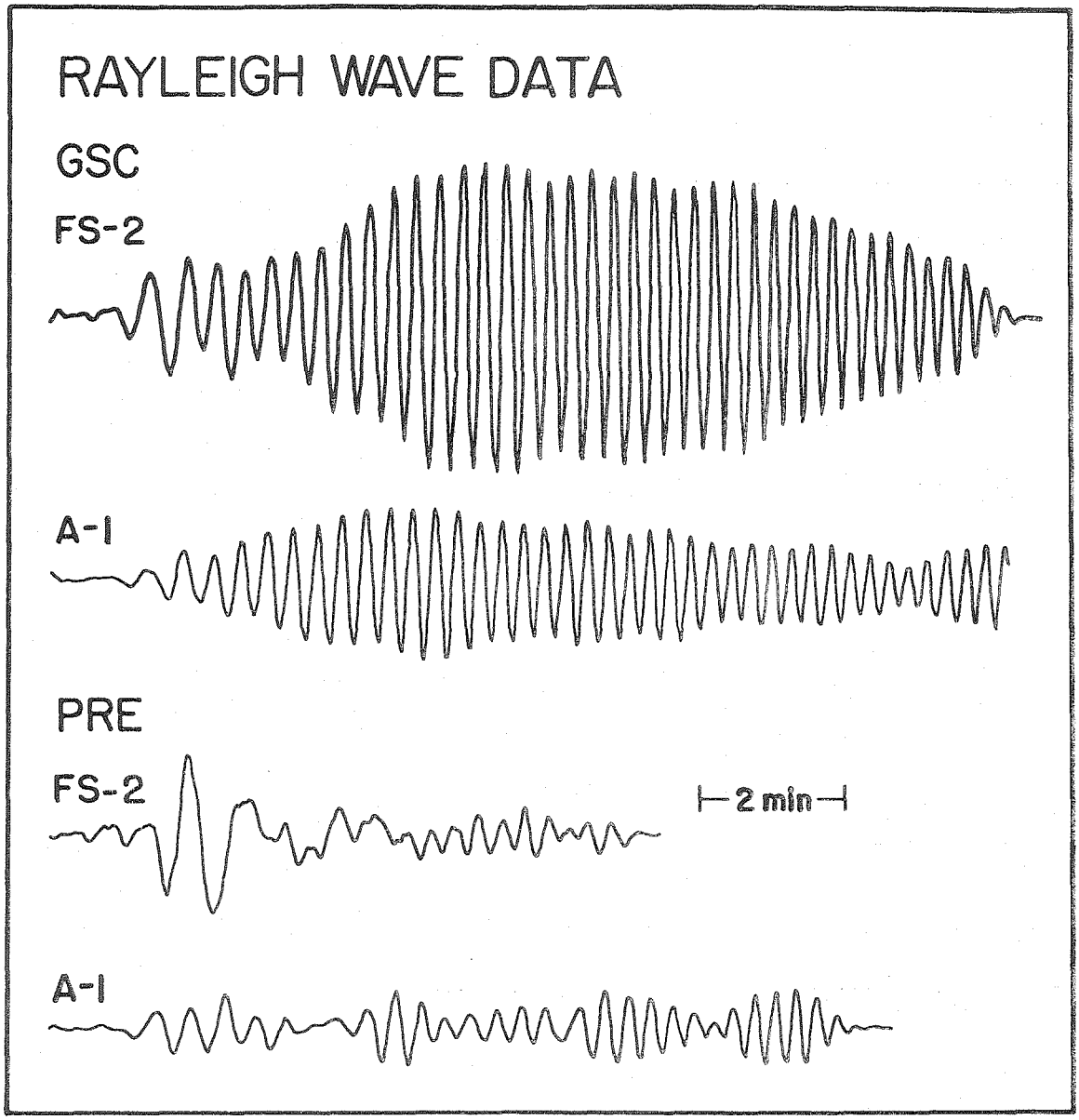

Figure 2-15. A comparison of the unfiltered Rayleigh waves (R1) at GSC and PRE for events A-1 and FS-2. The seismograms are all normalized to the same gain.

the slower deformations to which the surface-wave analysis is sensitive, but to which the body-wave analysis is not.

No obvious asymmetry due to source directivity is evident in any of the radiation patterns in Figures 2-11 and 2-12. However, the surface waves from FS-2 and M both displayed effects which may have been due to rupture propagation. Figure 2-15 shows the unfiltered seismograms for the R1 arrivals from FS-2 and A-1 at GSC and PRE. The amplitudes at periods of 60 to 80 seconds of the filtered records at GSC and PRE were roughly a factor of two larger for FS-2 than for A-1. For waves around a period of 20 seconds, the amplitudes at GSC for FS-2 were also about a factor of two larger than those for A-1. However, at PRE the amplitude of the 20 second waves for A-1 were larger than for FS-2. The radiation patterns for the 20 second waves (in all cases normalized to the maximum amplitude at COL which itself is arbitrarily normalized in Figure 2-11) for FS-2 and A-1 show that this happens at all the stations on the southwest radiation loop for FS-2. An explanation for this is that there was directivity from a source which ruptured toward the northeast for about 30 km at 3 km/sec. The effect of this unilaterally rupturing source on the amplitude spectra of the two different radiation maxima would be quite pronounced. The maximum amplitudes for Rayleigh waves of periods around 60 seconds radiated toward both the northeast and the southwest and for Rayleigh waves of periods around 20 seconds radiated toward the northeast should be the same as those for a point double couple source. However the 20 second Rayleigh waves generated toward the southwest should be a factor of four smaller for the unilateral

rupture than for the point source. Since A-1 seems to have behaved similar to a point source judging by the symmetry of its Rayleigh wave radiation patterns at periods of both 20 and 60 seconds, the asymmetry of the 20 second radiation pattern for FS-2 is consistent with this unilateral source model. This directivity argument also is consistent with the locations of two of the three events which immediately followed FS-2 in time (Figure 2-17(b)). If these three events are aftershocks of FS-2 and in some way define the fault plane for FS-2, then these events also indicate that this foreshock had a fault plane which elongated to the northeast.

The directivity argument for M is based upon the amplitudes of multiple Rayleigh waves at GSC. The ratio of the peak amplitudes of R2 to R3, where these waves were normalized to propagation distances of 270^{o} and 450^{o} respectively, is 3.84. The ratio of the amplitudes of R3 to R4, where R4 was normalized to a propagation distance of 630^{o}, is 1.34. These ratios should be 2.79 and 2.01 respectively if the source displayed no directivity, but in this case R3 is small compared to R2 and R4. This effect could have been caused by the earthquake rupturing away from GSC. All of the stations on the radiation maximum southwest of the source recorded higher amplitudes than the stations on the maximum to the northeast for R3 although only at GSC are the amplitudes for R2 and R4 significantly different from those expected from a source with no observable directivity. If the Rayleigh wave amplitude discrepancies at GSC are caused by directivity of the source, then M ruptured predominantly toward the southwest and updip on the fault plane

inferred from the body-wave analysis.

There are no obvious asymmetries in the Love wave radiation patterns for any of the events (Figure 2-12). Unfortunately, the station azimuthal density was not great enough for any of the events except FS-2 to clearly define the radiation patterns since theoretically the amplitudes should vary quite quickly with azimuth. The poor station coverage at the theoretical Love wave antinodal stations for M minimizes the usefulness of this data for detecting directivity. Also there were no anomalous azimuthal amplitude patterns found for the 20 second Love waves for FS-2 and A-1.

The directivity arguments for both FS-2 and M are based upon the assumption that the observed effects were not caused by anomalies in the attenuation and scattering properties of the earth along the paths in question. Unfortunately, details of the anelasticity and lateral heterogeneities of the travel paths discussed above in the directivity analyses were not modeled here, so it is only possible to guess what part of the travel paths could have caused the observed amplitude anomalies. For FS-2 and A-1 the proximity of the two sources means that the Rayleigh waves at far distances from the epicentral area shared common routes to the recording stations and therefore were affected by the same anelastic structure. Thus, the amplitude differences in the 20 second surface waves could have been caused only by scattering or attenuation in the source region if there was no source directivity. On the other hand, if the discrepancy in the amplitudes of R2, R3 and R4 recorded at GSC for M were not source related, they would probably have

been caused by attenuation between the New Hebrides and North America since this is the only part of the travel path not common to both R2 and R3. The attenuation and scattering along these travel paths have not been analyzed in this study, so it can only be claimed that there are possible indications of source directivity in the Rayleigh for M and FS-2. Conversely, since the details of these properties are not known, the suggestion that the Rayleigh wave amplitudes indicate source directivity for FS-2 and M cannot be completely ruled out.

STATIC DISLOCATION

One of the directly observable deformational effects of these earthquakes was an uplift of the coastline of Mallikolo which was first noted by Benoit and Dubois (1971). They reported that uplifts of 20 to 80 cm were found on the northern coast of Mallikolo while no vertical movements could be identified on the coast of either Malo or Espiritu Santo. They stated that the uplift took place on or before August 13 although they did not say whether or not it was coseismic with any of the large events. Taylor et al. (1980) have reexamined the uplifts on Mallikolo and present a much more detailed look at the deformation associated with the 1965 sequence. They found a maximum uplift of 1.2 meters at a place on the coast of northwestern Mallikolo with smaller vertical movements up to the east and south of this point. While they did not present evidence for uplift on Malo or Santo (except for one observation), Taylor (1979) did report an uplift of up to .4 m along the southern coast of Santo.

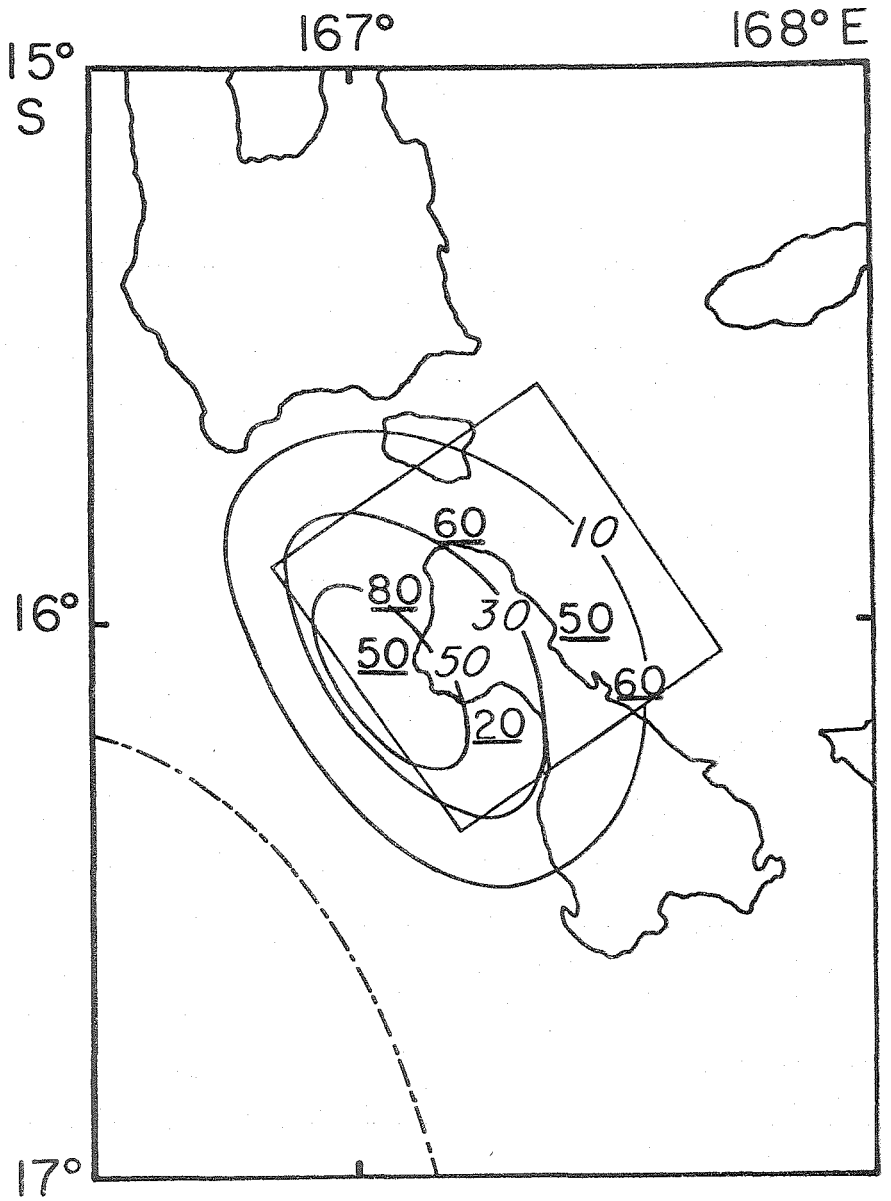

Figure 2-16. Model for the uplift of Mallikolo from the main shock. The heavy (underlined) numbers represent uplift values of the coastline in cm as reported by Benoit and Dubois (1971). Contours of theoretical static uplifts of 10, 30 and 50 cm are also shown. The rectangle is the projection of the assumed fault plane on the earth's surface.

These uplift observations are of interest in this study because they provide information on the very long-period (and permanent) deformation associated with these events which can also be used in a comparison with the deformation inferred from the far-field radiation which has been discussed above. The method used to model the uplift was that of Mansinha and Smylie (1971) in which the static displacements from a uniform dislocation on a rectangular fault are calculated for a uniform halfspace. In the case of the New Hebrides earthquakes, it was assumed that all of the uplift observed on Mallikolo was due to the main shock because that was the largest event and because all of the uplift occurred above the region where the aftershocks during the first 10 hours after the main shock were concentrated (see Figure 2-17 (c)). This zone of aftershocks was also used to define the fault area used in the model. The average dislocation assumed in the model was 1.5 meters which was computed from the surface-wave moment and the fault area shown in Figure 2-16. Contours of the uplift from this model are also shown in Figure 2-16.

The maximum uplift predicted by this model is about 25% smaller than the maximum observed uplift reported by Benoit and Dubois (1971). This model also agrees with the observations of Taylor et al. (1980), although there are some differences. While the shapes of the theoretical contours match the observed uplift contours reported by Taylor et al. (1980), the magnitudes of the theoretical vertical movements are only about one half of the uplifts they found on the west side of Mallikolo while the uplifts on the east side of the island are

greater in the model than those observed by Taylor et al. (1980). A model of the uplift computed by Taylor et al. (1980) with 5.3 meters of dislocation on a rectangular fault fit the amplitude of the data quite well. From a comparison of these two models it is apparent that the seismic far-field radiation contained information on only a fraction of the total deformation. The remainder of the dislocation must have taken place in very long-period deformations in the focal region either during or after the main event.

SEISMICITY PATTERNS

The seismicity patterns before, during and after this sequence of events show the evolution of the deformation process. Pascal et al. (1978) report that in the 4 years just prior to August, 1965, this zone had no teleseismically recorded events. The seismicity for the period July 1, 1965 to December 31, 1965 is shown in Figure 2-17. A magnitude 4 3/4 event, shown in Figure 2-17 as the open circle near the epicenter of FS-1, preceded FS-1 by about half an hour. This event was the first foreshock of the sequence. Most of the shocks after the occurrence of FS-1 and before FS-2 were located in the region near the epicenter of FS-2 as can be seen in Figure 2-17 (a). In this area were also located the three events that followed FS-2 and preceded M (Figure 2-17 (b)). While all of the foreshock activity was confined to the north of M, almost all of the seismicity during the first 10 hours after the main shock was south of the epicenter of M (Figure 2-17 (c)). From these locations it appears that the fault plane for the main shock was

Figure 2-17. Locations of events during different time periods in 1965. (a) All events from July 1, 1965 to, but not including, the occurrence of FS-2 on August 11, 1965. The open circles show the locations of events which took place prior to FS-1 (the large dot in the figure). (b) The large dot shows the location of FS-2 but prior to M. (c) The large dot shows the location of M. All other events are aftershocks of M which took place prior to A-1. (d) The large dot shows the location of A-1. The other events took place after A-1 and before A-2. (e) Location of A-2 (large dot) and events which occurred after A-2 on August 13 through August 28. (f) Locations of events which took place between August 29 and December 31.

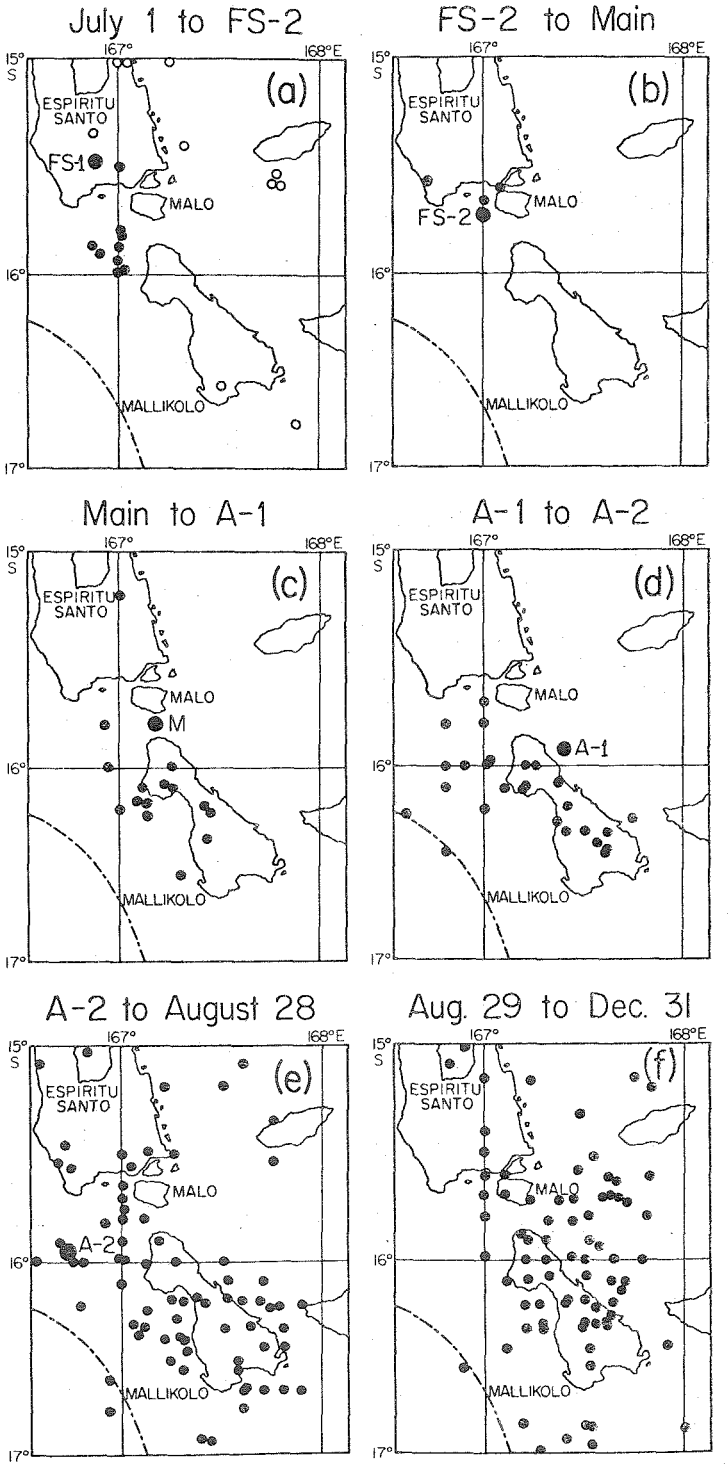

Figure 2·17. (See page 61).

confined to the region under northern Mallikolo. After A-1 the aftershocks spread away from the main shock fault plane (Figure 2-17 (d)), The seismic activity migrated to the west toward the hypocenter of A-2 (Benoit and Dubois, 1971). After A-2 the aftershocks continued to spread in all directions away from the main shock fault plane. Curiously, the aftershocks did not begin spreading east of the islands until after August 28 (Figure 2-17 (e)). Figure 2-17 shows very clearly the migration of the deformation first northwest to southeast along the fault plane during the occurrence of the foreshocks and the main shock, and then away from the fault plane toward the northeast and southwest during the aftershock sequence.

DISCUSSION AND CONCLUSIONS

The source models presented in this study are useful in making a detailed interpretation of the subduction process associated with the 1965 New Hebrides earthquake sequence. The focal mechanisms of all of the large events studied here are consistent with the convergence of the Indian and Pacific plates and are similar to the mechanisms of other events in the same area (Johnson and Molnar, 1972; Chung and Kanamori, 1978). The patterns of seismic activity, in terms of both temporal and spatial distribution of large and small events, are similar to those of the other subduction zones around the Pacific Ocean. Furthermore, the detailed source models for the different events are probably not unusual for plate boundary earthquakes.

Several conclusions can be drawn about the subduction process in

this area from the results of the body-wave and surface-wave analysis. The first is that the locations, depths and focal mechanisms of the events constrain the location of the contact zone between the two converging plates beneath Santo and Mallikolo. The focal mechanisms for FS-1, FS-2, M and A-1 demonstrate that beneath these islands the dip of the Benioff zone changes from 20^{o} to 50^{o} between the depths of 15 and 30 km respectively. The main shock probably ruptured around this bend in the fault plane, and it is possible that the dual nature of the main shock source was caused in some way by differences in the stress field around the bend. The second conclusion is that the source properties of A-2 may have been due to processes which were different from those which caused the other large events. In particular, the lack of short-period radiation from the earthquake together with the large tsunami it generated (Benoit and Dubois, 1971), and its location near the trench suggest that this event was caused by movements in the upper crust of the Indian plate. Fukao (1979) has found several other events with similar properties, and he attributes the lack of short-period energy from these events to deformations in the oceanic sediments. However, his model does not explain the large 30 km deep event which occurred half a minute or so after A-2 began. It appears that the rupture for A-1 propagated almost vertically downward into the underthrusting plate. This interpretation of the fault plane for A-2 is not unreasonable since events with steeply-dipping fault planes on or near trenches at subduction zones have been documented in a number of cases. Kanamori (1971) studied the 1933 Sanriku, Japan earthquake and concluded that it

was a normal faulting event located under the Japan trench which ruptured downward in an attempt to break the lithosphere. Stewart (1978) found similar properties for the 1977 Indonesian earthquake. Stauder (1968, 1973 and 1975) found normal faulting events under the Aleutian, Chilean and Peruvian trenches respectively. In addition, he found reverse dip-slip events under the latter two trenches (Stauder, 1973 and 1975). The similarities of the mechanism and inferred direction of rupture for A-2 and for some of these other events suggest that A-2 may have been an event associated with the formation of a trench west of Mallikolo. From the present analysis, though, it can only be argued that the event was associated with faulting which caused deformation in the underthrusting plate. A third conclusion is that different events may have had different rupture directions. An updip rupture propagation is common for thrust earthquakes at plate boundaries (Kelleher et al., 1973). However, the 20 second surface-wave data for FS-2 suggest that this event had a predominantly downdip direction of rupture. The main event may have been even more complicated. The two source models for the body waves for M is consistent with a downdip direction of rupture while the Rayleigh wave data for this event recorded at GSC can be interpreted as indicating source directivity toward the southwest which is primarily an updip direction on the fault. If the surface-wave directivity did take place, then one explanation for the behavior of M, similar to that proposed by Fukao and Furumoto (1975) for the Tokachi-Oki, Japan earthquake of 1968, can be given. They found for that event that smaller, more brittle breaks migrated in one

direction along the fault plane of their event and then a larger, smoother dislocation turned around and ruptured through the fault plane in the opposite direction. In the case of M the brittle fracture migrated in an east to southeast direction while the smoother fracture propagated predominantly toward the southwest. The inferred directions of rupture for both FS-2 and M provide insight into the temporal and spatial development of the deformation associated with these earthquakes.

The seismicity patterns and uplift data provide additional information on the development of the subduction history which took place during this sequence. The seismicity patterns shown in Figure 2-17 demonstrate that the seismic deformation migrated from northwest to southeast. Furthermore, since M and A-2 were much larger earthquakes in terms of seismic moment and fault dislocation than the foreshocks, the largest crustal movements occurred south and southeast of the epicenter of M. Conforming to the history of the last several thousand years of uplift of these islands deduced from geological studies by Taylor et al. (1978 and 1980), the deformation under and on Santo was different in magnitude and extent from that under Mallikolo.

Through time domain waveform modeling of the body waves and surface waves from the August, 1965 New Hebrides Islands earthquake sequence the focal mechanisms, fault depths, seismic moments and time functions for the five largest events have been determined. These source parameters are used to deduce details of the tectonic changes which accompanied these earthquakes as well as delimiting the location of the contact zone

between the two plates under the islands of Santo and Mallikolo. Some differences between the time functions of the foreshocks and the other events was also found. All of these results are useful in understanding the fracture properties and tectonic processes which are taking place in the central New Hebrides Islands.

Chapter 3

An Analysis of the Short-Period P Waves from the Borrego Mountain, California, Earthquake of 1968

INTRODUCTION

Time domain modeling of long-period, far-field body waveforms has proven to be a very effective tool for determining source parameters of earthquakes (Helmberger and Burdick, 1979). The power behind the technique lies in the fact that synthetic seismogram methods can correctly account for free surface effects along with near-source and near-receiver reverberations which can complicate far-field seismograms, especially those from shallow-focus events (Langston and Helmberger, 1975; Langston, 1978b). While time domain studies of long-period waveforms of moderately large, shallow-focus earthquakes have become quite popular, only a few investigators have attempted to model shorter period recordings (such as WWSSN short-period records) of events of comparable size (Bache et al., 1980; Cipar, 1980; Hartzell, 1980). The reason for this is simple; long-period seismograms contain much less detailed information about the faulting time history and the seismic structure along the source to receiver travel path than short-period records and consequently are much easier to model. However, the short-period records are of interest precisely because they contain a more detailed look at the earthquake source process. Thus, in-depth modeling of short-period body-wave data is a useful step toward

understanding seismic sources.

The Borrego Mountain, California earthquake of April 9, 1968 (M_L = 6.4; see Figure 3-1) is particularly well-suited for a short-period body wave study because it is an event for which there have been time domain studies of both the long-period body waves (Burdick and Mellman, 1976) and the strong-motion data (Heaton, 1977; Heaton and Helmberger, 1977). In addition, the surface rupture for the event was mapped in detail (Clark, 1972; Burford, 1972), aftershock locations and focal mechanisms have been determined (Allen and Nordquist, 1972; Hamilton, 1972) and a seismic crustal structure for the source has been found (Hamilton, 1970). This wealth of information simplifies the task of modeling the short-period body waves because it provides constraints upon the types of models which can be deemed acceptable. The philosophy used in this study was to try to find a source model for the teleseismic short-period data which was consistent with both the far-field long-period and strong-motion recordings of the event from El Centro, California.

THE DATA SET

The short-period P waves recorded at all of the stations located between 30° and 90° from the source are shown in Figure 3-2, and information on the station locations relative to the source region are given in Table 3-1. At first glance the waveforms appear rather complicated. The background noise on most of the records obscures the first arrival sufficiently that the initial polarities cannot be read

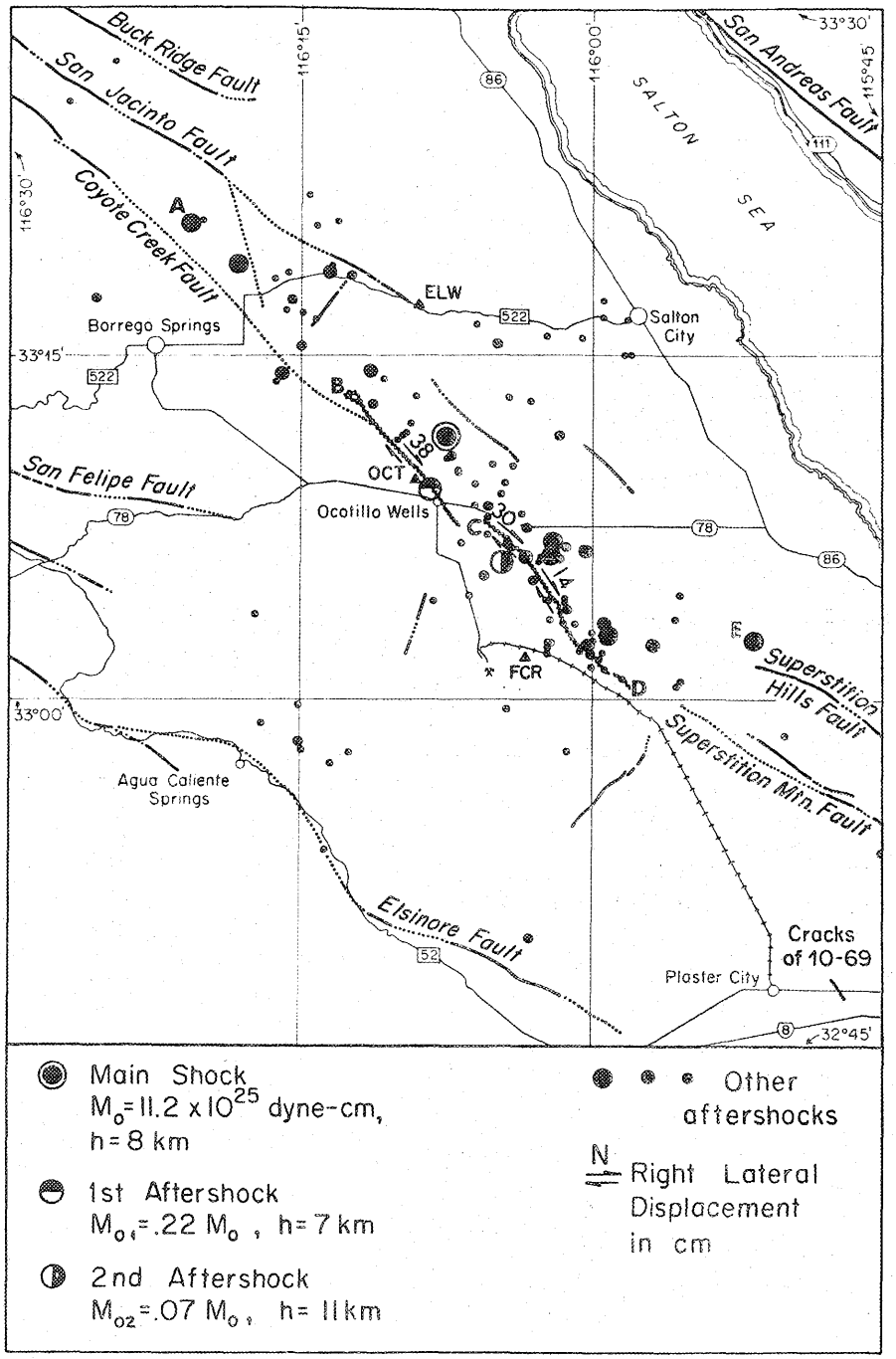

Figure 3-1. Map of the focal region of the Borrego Mountain earthquake in Southern California from Burdick and Mellman (1976). The aftershocks from the earthquake generally lay in segment AE, while the surface faulting was confined to segment BD (BC delineates the northern fault break and CD the central and southern breaks). The location, moment (M_o) and depth (h) of each of the three sources determined by Burdick and Mellman (1976) are also shown.

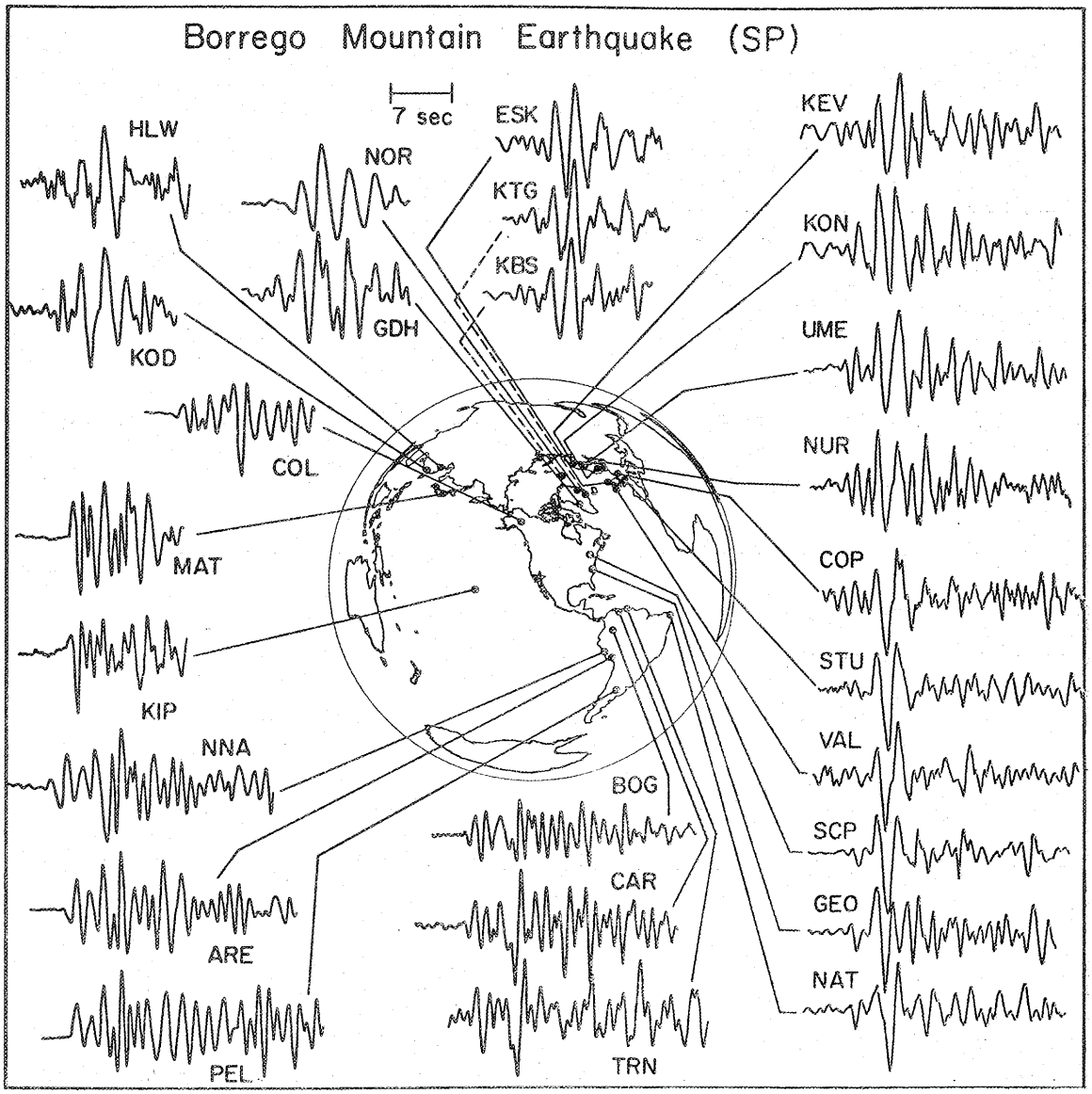

Figure 3-2. Short-period P waveforms recorded at 26 WWSSN stations. Note the coherence of the first several seconds of the waveforms from stations at similar azimuths. The star denotes the location of the earthquake.

TABLE 3-1

Station	Distance	Azimuth	Moment (t^*=1.0) ($\times 10^{25}$ dyne-cm) Short Period	Long Period
ARE	65°	132°	6.67	6.39
BEC	43°	76°		
BHP	42°	117°		
BOG	48°	117°	6.44	9.97
CAR	50°	105°		
COL	37°	338°	2.47	9.04
KEV	76°	14°	2.61	10.54
KIP	39°	263°		
KON	77°	25°	3.85	
LPB	67°	129°		
MAT	82°	308°	5.66	7.66
NAT	83°	100°	6.76	9.22
NNA	59°	133°	3.77	5.75
NUR	81°	18°	3.93	11.43
OGD	32°	64°		
PEL	79°	142°		
SCP	31°	65°	5.02	6.87
SEO	82°	308°		
STU	85°	33°	8.10	33.54
TRN	55°	101°		4.30
WES	36°	62°		5.43

with any certainty, and at some stations (particularly in South America) there are many seconds of high amplitude ringing after the first arrival which may be indicative of contamination from the local receiver structures. At other stations (especially those in eastern North America and some in Europe) the seismograms are characterized by a few seconds of high amplitude arrivals followed by a low amplitude coda. Even with these major differences in the waveforms for stations at different directions from the epicenter there is much coherence in the waveforms between stations at similar azimuths. In particular, the waveforms recorded at stations to the southeast of the source region (NNA, ARE, PEL, CAR and TRN) are very similar for the first ten seconds or so. This is likewise true of stations to the north (NOR, GDH, ESK, KTG, KBS, KEV, KON, UME and NUR) and stations to the northeast (STU, VAL, SCP, GEO and even NAT which lies somewhat southeast of the source). The similarity of the waveforms at these different stations is strong evidence that the recorded signals are dominated by information from the near-source region.

The first step taken in analyzing the data was to check the compatability of the short-period and long-period records. This was done by using the simultaneous deconvolution procedure outlined by Burdick (1977). The technique involves passing the data through a Gaussian filter, dividing instrument and Futterman attenuation operators from the long-period and short-period records from a station separately, and then adding together the spectra of the two deconvolved ground motions from the different frequency bands. The information in the

crossband of .125 Hz to .5 Hz where the responses of the two instruments overlap is averaged and the total response is then transformed to the time domain to get the broad-band ground motion. As a check on the stability of the procedure, the responses of the different instruments are reconvolved with the attenuation operator and the deconvolved ground motion and the results are compared to the original, filtered seismograms. If there is a mismatch in the relative timing or the relative amplitudes of the two records, if the signal-to-noise ratio is poor or if there are inaccuracies in the digitization of the records, the reconvolved traces may not match the initial, filtered traces very well. In these cases the amplitudes and timing of the data can be redetermined and the deconvolutions recomputed.

Simultaneous deconvolutions for the eight stations which had the best recordings on both long-period and short-period seismograms are shown in Figure 3-3 along with the filtered original and the reconvolved traces. A t^* of 1.0 and a width of 1.0 seconds at the half-maximum amplitude were used in the attenuation operator and the Gaussian filter respectively. The quality of the deconvolutions ranges from very good at ARE and MAT to very poor at STU even after the timing and amplitudes of the original records had been checked and rechecked. The problems with the quality of the results notwithstanding, there appear to some similarities among all of the deconvolutions. At all of the stations the largest arrival occurs several seconds after the beginning of the P wave coda. On many of the waveforms (especially those from which the best deconvolutions were obtained) this largest arrival is made up two

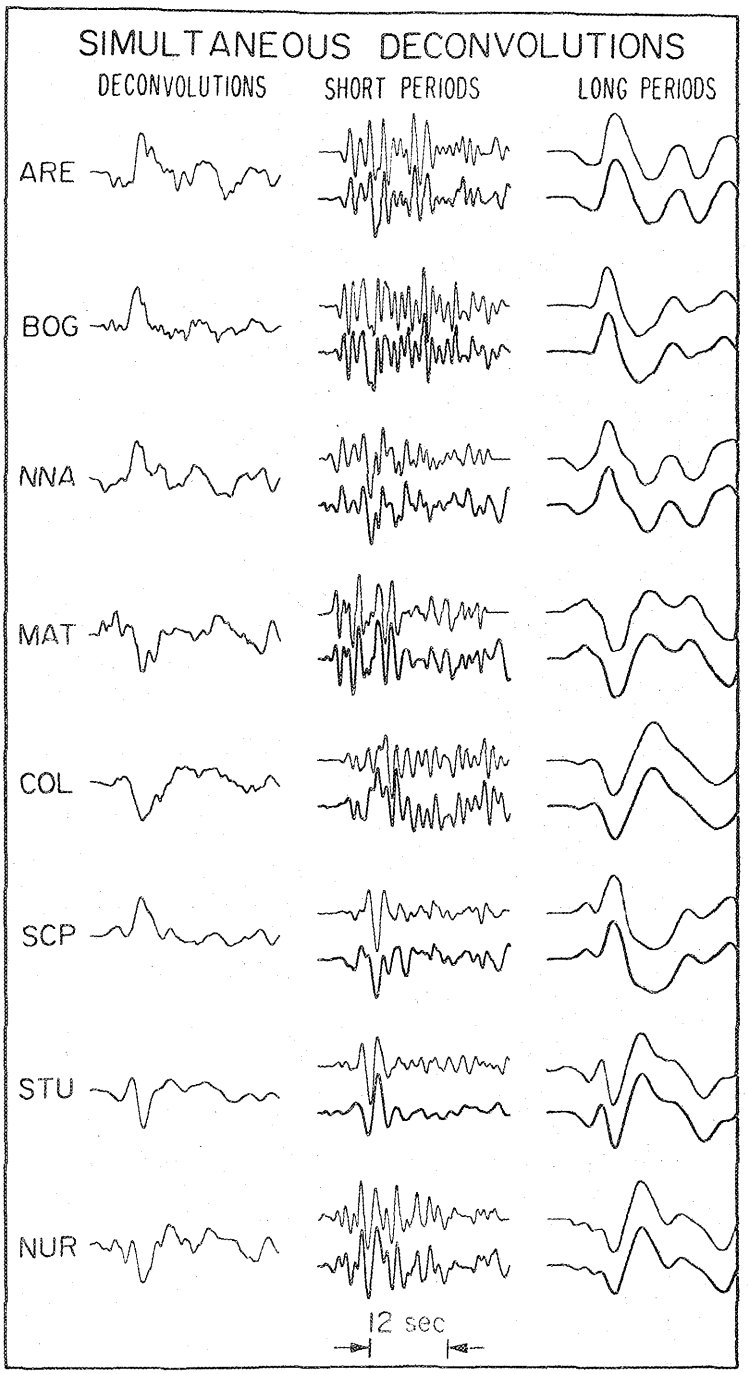

Figure 3-3. Simultaneous long-period-short-period deconvolutions of the P waveforms from 8 stations. For each station a filtered version of the original data (light trace) is plotted above the reconvolved waveforms (heavy trace). The amplitudes of the waveforms are arbitrary.

distinct pulses, both of which have the same polarity. The total duration of these two pulses is between 2 and 5 seconds at most of the stations. Based upon their analysis of the long-period P waves Burdick and Mellman (1976) have identified this arrival as the sP phase from the source region. The double-arrival nature of the sP phase evident in the simultaneous deconvolutions probably also had its origins in the near-source region. It was not due to receiver reverberations because it appears at different stations with undoubtedly dissimilar receiver crustal structures. This means that it must have been caused either by near-source reverberations or by two distant seismic sources which took place within a couple of seconds of each other.

A number of unusual features of the data set are obvious from the simultaneous deconvolutions. One is that the time difference between the arrival time of the sP pulse and the initial P phase is about 2 seconds greater at MAT than at any other station with the possible exception of COL. Since source directivity affects the shape of the time functions of different phases much more than their relative arrival times, the similarity of the sP phase at MAT and ARE (stations at well-separated azimuths) implies that this discrepancy cannot be attributed to source directivity. One possible explanation for this observation is that a laterally-varying near-source surface structure such as a localized deep sedimentary basin northwest of the epicenter could have delayed the sP phase. However, this idea is difficult to reconcile with the fact that the area on the earth's surface where sP for MAT reflected was in the vicinity of Borrego Mountain where the

seismic velocities are faster than the local average (Hamilton, 1970). Thus, while this sP arrival time problem has no satisfactory explanation, it does adversely affect the fit of the long-period synthetic to the observation at MAT (the first swing of the Burdick and Mellman (1976) synthetic at MAT is shorter period than that of the observation) as well as the match of the short-period synthetics and observations in this study.

A second unusual feature of the data is evident in the long-period and short-period records from BOG. The sP arrival on the long-period record from this station is approximately 13 times larger than the amplitude of the direct P wave, while on the short-period record the P and sP phases are about the same size. The reconvolutions of the long-period and short-period data match the initial seismograms closely which means that there was almost no mismatch of information between the waveforms digitized from the two different records. Since the focal mechanism for this event indicates that the P arrival should be nodal at this station, the amplitude of the first arrival on the short-period record appears to be anomalously large. This high frequency, high amplitude P arrival was probably due either to a rotation in the orientation of the fault plane which radiated the initial short-period energy relative to that for the long-period energy or to some sort of diffraction around the southern end of the fault which would occur if the seismic velocities to the west of the fault are higher than those to the east. Hamilton (1970) found some evidence that a velocity contrast does exist across the fault in the Borrego Mountain epicentral region

although he does not quantify what this contrast might be or to what depth it may extend. If there is a velocity difference in the basement rock across the fault which affected the apparent short-period radiation pattern, it must be confined to the upper crust since the long-period P and sP radiation do not have anomalous relative amplitudes. On the other hand, if the amplitude discrepancy was caused by different focal mechanisms at short and long periods, it should be evident from the modeling of the short-period records. Unfortunately, the short-period observations were not of high enough quality to resolve any short-period-long-period radiation pattern differences. Therefore, a strong argument for the cause of the anomalously high amplitude short-period P wave at BOG cannot be made with the data set at hand.

A third problem in the data set is that there is an unusual pattern of waveforms recorded at SCP and STU. These stations are at similar azimuths from the source region, but STU is more than twice as far away as SCP. The short-period waveforms recorded at these two stations are virtually identical, but the STU long-period record is an upside-down version of that from SCP. While a poor but acceptible deconvolution was found for SCP (one which was very similar to the good deconvolution found by Burdick and Mellman (1976) for WES, a station a few hundred kilometers north of SCP), a satisfactory deconvolution could not be found for STU. The polarities of the short-period instruments at STU and SCP were checked using first arrivals from nuclear tests and nothing unusual was found. Certainly the waveform differences between STU and SCP would not be unexpected if the short-period and long-period

radiation had different focal mechanisms. However, the apparent mismatch of the short-period and long-period waveforms recorded at STU casts doubt upon the reliability of the data from that station. Thus it is not possible to ascribe the cause of the differences in the seismograms from SCP and STU to effects located in the source region of the earthquake.

SHORT PERIOD MODELING

The short-period body waves from the earthquake were modeled using the time-domain synthetic seismogram method of Langston and Helmberger (1975). Synthetic seismograms for the short-period P waves were generated by computing the response of a layered earth to one or more point sources and convolving it with a trapezoidal time function for each point source, a Futterman (1962) attenuation operator with a t^* of 1.0 (unless other noted) and a WWSSN short-period instrument response. The parameterization of the time functions was the same as that of Helmberger and Malone (1975) where the rise, top and fall times of the trapezoid are designated as δt_1, δt_2 and δt_3 respectively. The time functions for all P and S rays which took off from a particular source were assumed to be identical, and the interaction of the incident arrivals with the near-receiver structure was not included in the models since the receiver structures for the stations used are not known.

The first step taken in analyzing the short-period P records was to generate synthetics using the strike-slip source model found by Burdick and Mellman (1976) from studying the long-period body waves (Table 3-3).

The earth response used for these synthetics was computed using the direct P wave and the surface reflections pP and sP in the crustal model of Hamilton (1970) which is summarized in Table 3-2. These synthetics are compared to the observed data in Figure 3-4. It is obvious that while the synthetic waveshapes do not match the observations well at all, there are several aspects of the synthetics which bear some resemblance to the data. In particular, the ratio of the amplitude of the initial arrival to the highest amplitude swing of the synthetics is approximately that of the data at many of the stations (i.e. ARE, TRN, SCP and KIP). Also, the arrival time of this large pulse with respect to the start of the waveshape on the synthetics appears to be close to that of the data at stations where the first arrival can be isolated from the noise (ARE, SCP, TRN and PEL are examples). The similarities between the synthetics and data suggest that the focal mechanism and source depth found by Burdick and Mellman (1976) are consistent with the short-period observations. The discrepancies between the synthetics and data, in particular the fact that the synthetics lack some of the high frequency nature of the observations, is evidence that the source time function of Burdick and Mellman (1976) is not entirely appropriate at shorter periods.

On all of the synthetics from the Burdick-Mellman model (Figure 3-3) the large arrival which occurs several seconds into the waveforms is the sP phase, and from the simultaneous deconvolution analysis it was evident that there were two separate pulses which contributed to making up the sP phase. This suggested that more than one source was needed to

TABLE 3-2

P velocity (km/sec)	S velocity (km/sec)	Density (g/cm^3)	Thickness (km)
	Hamilton (1970)		
2.5	1.6	1.4	0.4
5.1	3.0	2.3	2.5
6.0	3.5	2.7	11.1
7.1	4.2	3.2	11.0
7.9	4.6	3.6	--
	Mooney and McMechan (1980)		
--	1.35	1.7	1.4
--	1.98	2.2	1.4
--	2.59	2.5	1.4
--	3.09	2.6	1.0
--	3.28	2.65	1.9
--	3.3	2.67	1.9
--	3.33	2.69	1.9
--	3.36	2.7	1.85
--	3.59	2.78	0.1
--	3.81	2.84	0.95
--	4.16	2.9	10.0

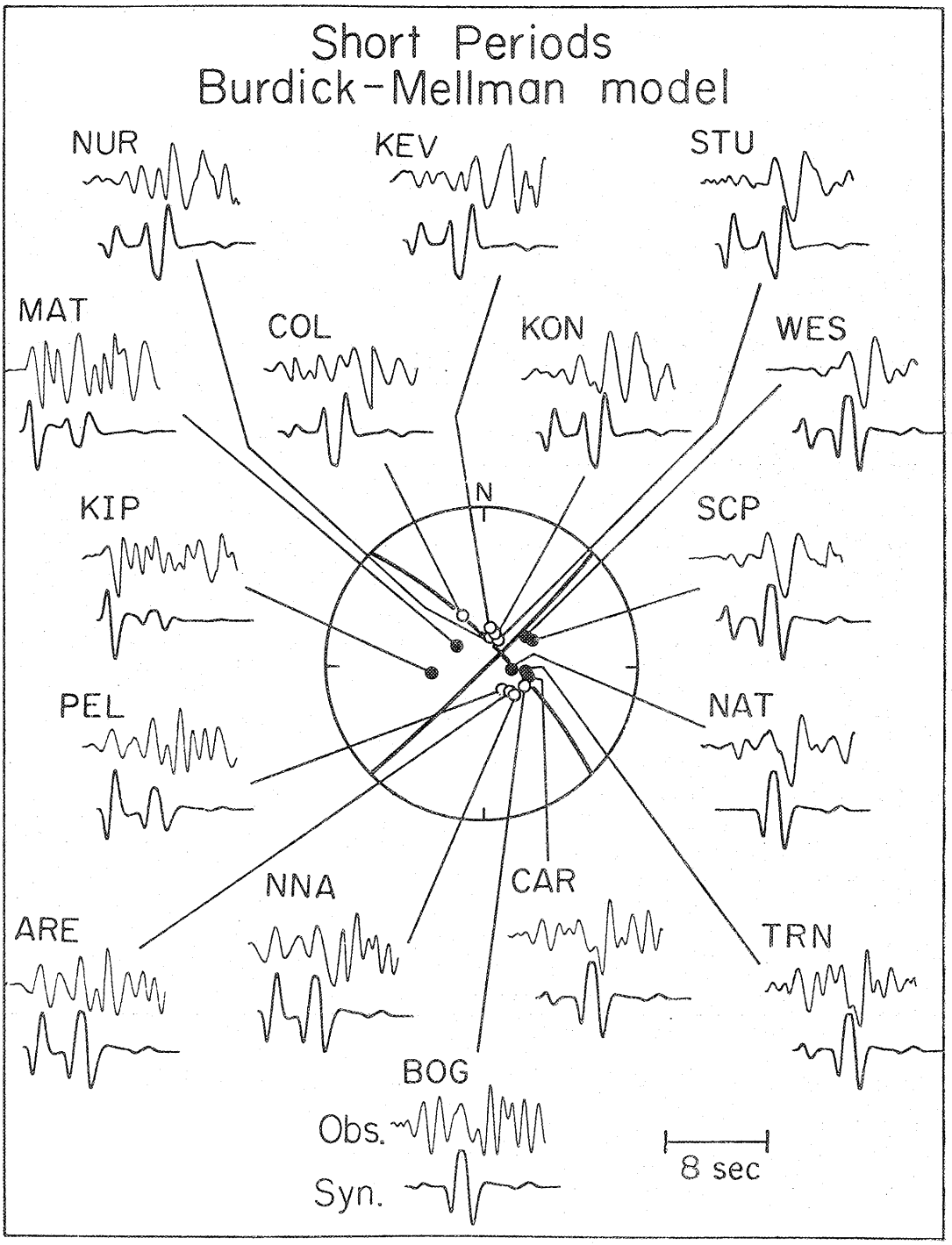

Figure 3-4. Synthetic short-period P waveforms computed from the Burdick and Mellman (1976) strike-slip source model compared to the data. The closed circles in the focal mechanism represent compressional arrivals, while the open circles are dilatational arrivals. The amplitudes of the waveforms in this and all of the following figures are arbitrary unless otherwise noted.

model the short-period records. Several different sets of synthetics computed with two point sources were found to give a fit which was much better than that from the single point-source model of Burdick and Mellman (1976). With the two-source models the fit of the synthetic P arrival to that of the data at most stations was still not very good, but this is not surprising since the signal-to-noise ratio is generally poor for this part of the record. However, the similarity of the synthetic sP phase to that of the data was improved for most of the records. The synthetics generally fit the data quite well at stations in Europe (with the exception of STU which was found to be a questionable station in the deconvolution analysis) and eastern North America, but for the South America stations they lacked some of the high frequency characteristics of the data.

INVERSION MODELS

An effort was made to improve the fit of the synthetics to the short-period data and to explore the uniqueness of the source models by employing the waveform inversion technique used by Burdick and Mellman (1976) to model the long-period body-wave records. The procedure involves computing changes in the source model based upon cross-correlations of the synthetic and observed waveforms at each station. In practice the inversion program was allowed to iterate a number of times on the source model until it could no longer improve the cross-correlations. For the Borrego Mountain data set the only rays used in the inversion process were the same three as those used in the

initial forward modeling. The only short-period waveforms that were used were those where the signal-to-background-noise ratio was large and where it was felt that there was the least contamination by receiver reverberations. Since each station was given a weighting, stations with waveforms of questionable quality could be deemphasized in the inversion process so that they did not contribute very much to the final model which the program found.

The parameters which were allowed to vary in the inversion runs were the three parts of the trapezoidal time function, the focal mechanism and depth of each of the two sources and the time lag of the second source with respect to the first. The program was first used on a data set of six short-period records (STU, ARE, BOG, KON, ARE and SCP) using the starting model listed in Table 3-3. The final model from this inversion is given as the short-period inversion model in Table 3-3 and synthetics for all of the short-period records are shown in Figure 3-5. A comparison of the cross-correlation values between the final and the starting model reveals that the inversion procedure improved the fit by about 10% at each station. The inversion made only minor alterations in the parameters for the first source, but it made rather substantial changes in the focal mechanism and time function of the second source. The result of these changes was to make the second source have a focal mechanism with the approximate strike of but with a time function very different from those of the first source. The inversion program left both sources at depths of about 8 km. Long-period synthetics were also computed using this model and they are shown in Figure 3-6. In general

TABLE 3-3

	Mechanism			Time Function				Depth	Delay time
	strike	dip	rake	δt_1	δt_2 (sec)	δt_3	amp	(km)	(sec)
Burdick-Mellman Model	-45°	81°	178°	.36	0.0	.45	1.0	8.0	---
Starting Model									
Source 1	-45°	80°	180°	0.3	1.0	0.3	1.0	8.0	0.0
Source 2	-30°	80°	180°	0.3	1.0	0.3	1.0	8.0	2.0
Short Period Inversion Model									
Source 1	-43°	78°	178°	.89	.82	.76	1.0	8.2	0.0
Source 2	-30°	63°	193°	.31	.64	.73	.34	9.0	2.3
Simultaneous Inversion Model									
Source 1	-43°	78°	178°	.54	.89	.75	1.0	7.3	0.0
Source 2	-38°	68°	197°	.05	.05	1.2	.35	8.4	2.2

For all models the second source was located 5.4 km southeast of the first.

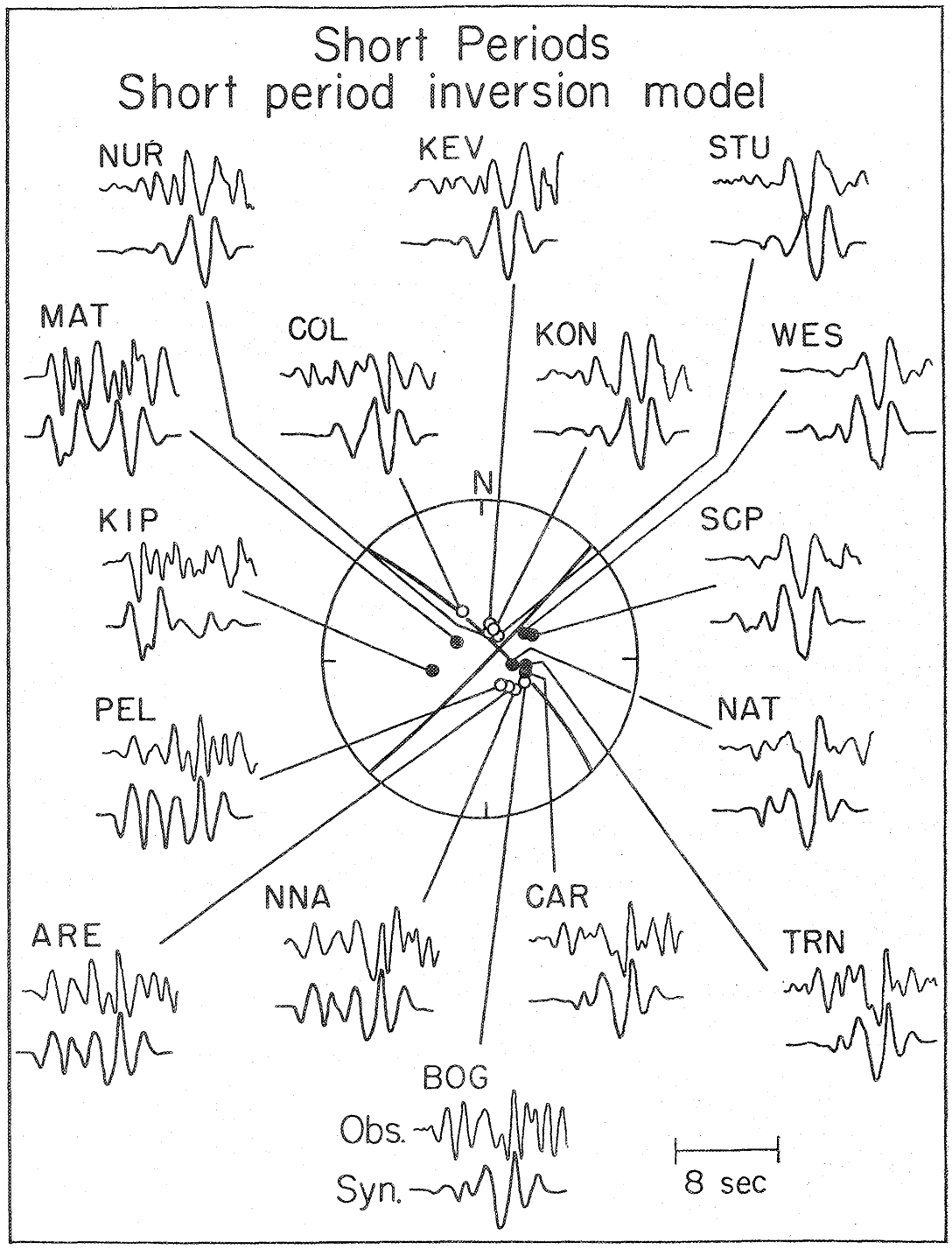

Figure 3-5. Short-period synthetics from the short-period inversion model compared to the data.

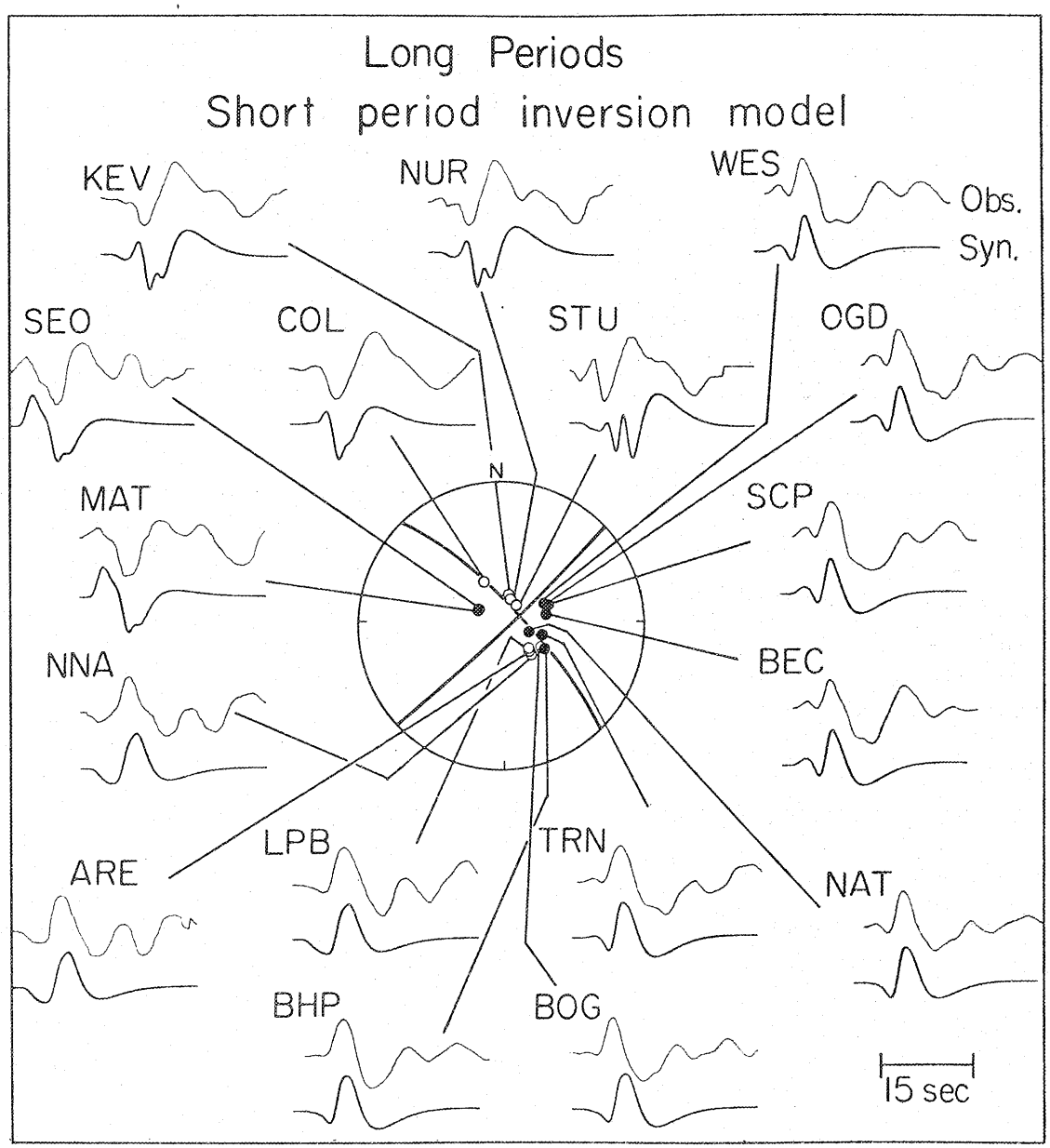

Figure 3-6. Long-period synthetics from the short-period inversion model compared to the data.

they fit the observations reasonably well.

The inversion process was also performed on a data set which included all the seismograms used in the short-period inversion plus records from 17 long-period stations used by Burdick and Mellman (1976). Once again, focal mechanisms, depths, time functions and relative time of the events were freed in the inversion program, and the starting model was the same as that used for the inversion of the short period data set. The source models which resulted from the inversion of this data set are given as the simultaneous inversion model in Table 3-3 and the synthetics are shown in Figures 3-7 and 3-8. The cross-correlations were once again improved by about 10% at each station. Here also the inversion program changed the parameters of the second source much more than those of the first and the final models for the two sources are similar to those found from the short-period inversion except for the shape of the time function and the strike of the second source. This simultaneous inversion demonstrates that the two source model which is necessary to fit the short-period data is also quite compatible with the long-period waveforms. The difference in the time functions of the second source found from inverting the two different data sets also gives a good feeling for the resolution of the modeling process. From comparing the models in Table 3-3, it appears that the methods used here are much more capable of determining the source parameters for the larger, first source than for the smaller, second source. Nevertheless, many parameters of the two sources are well determined from the modeling. The first source was at about 8 km depth, had a duration of

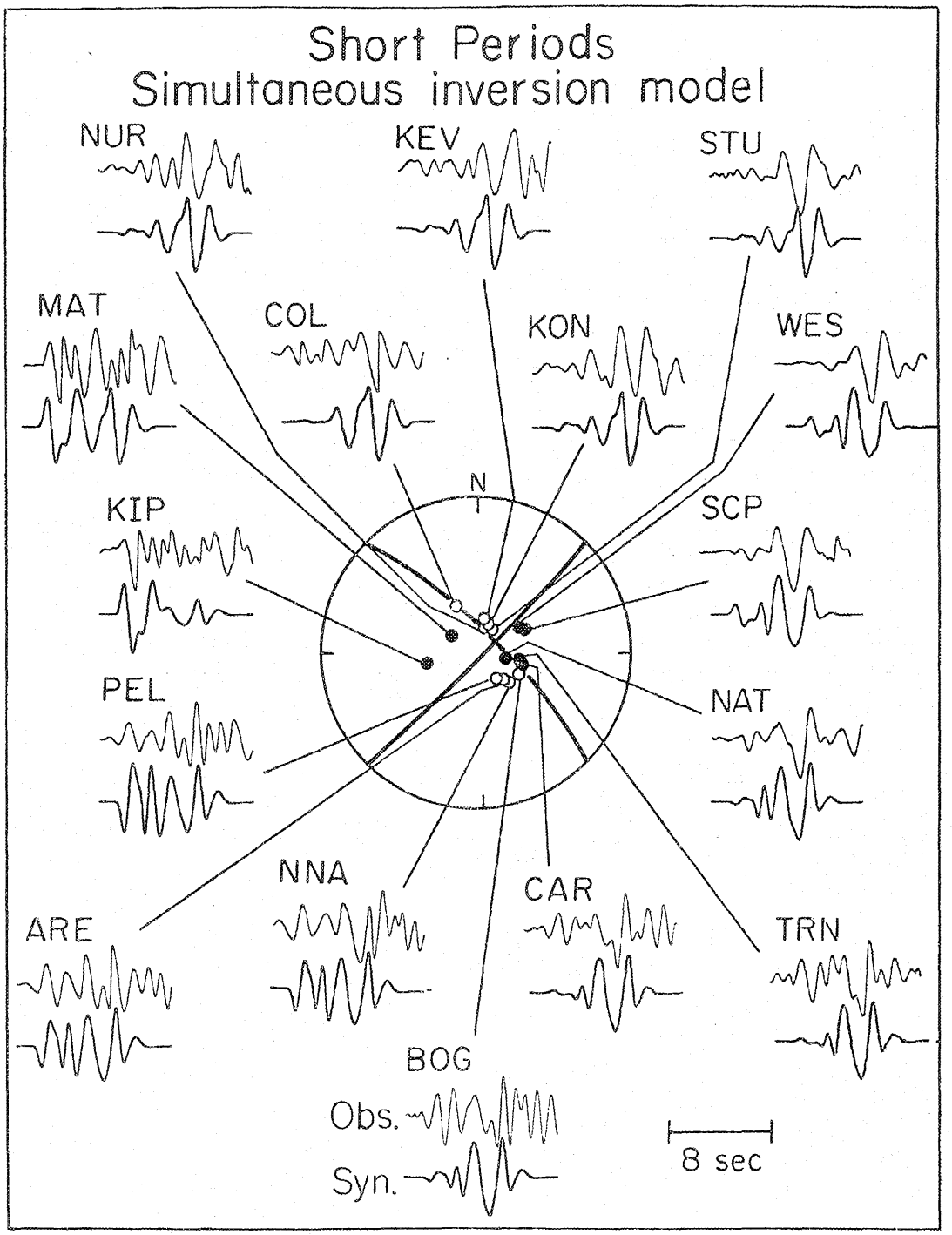

Figure 3-7. Short-period synthetics from the simultaneous inversion model compared to the data.

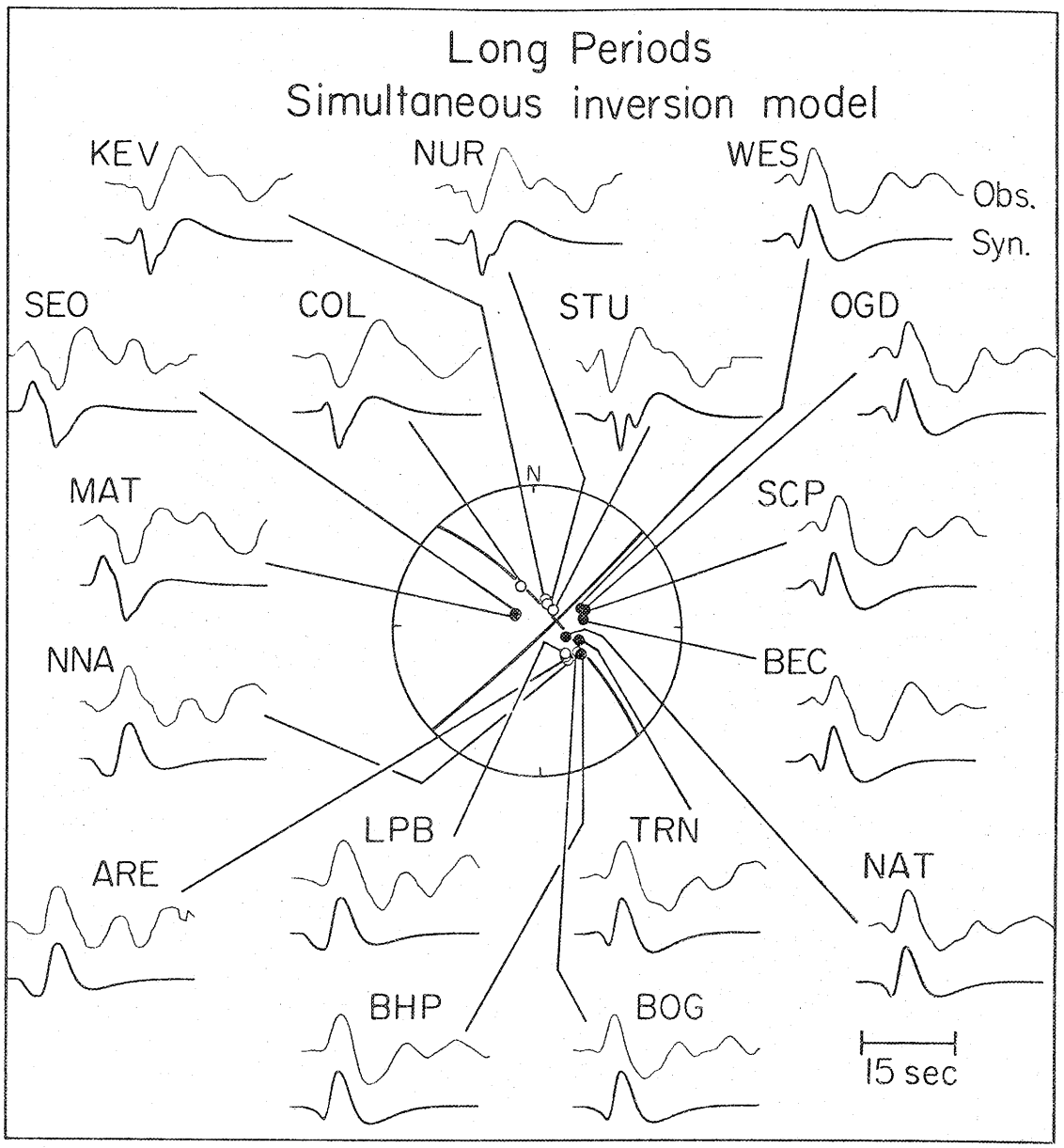

Figure 3-8. Long-period synthetics from the simultaneous inversion model compared to the data.

about 2.2 seconds and had a strike, dip and rake of -43^{o}, 78^{o} and 178^{o} respectively. The second source took place about 2.2 seconds after the first, was only about a third of the amplitude of the first, was located at a depth of about 8.5 km and had a strike, dip and rake of -38^{o}, 68^{o} and 194^{o}.

None of the inversion runs on either of the two data sets was able to resolve the simultaneous waveform problems found at BOG and STU, nor were they able to find a model which satisfactorily fit the waveforms at MAT. In fact, there are noticeable differences between all of the short-period synthetics and data in Figures 3-5 and 3-7. While this is not surprising because of the low signal-to-noise ratio for the data set, it does make it difficult to judge how well the synthetics model the data. A better feeling for the quality of the fits can be obtained by considering how well the deconvolved waveforms can be matched. Synthetics which have been computed without either instrument response or attenuation are compared in Figure 3-9 to the results of the simultaneous deconvolution analysis presented in Figure 3-3. The model used for the synthetics in Figure 3-9 was that found from the simultaneous inversion modeling. In general the fit is very good at ARE and NNA, and, except for a somewhat strong synthetic pP phase at BOG and SCP, the synthetics match the data at these stations also. The deconvolved synthetic at MAT was found to match the data best if the synthetic sP phase was aligned with the arrival which was identified as the sP phase in the data, and so this is the way that the comparison at MAT is plotted in Figure 3-9. Because of this, the first arrivals of

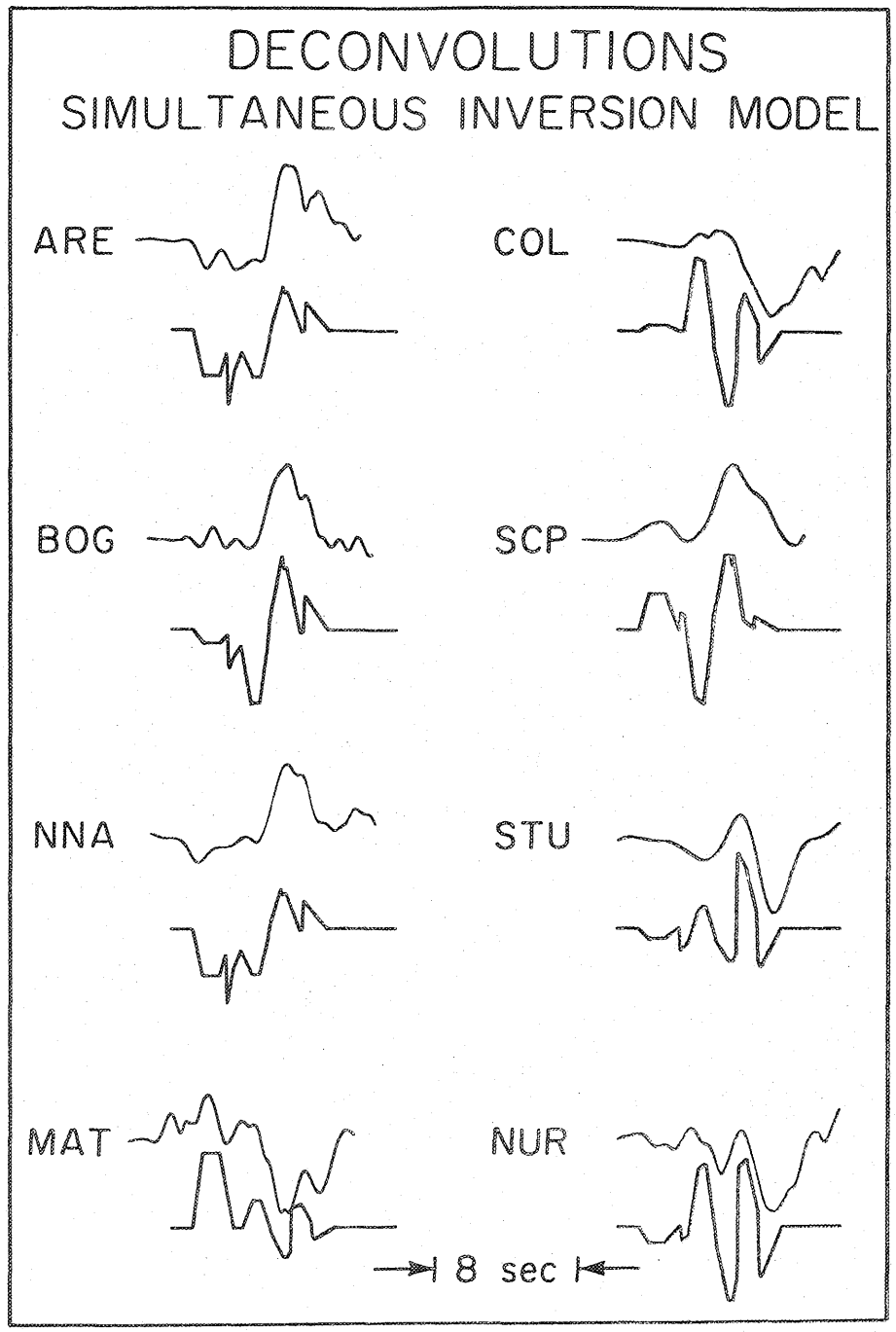

Figure 3-9. Comparison of synthetics computed from the simultaneous inversion model without instrument or attenuation and the deconvolved observations. The synthetic at MAT was time shifted by about 2 seconds so the sP phases of the datum and synthetic are matched. The alignment of the synthetic waveforms at COL, STU and NUR with the data is somewhat arbitrary since the traces have very different shapes.

the synthetic and observation do not coincide. The fits at COL, STU and NUR are poor, but this is not surprising since good deconvolutions at STU and COL could not be obtained and the signal-to-noise ratio was very low for the data from NUR. The deconvolution synthetics show that, while the theoretical time functions lack some of the details of the data (especially the long-period information), the source model is a reasonable interpretation of the data.

The inversion modeling was all done assuming that the short-period records could be closely modeled using only the direct P wave and the P and SV free-surface reflections. This assumption was justified by comparing synthetics computed from these three rays with those calculated from a full crustal response. The similarity of the synthetics computed from these two methods is demonstrated in Figure 3-10. The source parameters used for both synthetics were those found from the simultaneous inversion modeling, and the full crustal response synthetics were calculated using Fuchs (1966) modification of the Thomsen-Haskell layer matrix method with the near-source crustal structure being that reported by Hamilton (1970). The two sets of synthetics are very similar for NAT, KON and SCP. For ARE the amplitudes of the peaks and troughs of the two synthetic waveforms are somewhat different while the phases of the two waveforms are quite similar and in fact match the phase of the observation very closely. From these examples it is evident that the waveforms contain much more information about the earthquake source time history than about the near-source structure and that the direct P wave and the free surface

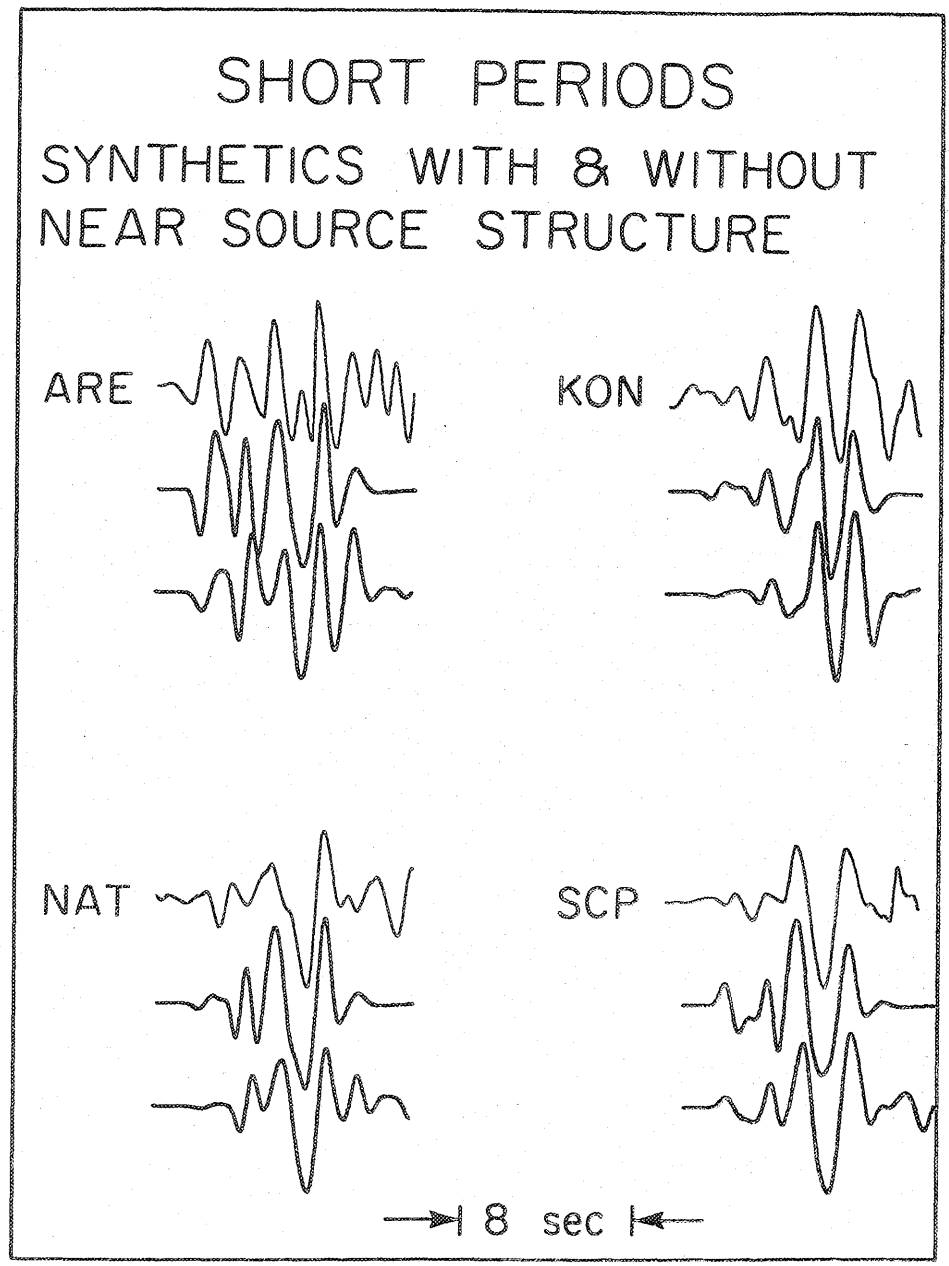

Figure 3-10. Comparison of the data (top trace; light line) with synthetics computed from just P, pP and sP (middle trace; heavy line) and with synthetics computed from the full response of the near-source crustal structure (bottom trace; heavy line) at ARE, KON, NAT and SCP.

reflections are by far the most important phases for determining the shapes of the synthetic waveforms.

Seismic moments for the earthquake were computed from the simultaneous inversion model by averaging the moments calculated from several of the stations. Values for the short-period and long-period moments computed from the simultaneous inversion model for $t^* = 1.0$ are given in Table 3-1 for those stations where moments were computed. The average moments for all the short-period records are 5.0×10^{25} dyne-cm for a t^* of 1.0 and 7.7×10^{25} dyne-cm for a t^* of 1.3. The corresponding average moments for the long-period data (excluding STU where the value was found to be clearly inconsistent with the rest of the data) are 7.6×10^{25} dyne-cm and 8.8×10^{25} dyne-cm respectively. The differences between the short-period and long-period moments must be due to the existence of a very long-period part of the time function which was not found during the modeling process. Since the fault length determined from surface cracking and aftershock locations (Clark, 1972) is much larger that that which was estimated from the long-period body wave modeling (Burdick and Mellman, 1976), the existence of a long-period part of the source time history is quite reasonable.

STRONG MOTION MODELING

Data from the earthquake were also recorded on a good set of acceleration and Carder displacement seismograms at El Centro, California, located about 60 km to the south-southeast of the epicenter. The highest acceleration, which was measured on the north-south

component of the accelerometer, was 128 cm/sec^2, while the maxima on the vertical and east-west components were 30 cm/sec^2 and 56 sec/cm^2 respectively. The accelerometer triggered sometime during the arrival of the P-wave train so it did not record the initial arrival of energy. However, the S-wave and some surface waves were well-recorded by the instruments which remained triggered for about 60 sec.

The acceleration records have been integrated into velocity and displacement waveforms, and the horizontal displacement traces were found to match the Carder displacement records quite well, as discussed by Heaton (1977). The north-south record, which is shown in Figure 3-11, is of particular interest because it represents primarily SH motion. Heaton (1977) and Heaton and Helmberger (1977) have done extensive modeling of the SH displacement record. They determined that the long-period oscillations which characterized most of the later part of the displacement record were due to SH rays trapped in a near surface crustal layer and that they could isolate a source time function by modeling the initial part of the SH wavetrain. The time function from their best model was actually the sum of three different time functions--two triangles of one second duration each located at a depth of 8 km and occurring 2 seconds apart, and a third low amplitude, long-period time function put at 4 km depth and beginning at the same time as the first source. The shape of the time function of Heaton and Helmberger (1977) as it would appear to teleseismic stations is shown in Figure 3-12 along with that of Burdick and Mellman (1976) and the time history determined from the simultaneous inversion as listed in

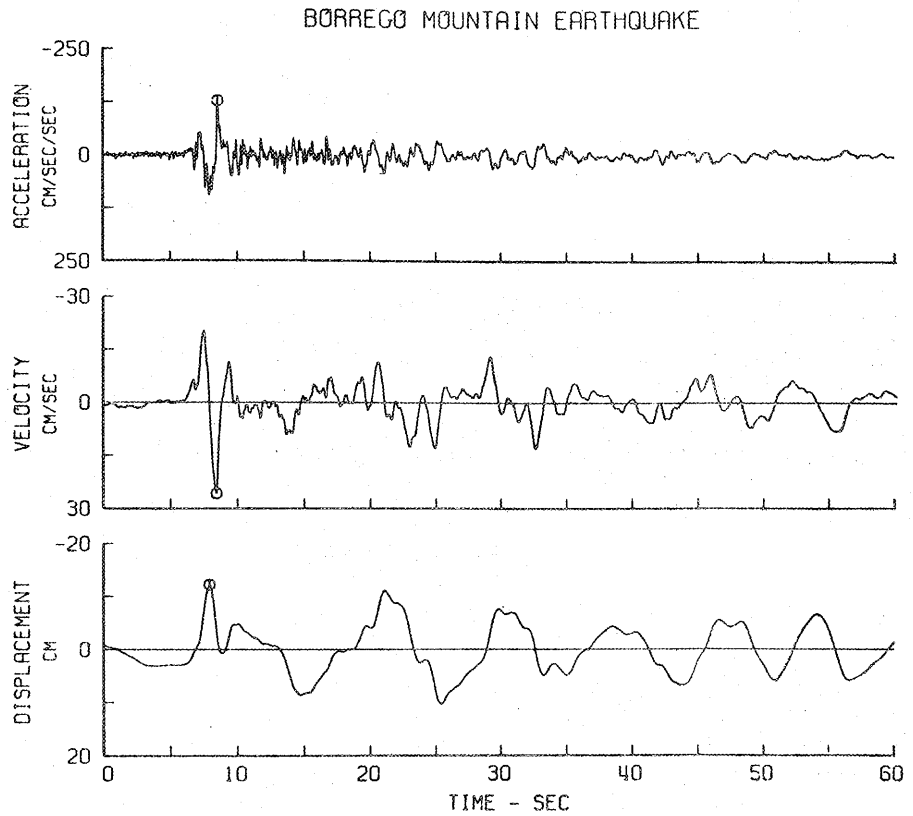

Figure 3-11. Corrected acceleration, velocity and displacement records from the north-south component of the strong ground motion recorded at El Centro, California (from U. S. Coast and Geodetic Survey et al., 1968).

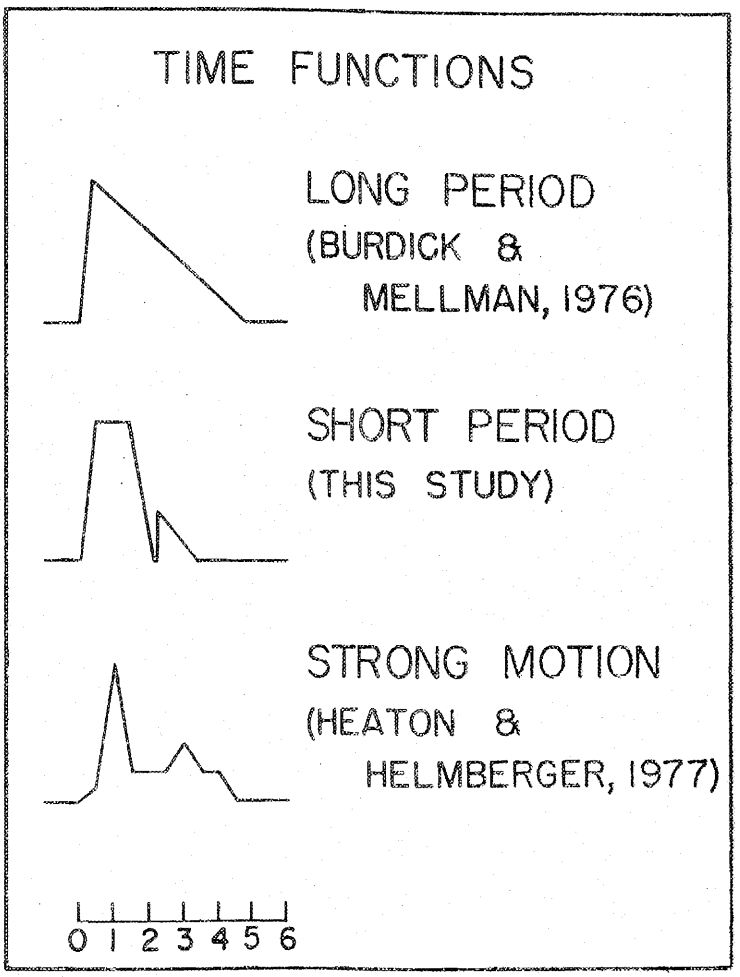

Figure 3-12. Comparison of the time functions for the Borrego Mountain earthquake determined from the long-period body waves (top), short-period body waves (center) and strong motion data (bottom). The time scale at the bottom is in seconds.

Table 3-3. It can be seen that the Heaton and Helmberger (1977) time function and that determined from this study are quite similar, and that the Burdick and Mellman (1976) time function is a smoothed version of the other two.

The success in modeling both the teleseismic short-period P waves and the strong-motion SH ground displacements at El Centro was an inducement to try to understand the north-south velocity and acceleration records at El Centro. This is not an easy thing to do since the synthetic velocity and acceleration traces are calculated from derivatives of the synthetic displacement record, and small changes in the shape of the displacement record have large effects on the waveshapes and amplitudes of the synthetic velocity and acceleration. On the other hand, the modeling is simplified somewhat since by far the highest amplitude velocity and acceleration arrival is that of the S wave (Heaton, 1977; Heaton and Helmberger, 1977) which is found between about 7 and 10 seconds after the beginning of the record (Figure 3-11). Attention was restricted to understanding this part of these two records.

Initial modeling of the S wave on the velocity and acceleration records revealed that the waveform is not made up of a single direct arrival from the source as assumed by Heaton (1977) and Heaton and Helmberger (1977) but that there are some important crustal complications involved in it. The differences can be seen in the step function responses shown in Figure 3-13. The response in Figure 3-13 (a) is that of Heaton (1977) and Heaton and Helmberger (1977) and

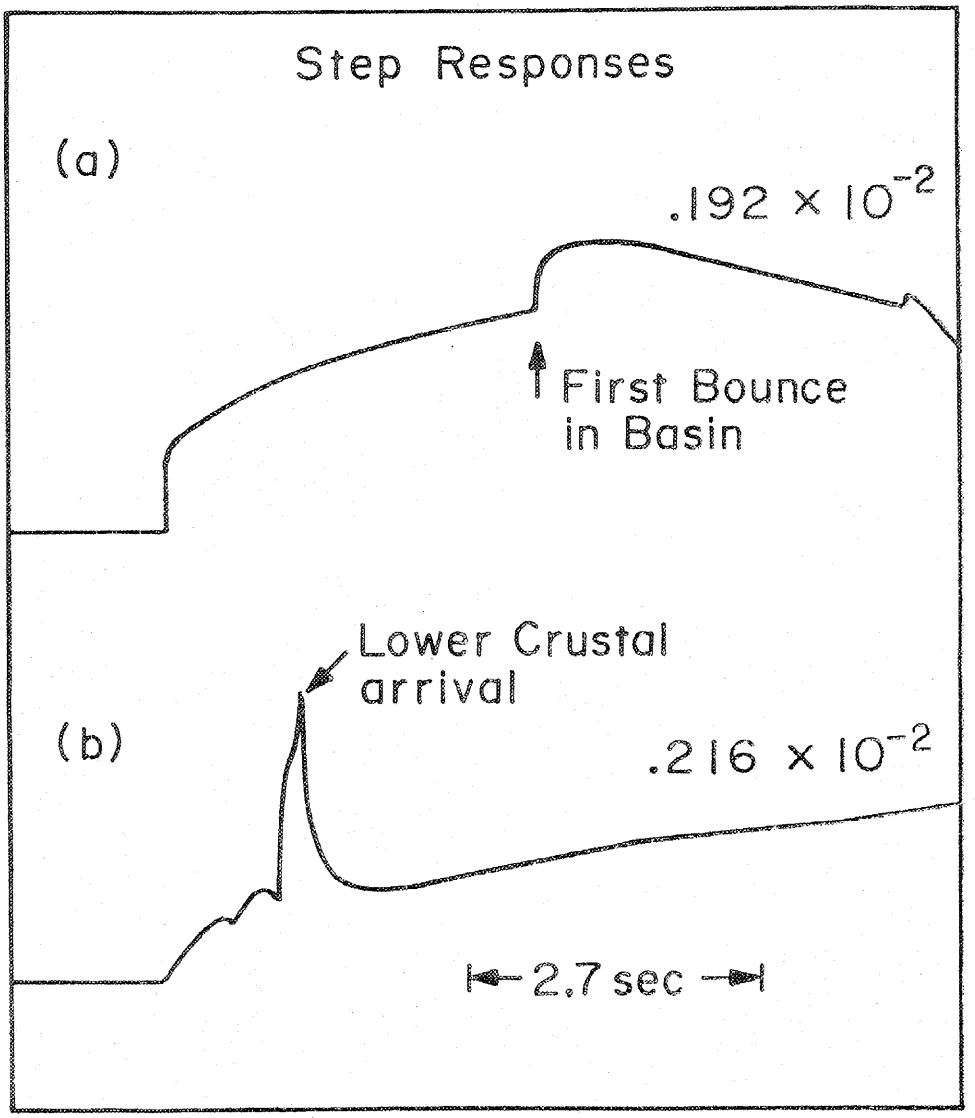

Figure 3-13. Step function responses for initial SH arrivals from (a) the study of Heaton and Helmberger (1977) and (b) the crustal model of Mooney and McMechan (1980) as computed in this study. Peak amplitudes from a unit point source are given in each case.

is made up of a simple direct arrival plus later reverberations in a near-surface sedimentary basin. The response in Figure 3-13 (b) shows the response from a source located in a crust with a modification of the crustal structure of Mooney and McMechan (1980) listed in Table 3-2 (the basin bounces are not included in this response). The latter response, in which only the most significant rays are included, has a strong reflection from the lower crust which occurs a little over a second after the initial arrival. This response was the one used in the calculation of the synthetics.

From the initial modeling it was also found that large initial source time function needed to be symmetric in shape. The best trapezoidal time function was found to be one with durations of the legs and top of .8 sec and .2 sec respectively. It was necessary to filter this time function in order to make it smoothly differentiable. A symmetric time-domain triangle was used as this filter. It was discovered that the synthetics were quite sensitive to the width of this smoothing filter. Synthetic displacement, velocity and acceleration records for the trapezoidal source smoothed with triangles which have legs of duration (τ) .2 sec, .3 sec and .4 sec are shown in Figure 3-14. The general shape of the synthetics fit the observations fairly well, but the frequency content and amplitude of the velocity and especially the acceleration records are strongly affected by the choice of the filter duration. Thus a time function which best fits the data could be found by varying the width of this smoothing filter.

The second source, which had been inferred by both the teleseismic

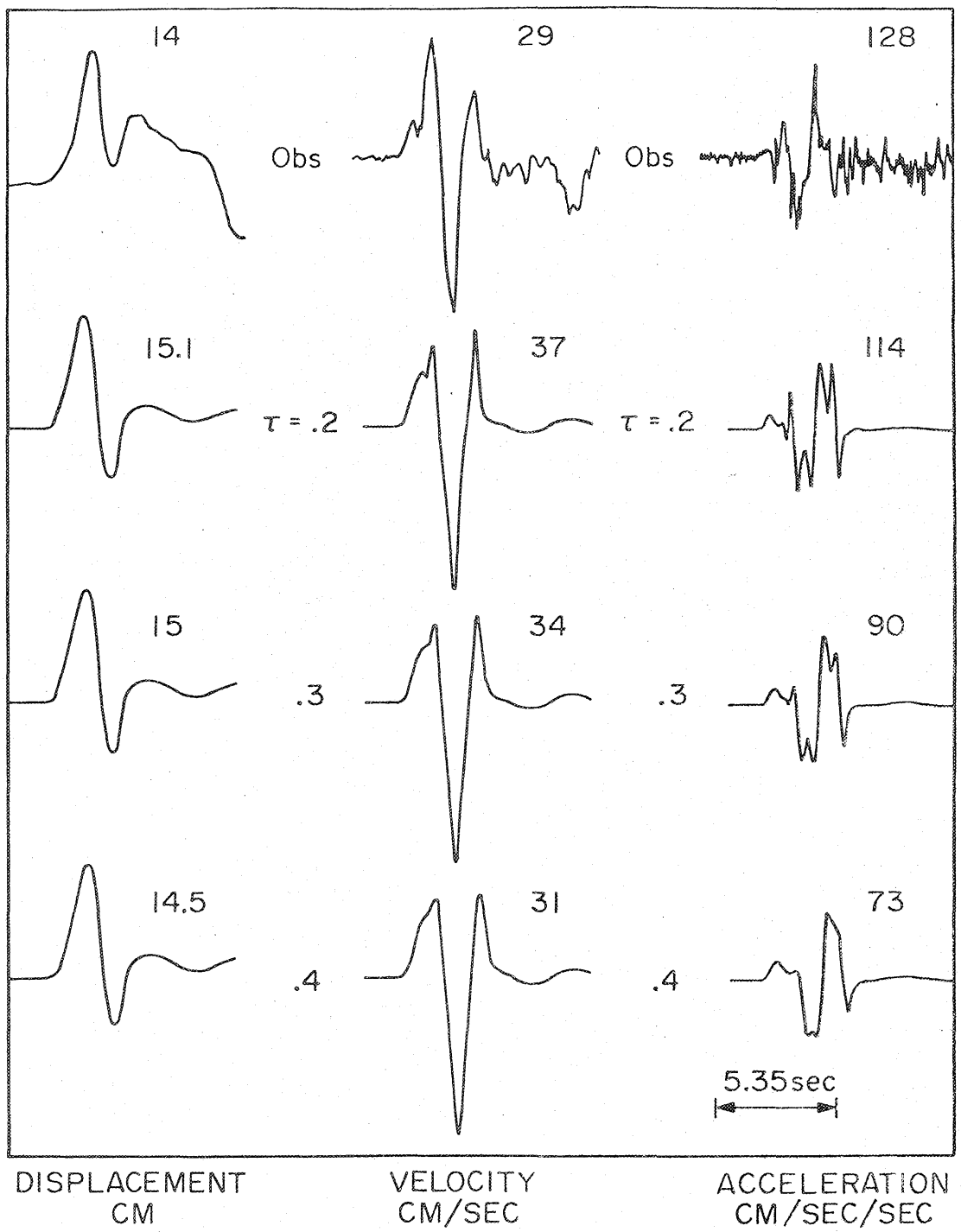

Figure 3-14. Synthetic displacement, velocity and acceleration records (lower three lines) for the first source are compared to the data (top line) from the north-south El Centro strong ground motion record. Peak amplitudes for each trace are shown with the units at the bottom of each column. The duration of the legs of the triangle filter τ are also given.

short-period P wave and the strong-motion displacement modeling, was added to the model and synthetics were again computed in an effort to understand how it may affect the waveforms. This source was approximated by using the analytic time function of Haskell (1967). This source time history, which is shown together with its displacement, velocity and acceleration time functions in Figure 3-15, has been used in the description of the source time functions of large explosions. The reason for using it here was twofold: the source could be smoothly differentiated to find accelerations and the accelerations from the source are basically a pulse with a sharp rise followed by a long tail. The latter was felt to be important because the highest peak on the acceleration record has this one-sided nature. This source is parameterized by one independent constant k which was varied until the pulse had roughly a 1.2 sec duration. Synthetic accelerograms with two sources where the second source has k = 5 and k = 7 (τ = .3 for both) and a moment of 6.4×10^{25} dyne-cm are shown in Figure 3-16 along with plots of the displacement time histories of the second sources. The time separation of the two sources necessary to best fit the data was 1.6 sec. While this is less than the 2.2 sec found from the teleseismic modeling, the peak of the displacement time function with k = 5 occurs about 2.2 sec after the first source. Thus, if the Haskell (1967) time function is thought of as a smoothed version of the teleseismic short-period triangular source, the discrepancy in the timing of the two sources found at El Centro and in the teleseismic short-period body waves is unimportant. It is evident from Figure 3-16 that the effect of

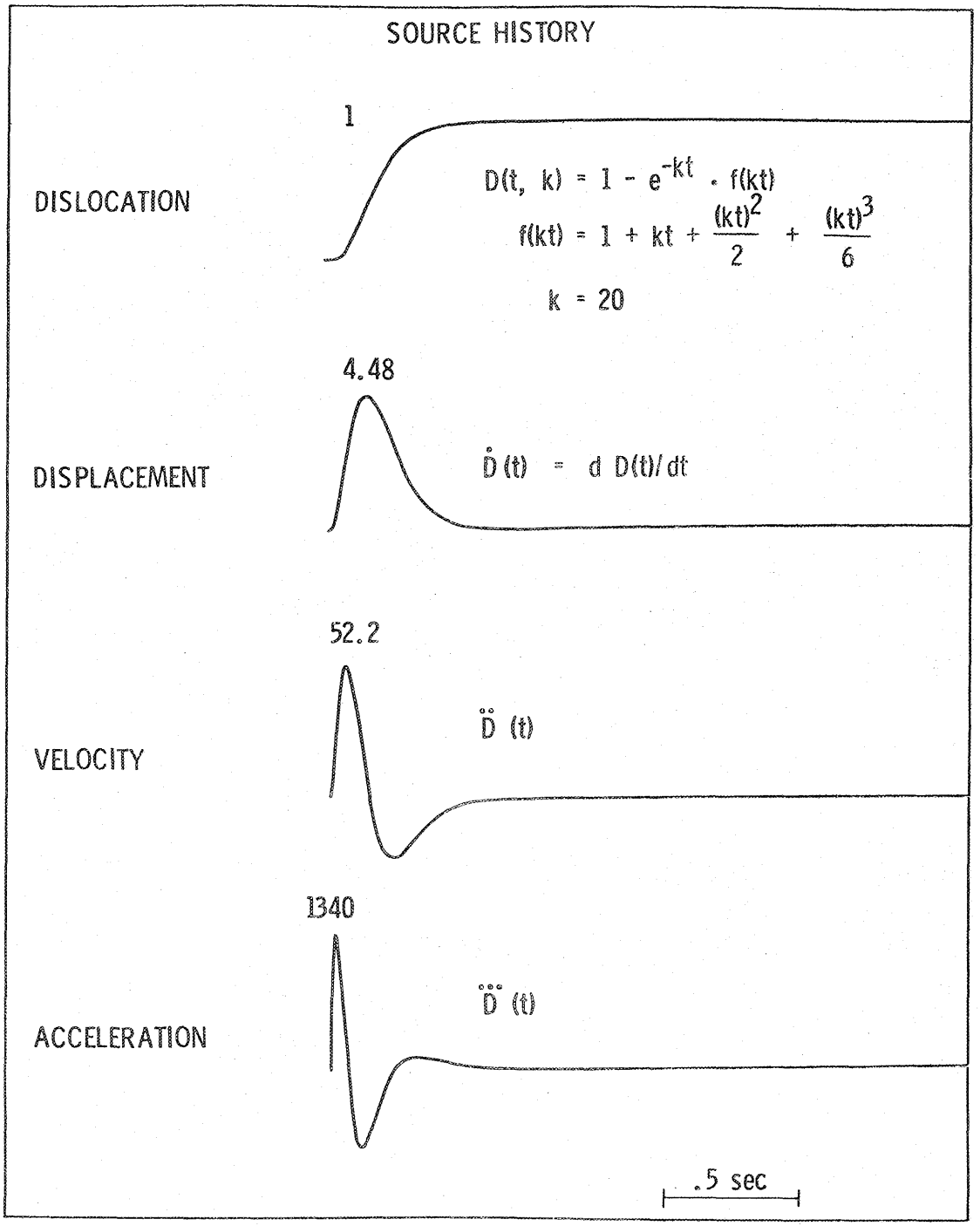

Figure 3-15. Description of the Haskell (1967) source. The peak amplitude of each waveform is given above the trace.

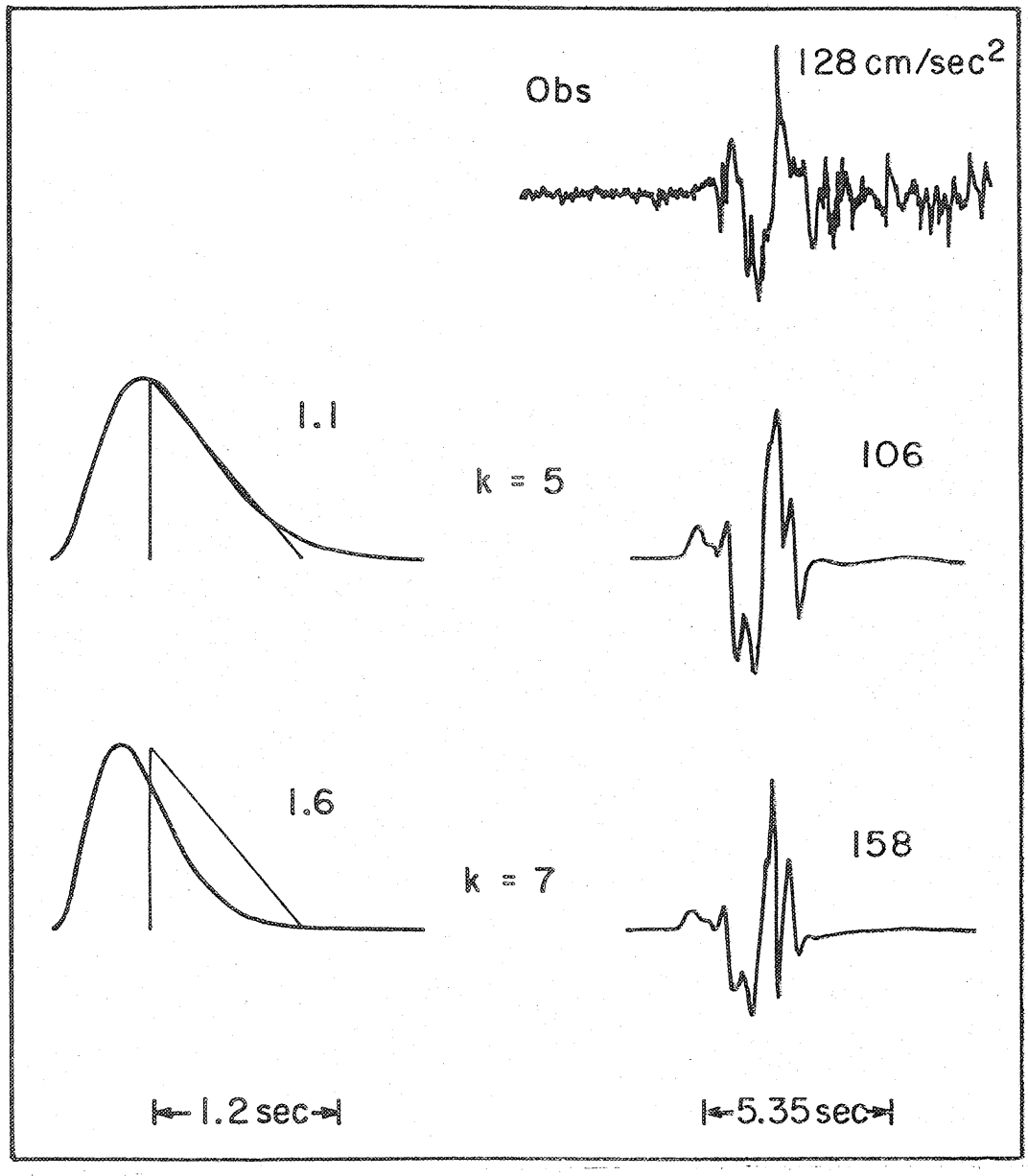

Figure 3-16. Synthetic accelerations (lower traces) computed from the two-source model are compared to the observed north-south acceleration record from El Centro (top trace). Also plotted on the left are the time functions for the second source computed from the Haskell (1967) formulation and the shape of the second source (the trangles) found from the simultaneous inversion. The triangles have been shifted .6 sec relative to the beginning of the Haskell (1967) source. Peak amplitudes of the accelerograms in cm/sec^2 are given next to the traces, as are the peak amplitudes of the Haskell (1967) time functions (units are arbitrary).

the second source is to add high frequency information to the acceleration record synthesized with just the first source. The velocity and displacement synthetics are almost totally unaffected by the addition of the second source.

The results of the strong-motion modeling demonstrate that the sources inferred from the teleseismic short-period study were the ones that contributed the high amplitude part of the acceleration record at El Centro. The main source, which was less than 2 sec in duration, was responsible for the long-period (1 to 3 sec) part of the S-wave shape, while a combination of crustal reflections of the first source and a smaller, sharper second source add high frequency accelerations. The short duration of the time functions for the two sources is evidence that motions on only a small section of the fault caused the highest and most hazardous part of the accelerations recorded at El Centro.

CONCLUSIONS

The short-period teleseismic P waves from the 1968 Borrego Mountain earthquake have been studied and source models have been found which fit not only those records but the teleseismic long-period body waveforms and the strong motion SH record at El Centro as well. From the deconvolutions and the forward and inverse modeling of the waveforms it was found that the source radiation came in two pulses separated by about 2.2 seconds. The sources for each of these pulses were located at about 8 km depth and had similar focal mechanisms, but the second was only about a third the amplitude of the first. The duration of the time

function for the first source is fairly well constrained at about 2.1 seconds while there is less resolution on that of the second source. The moment at short periods is 12% to 33% less than that calculated from the long-period data and is 80% to 85% less than that from the surface waves.

There were some problems with the short-period data set. The signal-to-noise ratio is poor on many records and at some stations there is an apparent mismatch of information between the short-period and long-period records. There is also some evidence for either laterally varying structure in the source region or for different focal mechanisms at short and long periods. Even so, the short-period waveforms contain much detailed information on the source time history of the earthquake.

Chapter 4

Evidence for Fault Asperities in the New Hebrides Islands and Borrego Mountain Fault Zones

INTRODUCTION

It has long been evident that the fracture properties of the earth are very heterogeneous over length scales ranging from meters to kilometers. Certainly there are many observations that can be given as evidence of this--the tremendous range in the sizes of earthquakes, the great variation of fault lengths which can be found in seismically active areas and the nonuniform surface displacements on fault breaks observed after earthquakes. The abundance of high frequency radiation from an earthquake is probably due to heterogeneity in the energy release on the fault (Richter, 1958). Mogi (1962, 1963, 1968) used laboratory fracturing experiments performed on several different kinds of rocks to show that the time occurrence and size distributions of shocks vary depending upon the amount of heterogeneity in the composition of a sample. Using his laboratory work as a guide, Mogi (1963, 1969) related the patterns of earthquake occurrence in Japan to the heterogeneity of the crust in the source regions.

A knowledge of the distribution of the fracture properties in the earth is of more than academic interest to seismologists. It is important for deciphering the conditions which lead to the initiation of fracture in the earth and for assessing the spectrum of the dynamic

radiation expected from an earthquake on a given fault. Unfortunately, establishing the relationship between the seismicity and fracture properties of a region is not easy, and documenting the heterogeneity of a given fault zone using seismograms from an earthquake which took place on that fault is more difficult still. Nevertheless, the latter is an important step toward understanding the triggering and development of a rupture on a fault.

Recent studies of seismic sources have provided detailed observations of the heterogeneous radiation from some particular earthquakes. Wyss and Brune (1967) isolated 5 different arrivals of energy on seismograms of the 1964 Alaska earthquake (M_S = 8.5), and they used these observations to locate the places on the fault which radiated the individual pulses. Fukao and Furumoto (1975) combined analyses of the body waves and surface waves of the Tokachi-Oki earthquake of 1968 (M_S = 7.9) to argue for a complicated rupture process where a number of small shocks preceded a larger and smoother dislocation on the fault plane. Kanamori and Stewart (1978) and Rial (1978) studied the 1976 Guatemala earthquake (M_S = 7.5) and the 1967 Caracas earthquake (M_S = 6.7) respectively and each found that the main shock was composed of a number of distinct sources. These studies all show that many large earthquakes tend to radiate seismic energy quite strongly from a few source areas on their fault planes and that in each case these areas are only a fraction of the total fault surface involved in the seismic event. Some of the investigators were able to infer locations for each of the sources of the earthquakes they studied. Their results indicate

that there are just a few large heterogenities on the fault planes of large events.

The studies of the New Hebrides Islands earthquakes and the Borrego Mountain earthquake presented in the previous two chapters of this thesis provide an excellent data set for determining some of the properties of the fracture heterogeneities on the faults in these two source regions. The purpose of this chapter is to discuss the existence of areas of high strength or high stress concentration on a fault, describe the aspects of these asperities which may be observed in seismic source studies and then apply these ideas to the data from the New Hebrides Islands earthquakes and the Borrego Mountain earthquake in an effort to quantify the properties of asperities on the faults in each area.

BARRIER AND ASPERITY MODELS

Two models which relate faulting to fracture heterogeneities have been proposed in the literature--the barrier model and the asperity model. Within each model there is the assumption that there exist areas of high and low breaking strength on a fault and that the distribution of these areas controls the history of stress release during a seismic rupture. From each model predictions about the time history of the rupture process on a fault can be made. The quantitative differences between the two models are not great and, with present methods, are difficult to observe. Nonetheless, the models are useful for describing and understanding the strength distribution on observed faults.

The barrier model as proposed by Burridge and Halliday (1971) and Das and Aki (1977) is one where a seismic rupture, once started, will continue propagating through a region with some relatively low level of breaking strength until it runs into a place, called a barrier, where the breaking strength of the material is significantly larger than average. If certain energy considerations needed for breaking this high strength material are not met, the fracture cannot penetrate the barrier and the rupture front stops. Das and Aki (1977) generalized this idea by studying the radiation from a fault with several barriers of different strengths distributed on it. They showed that the high frequency part of the source radiation from their fault model would be enhanced over that radiated from a fault with no barriers due to the complicated time history of the rupture as it interacts with the barriers. Aki (1979) applied the barrier idea to the 1966 Parkfield, California, earthquake. He analyzed the aftershock distribution of that event and argued that the rupture ran into a significant barrier near the south end of the fault. From the size of the barrier he calculated that this part of the fault had a breaking strength energy of about 8 x 10^8 erg/cm^2. This value is comparable to the largest measurements of breaking strengths heretofore determined for earthquakes (Husseini et al., 1975).

The asperity model is an outgrowth of studies of the mechanisms of frictional sliding. The idea that the tendency for movement on a fault is controlled by the existence of areas of high strength was proposed by Byerlee (1970) and Scholz and Engelder (1976) to explain the friction of

rocks as observed in laboratory experiments. In this model the two surfaces of a fault are held together by a number of areas of high breaking strength called asperities. Sliding on a fault is initiated when the shear stress on the fault surface exceeds the yield stress of the asperities. Kanamori (1977) applied this asperity idea on a much larger scale to explain the multiple rupture nature of some large earthquakes. Kanamori and Stewart (1978) suggested that the complicated rupture history of the Guatemala earthquake of 1976 (M_s = 7.5) is an example of this phenomenon. The individual shocks, which together comprised the seismic energy release from the earthquake, were thought to each represent the breaking of an asperity as the rupture front propagated along the fault.

The asperity model has been used by Jones and Molnar (1979) to explain the existence of foreshocks which take place immediately prior to a main shock. In their model the failure of asperities of low breaking strength increases the stress on stronger asperities on some portion of a fault surface. Some of these newly-loaded asperities eventually break, increasing the stress on still stronger places on the fault. The strongest asperities eventually are induced to fail by the increased load and this results in the initiation of the main shock.

The tendency of the hypocenters of foreshocks to cluster near those of main shocks (Mogi, 1968; Kelleher and Savino, 1975) and of foreshocks to increase in number just before the occurrence of main shocks (Mogi, 1968; Jones and Molnar, 1976) can be taken as evidence to support the idea of Jones and Molnar (1979). However, these behavior

patterns have also been noted in the laboratory where microfractures tend to cluster along the eventual fracture plane in previously unfractured samples of rock (Mogi, 1968; Scholz, 1968). Thus the existence of foreshocks by themselves may not necessarily be indicative of the failure of asperities on a fault.

While there are quantitative differences between the barrier and asperity models (Husseini et al., 1975; Rudnicki and Kanamori, 1980), there are many similarities between the observable parameters expected from the models. In particular both models predict that on a fault surface which fractures during an earthquake there should be areas of high stress drop, but that the stress drop averaged over the entire fault plane for the event would be much lower. Likewise, both models predict that there should be some areas on a fault where all of the shear stress is relieved (to some low level) while there should be other areas where only a part of the stress is released. The major differences between the two models is that in the barrier model rupture initiates in a weak zone on the fault and propagates into an area of high breaking strength while for the asperity model rupture begins at a strongly held place on the fault and propagates into weaker areas. However, it is reasonable to think that both processes occur in the earth. For instance, local asperities may break and initiate a rupture into a weak zone on a fault. The rupture could continue to propagate until it later encounters a region of high breaking strength which it may or may not penetrate. If it does penetrate it, the failure of the barrier causes a significant amount of energy to be radiated and it

appears as another "source" to those observing in the far-field. If it does not penetrate it, the rupture is stopped and the earthquake ends. On the other hand, if no barriers are encountered by the rupture, it will continue to propagate until the average stress drop over the entire fault surface reaches some low value.

In most of the following discussions, the terms "barrier" and "asperity" are used interchangeably to refer to an area on a fault surface with higher-than-average breaking strength. If some observation from an earthquake is specifically related to the asperity model or to the barrier model, this will be stated explicitly and the appropriate terminology will be used for that particular discussion.

THE NEW HEBRIDES ISLANDS EARTHQUAKES

The analysis presented in Chapter 2 provides a detailed history of the seismic failure process which occurred during the 1965 New Hebrides Islands earthquake sequence. This history is, in turn, useful for isolating the locations of suspected asperities in the fault region and for providing some information on the size and strength of the asperities at these places. Three asperities are inferred to lie in the fault zone of these earthquakes.

As was noted in Chapter 2, the two large foreshocks of the sequence, FS-1 and FS-2, occurred to the north of the rupture zone of the main shock, and the large events migrated from north to south during the seismic failure process. The time functions for the two foreshocks to the north were found to have longer rise times than those for the

main shock and the first large aftershock. The time function shapes as well as synthetic and observed waveforms at KIP and MAN for FS-1, FS-2, M and A-1 are summarized in Figure 4-1.

The time function differences for these events can be related to stress drop differences. This can be done by computing the area of the part of the fault which radiated the pulse which was modeled with some particular time function, and then relating this area S to the stress drop ($\Delta\sigma$) using the relation

$$\Delta\sigma = \frac{C\ M_o}{S^{3/2}} \qquad (4\text{-}1)$$

where M_o is the appropriate seismic moment (that for body waves in the cases where the fault dimensions were found from time functions) and C is a constant which depends on the geometry of the fault (Kanamori and Anderson, 1975). The fault areas were calculated using the method of Ebel et al. (1978) which relates time function duration to fault area. In the case of these events the method was modified somewhat to take into account an assumed rectangular shape of the fault planes. Fault areas and stress drops for FS-1, FS-2, M and A-1 are given in Table 4-1. The stress drops computed for the foreshocks are smaller than those for M-1, M-2 and A-1, while the stress drop for the entire main shock M, that found from the aftershock fault area and the surface-wave moment, is smaller than that for any of the other events. It is also evident from a comparison of the sizes of the fault areas for M-1 and M-2 that each of these events represented the breaking of only a small percentage

TABLE 4-1

Event	Characteristic Fault Dimensions (km)	Fault Area (km^2)	Seismic Moment b-Body Wave s-Surface Wave (dyne-cm)	Stress Drop (bars)
New Hebrides Islands Earthquakes				
FS-1	16 x 8	128	1.6×10^{26} b	31
FS-2	16 x 8	128	1.0×10^{26} b	19
M-1	14 x 7	98	1.6×10^{26} b	49
M-2	18 x 9	162	1.0×10^{27} b	129
M	60 x 50	3000	3.4×10^{27} s	15
A-1	12 x 6	72	8.0×10^{25} b	43
Borrego Mountain Earthquake				
Source 1	7.7 (diameter)	47	6.4×10^{25} b	436
Source 2	4.0 (diameter)	13	0.9×10^{25} b	366
Total Fault	12 x 30	360	3.0×10^{26} s	20

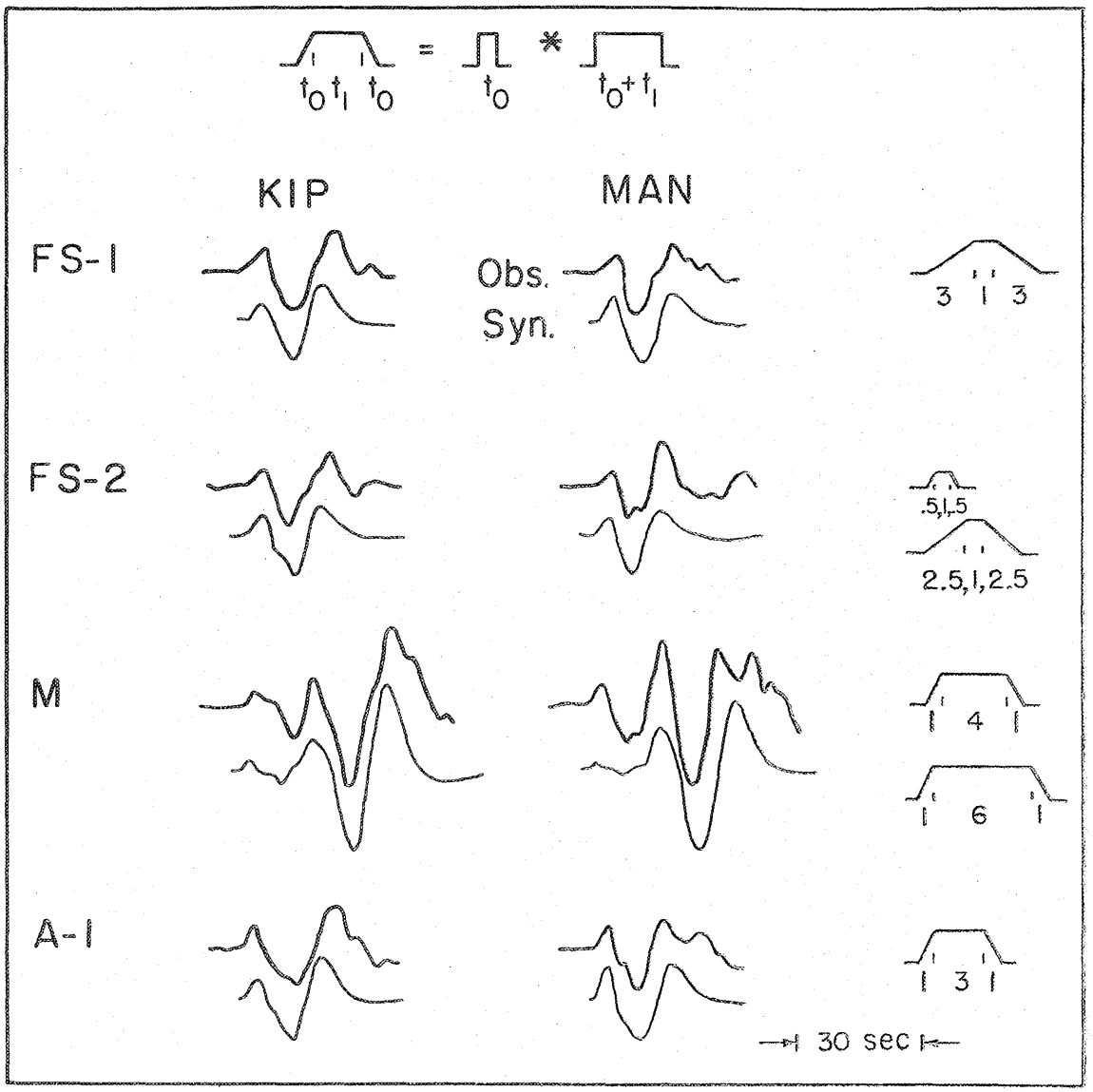

Figure 4-1. Comparison of the synthetic (heavy line) and observed (light line) waveforms and time functions for FS-1, FS-2, M and A-1 from the 1965 New Hebrides Islands earthquake sequence. The numbers under the time functions show the durations of the corresponding parts in seconds.

of the main shock fault area. This confirms the suggestion in Chapter 2 that M-1 and M-2 were only a small part of the entire deformation associated with the main shock.

This pattern of stress drops is similar to that predicted by the asperity model for foreshocks as suggested by Jones and Molnar (1979). The first foreshock can be viewed as the breaking of a relatively weak asperity under Santo which then loaded stronger asperities between the islands of Santo and Mallikolo. While the breaking of one of these asperities resulted in FS-2, the failure of another of these strong asperities (M-1) initiated the main shock, which ultimately broke a large area over which the average stress drop was very low. A-1, another higher stress drop event, may have been due to the failure of an asperity which did not break during the main shock.

The epicenters for FS-1, FS-2, M-1 and A-1 provide constraints on the locations of these asperities on the contact zone between the two converging plates under the central New Hebrides Islands. One area is presumed to be located around the hypocenter of FS-1. This asperity is a few kilometers south of the region where the northern ridge of the D'Entrecasteaux fracture zone is being subducted and it appears that the focal mechanisms and sizes of the earthquakes to the north and to the south of this ridge are different (Chung and Kanamori, 1978). FS-1 itself was preceded by a couple of hours by a foreshock (m_b = 4.4) which also suggests that there may have been the gradual breaking of asperities in this region. A second asperity is suspected to lie on the fault contact between the islands of Santo and Mallikolo. Almost all of

the earthquakes which took place after FS-1 and before FS-2 occurred in this general area (Figure 2-17(a)), the hypocenters of both FS-2 and M were located in this area and the region was the northern boundary of the aftershock zone for M (Figure 2-17(d)). A third possible asperity is located at the southern end of the main shock aftershock zone (Figure 2-17(c)). This asperity lies under the part of Mallikolo where some east-west trending surface faults cut across the island (Benoit and Dubois, 1971). The general locations of these three asperity areas are shown in Figure 4-2.

It appears that the locations of these suspected asperities correlate quite well with details of the recent deformation history of Santo and Mallikolo. Taylor et al. (1980) report that the southern part of the island of Santo has been tilting toward the south during the last several thousand years, while during that same time period the northern part of Mallikolo has been tilting toward the north. Their interpretation for the cause of this is that the subduction of the D'Entrecasteaux fracture zone is deforming the islands under which it is subducting. Specifically, the northern ridge of the fracture zone is subducting under central Santo, causing the northern of that island to tilt toward the north while the southern part tilts toward the south. The southern ridge of the fracture zone is subducting under central Mallikolo (in the area of the east-west surface faults). In a situation similar to that on Santo, the northern part of Mallikolo is tilting north while the southern part is tilting south. This model predicts the existence of a synclinal hinge located somewhere between the two

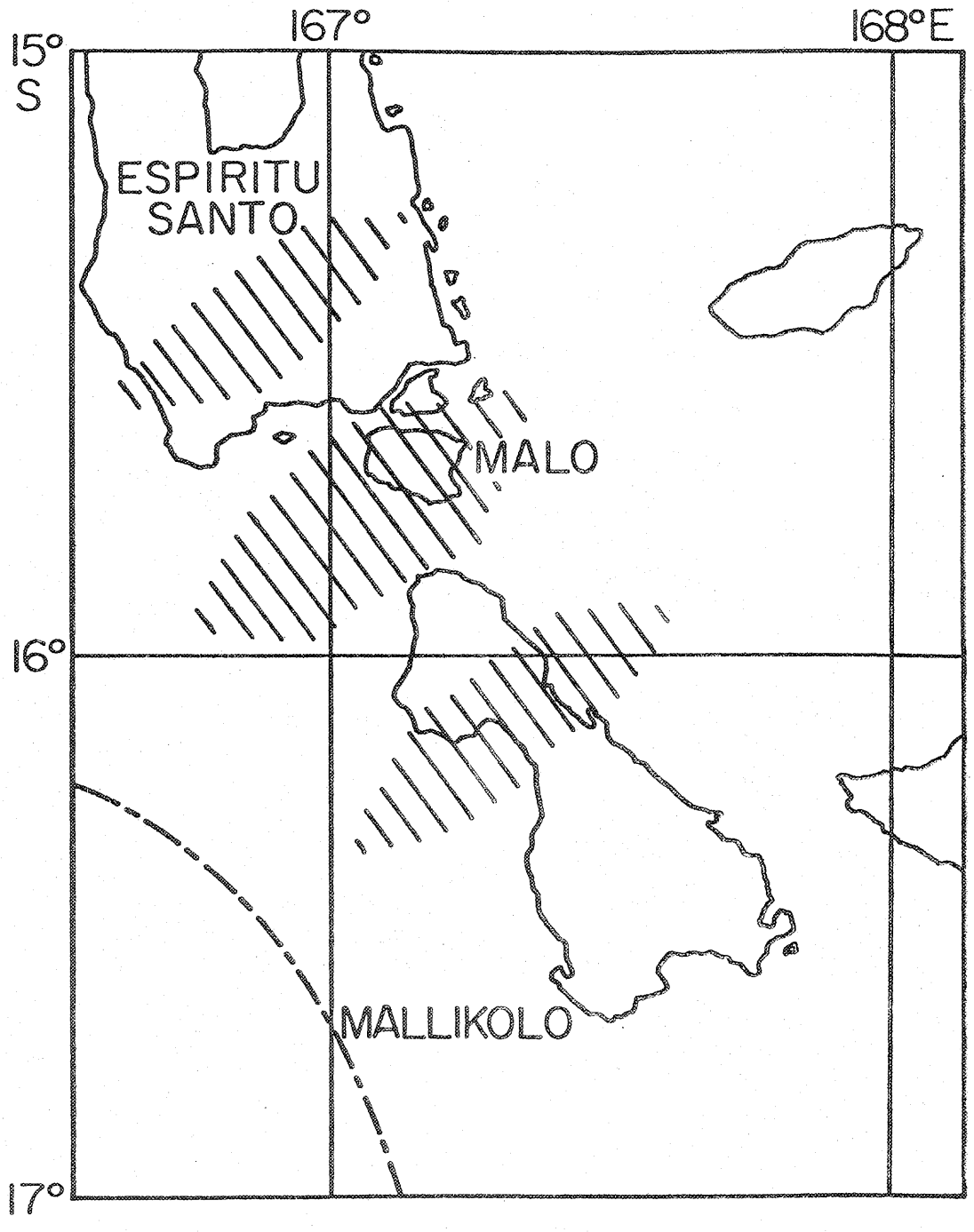

Figure 4-2. Locations of the three proposed asperities (striped areas) in the central New Hebrides. The shapes of the three areas are arbitrary and are not meant to represent the sizes of the asperities.

islands. The locations of the asperities found from studying the 1965 earthquakes are inferred to be in the areas where the two ridges of the D'Entrecasteaux fracture zone are being subducted and where the hinge line between the two islands should occur. Thus it appears that the asperities in this region lie in places where there are local changes in the thrust contact between the two plates and where these local changes are caused by the subduction of an irregular topographic feature.

Three conclusions can be drawn from this analysis of the New Hebrides Islands earthquakes study. The first is that the relatively lower stress drops of the foreshocks compared to the main shock and the first aftershock are consistent with the idea that the breaking of weaker asperities loaded stronger asperities on the fault, which eventually broke during the main shock. The second conclusion is that asperities which made up only a small fraction of the main shock fault plane participated in a high stress drop part of the earthquake. The asperities which were thought to have broken during the main event had a total area of only about 8% of the main shock fault area. Third, there is strong evidence that somewhat irregular tectonic features in the fault zone are related to the existence and locations of these asperities. The deformations associated with the subduction of the D'Entrecasteaux fracture zone correlate quite well with the locations of the asperities on the fault.

THE BORREGO MOUNTAIN EARTHQUAKE

The Borrego Mountain earthquake was preceded by one foreshock

(M_L = 3.7) which occurred about 90 seconds before the main event, so it is in actuality an earthquake which was part of a foreshock-mainshock-aftershock sequence. Unfortunately, the foreshock was too small and poorly recorded to allow a quantitative study of its source properties. However, the analysis presented in Chapter 3 gives a detailed picture of the rupture history of the main shock, and this history does provide some information on the stress distribution on the fault which broke during the event.

In Chapter 3 it was demonstrated that the short-period and long-period P waves could be adequately modeled by two point sources of 2.1 and 1.2 seconds duration respectively with the second one occurring 2.2 seconds after the first. The body wave moments of these two sources indicate that much of the total moment of the earthquake was contained in these two pulses. The fault areas which radiated these two pulses were computed using the method of Ebel et al. (1978) and are given in Table 4-1 along with an estimate of the entire fault area which was made from the aftershock data. It is evident that the two sources found from short-period body wave analysis broke only a fraction of the total fault plane. The area which radiated the pulse which was modeled as the first source in Chapter 3 was only about 12% of the total fault area. Thus, as in the New Hebrides Islands sequence, the main shock fault area was many times the size of the asperity which failed at the beginning of the earthquake.

Stress drops for the two individual sources were computed from the fault areas and moments found in the body wave analysis. These values

were found to be several hundred bars each for the two events (Table 4-1). A much lower estimate of 96 bars for the stress drop from this event was determined by Burdick and Mellman (1976) from their study of the long-period body waves, and a stress drop of 20 bars can be computed from the total fault area given in Table 4-1 and the surface moment of 3 x 10^{26} dyne-cm (Burdick, 1978). These stress drop estimates show that while the rupture initiated with two very high stress drop events, the total rupture had a much lower average stress drop.

The location of the region which radiated the two high amplitude pulses was probably near the northern end of the fault zone where the largest surface displacements were measured (Clark, 1972; Figure 4-3) and where the epicenter of the event as well as that of the immediate foreshock were located (Allen and Nordquist, 1972). The distribution of aftershocks projected on the fault determined by Hamilton (1972) which is reproduced in Figure 4-4 has an interesting feature. At the northern end of the fault trace there is a gap of about 6 km where there were almost no aftershocks. The size of this gap (which has been outlined in Figure 4-4) is approximately the same size as that which radiated the high amplitude body wave pulses. The surface faulting on the northern segment of the fault breakage did not have any noticeable aftercreep on it while the central and southern parts underwent significant post-seismic displacements (Clark, 1972; Burford, 1972; Figure 4-3). Burford (1972) notes that the basement under the northern part of the surface faulting is covered by a thin layer of sediments, while the basement under the central and southern traces lies under several

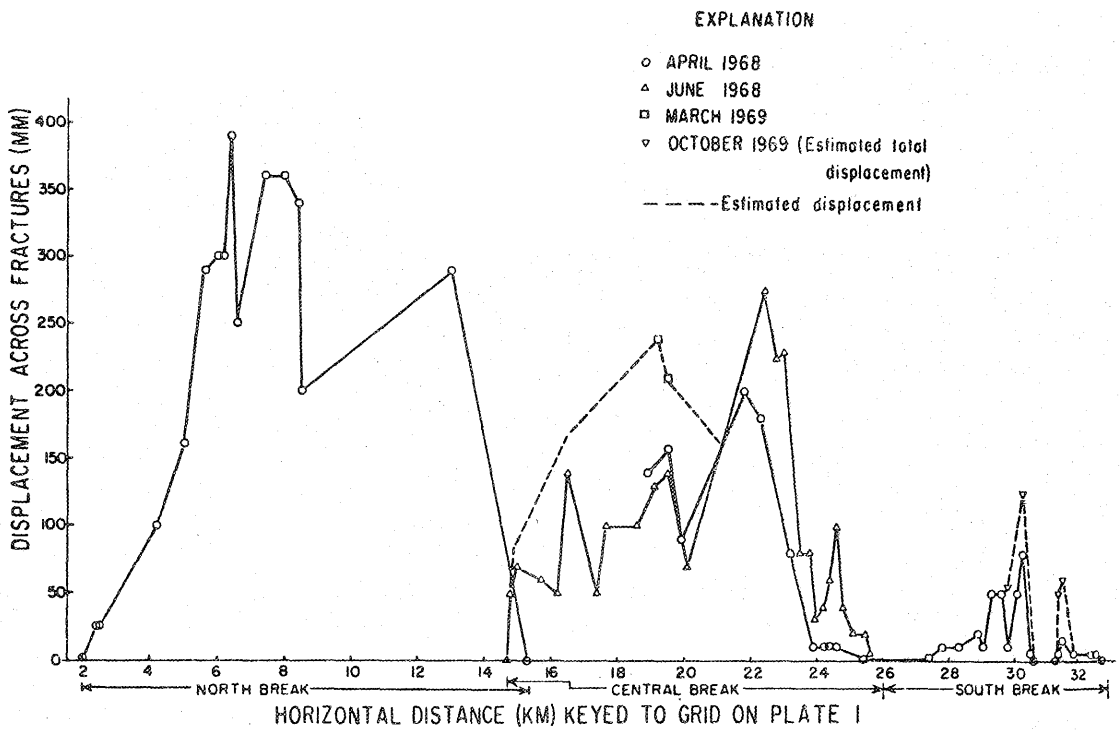

Figure 4-3. Graph of the surface faulting of the Borrego Mountain earthquake from Clark (1972).

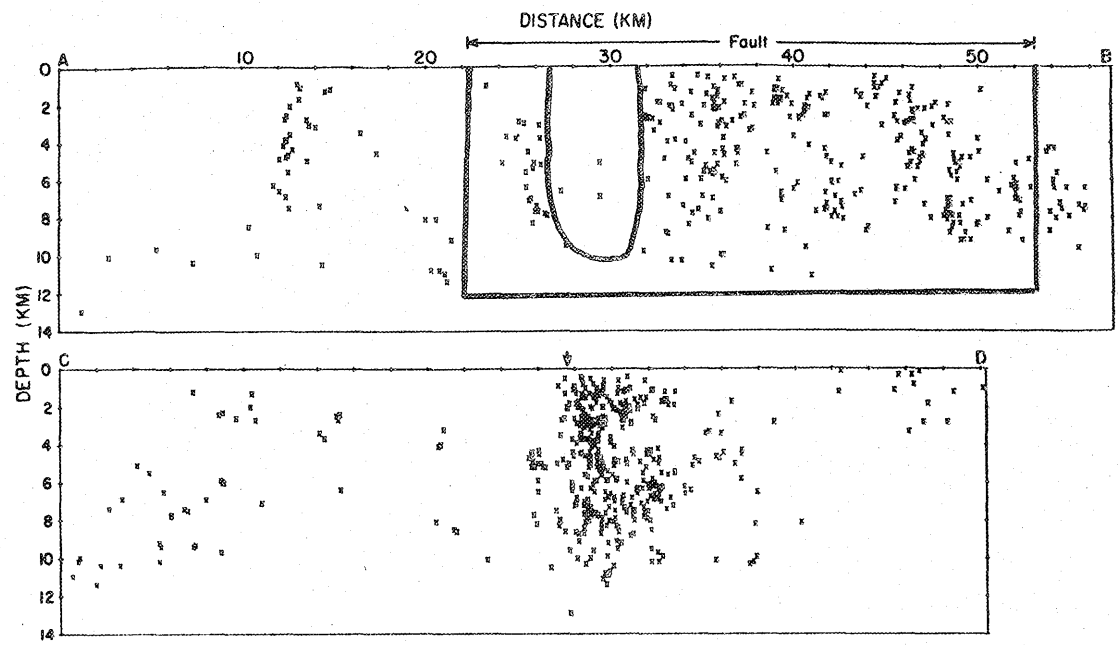

Figure 4-4. Plot of aftershock locations with depth on a plane parallel to the surface faulting (AB; A is to the north) and perpendicular to the surface faulting (CD; C is to the west) from Hamilton (1972). The arrow in the lower figure denotes the location of the surface faulting. The rectangular box in the upper figure shows the approximate fault area which probably participated in the main shock, and the outlined region under the northern part of the surface break shows the possible location of the asperity on the fault.

hundred meters to several kilometers of sedimentary rock. He argues that the aftercreep may have been a delayed response of the sediments to the initial coseismic displacement of the basement rock. However, since the aftercreep died away at the same time that the aftershock activity dropped to a very low level (Burford, 1972), it may reflect the existence of post-seismic movements in the basement rock.

This evidence all indicates that the asperity which broke at the beginning of the main event relieved all of the stress in a region about 6 km in radius at the northern end of the the fault and that the rest of the fault breakage was probably some sort of readjustment to the initial break. The existence of aftercreep on the central and southern parts of the fault zone suggest that not all of this readjustment managed to take place at the time of the main shock.

The evidence is good that there was a strong asperity at the northern end of the surface breakage of the Borrego Mountain earthquake which was ruptured during the initiation of faulting for that event. The question immediately arising from this evidence is whether or not there is any tectonic reason for the existence of an asperity on this part of the fault. Since this fault is part of the San Jacinto fault zone which has undergone at least 24 km of displacement (Sharp, 1972), it is possible that the bedrock is different on the two sides of the fault. At the surface the part of the fault where the maximum coseismic displacement took place is in a zone where Tertiary and Quaternary sedimentary rock on the east abut a part of Borrego Mountain which is made up of crystalline rock on the west (Sharp, 1972). This place is

the only location along the 1968 rupture where on the surface there is anything but sedimentary rock in contact across the fault. If there is a contrast of the basement rock across the fault in this area, then the results of this study indicate that this contrast may locally cause the fault zone to have a very high breaking strength. The size and the stress drop of the asperity would indicate a fracture strength of about 4×10^{10} erg/cm^2, which is even larger than the high value that Aki (1979) calculated for the 1966 Parkfield earthquake. While the surface geology may not be representative of the structure at depth along the fault zone, it can be said that in this case the location of the asperity correlates with a change in surface geology along the fault zone.

CONCLUSIONS

There were several similarities between the rupture histories of the New Hebrides Islands main shock which was a subduction zone thrust event and the Borrego Mountain earthquake which was a strike-slip event near the edge of a continent. Both events were initiated with the fracture of an asperity which had a stress drop much higher than that for the entire fault area. In each case the size of the asperities was inferred to be only a fraction of the total fault surface--approximately 5% of the total fault area for the Borrego Mountain event and about 20% of the fault plane for each of the two asperities of the New Hebrides Islands events. The locations of the asperities in the New Hebrides Islands fault zone correlate quite well with changes in the local

tectonic deformation of the region, while in the Borrego Mountain fault zone the one asperity lay beneath an unusual surface geological feature.

While these results are not intended to be generalizations which are true for all earthquakes, they do represent observations which can be made for other earthquakes and compared to those presented here. In particular, detailed source studies of other foreshocks (as defined in Chapter 1) may not only provide information which may be useful for predicting large future earthquakes but which may be important in understanding the initiation of seismic failure on a fault. Attention paid to the details of the sources from earthquakes is also useful for understanding the reasons for the existence and locations of stress heterogeneities on a fault, and ultimately perhaps, for assessing the earthquake risk from a particular fault zone. The most important contribution of this thesis is simply a documentation of the existence of fault heterogeneities found from the far-field seismic radiation from earthquakes in two different fault zones.

REFERENCES

Aki, K., (1979). Characterization of barriers on an earthquake fault, J. Geophys. Res., 84, 6140-6148.

Allen, C. R., and J. M. Nordquist, (1972). Foreshock, main shock and larger aftershocks of the Borrego Mountain earthquake, U. S. Geological Survey Professional Paper 787, 16-23.

Bache, T. C., D. G. Lambert, T. G. Barker, (1980). A source model for the March 28, 1975 Pocatello Valley earthquake from time-domain modeling of teleseismic P waves, Bull. Seism. Soc. Am., 70, 419-436.

Benoit, M., and J. Dubois, (1971). The earthquake swarm in the New Hebrides Archipelago, August, 1965, Bull. R. Soc. N. Z., 9, 141-148.

Berg, E., (1968). Relation between earthquake foreshocks, stress and main shocks, Nature, 219, 1141-1143.

Brady, B. T., (1977). Anomalous seismicity prior to rock bursts: Implications for earthquake prediction, Pageoph, 115, 357-374.

Burdick, L. J., (1977). Broad-band seismic studies of body waves. Ph. D. thesis, Calif. Inst. of Tech.

Burdick, L. J., and G. R. Mellman, (1976). Inversion of the body waves of the Borrego Mountain earthquake to the source mechanism, Bull. Seism. Soc. Am., 66, 1485-1499.

Burford, R. O., (1972). Continued slip on the Coyote Creek fault after the Borrego Mountain earthquake, U. S. Geological Survey Professional Paper 787, 105-111.

Burridge, R. and G. S. Halliday, (1971). Dynamic shear cracks with friction as models for shallow focus earthquakes, Geophys. J. R. astr. Soc., 25, 261-283.

Byerlee, J. D., (1970). Static and kinetic friction of granite under high stress, Int. J. Rock Mech. Min. Sci., 7, 577-582.

Chung, W. and H. Kananori, (1978). Subduction process of a fracture zone and aseismic ridges--the focal mechanism and source characteristics of the New Hebrides earthquake of January 19, 1969 and some related events, Geophys. J. R. astr. Soc., 54, 221-240.

Cipar, J. C., (1980). Broad-band time domain modeling of earthquakes from Fruili, Italy, submitted to Bull. Seism. Soc. Am.

Clark, M. M., (1972). Surface rupture along the Coyote Creek fault, U. S. Geological Survey Professional Paper 787, 55-86.

Colenan, P. J. and G. H. Packham, (1976). The Melanesian borderlands and India-Pacific plates' boundary, Earth-Sci. Rev., 12, 197-233.

Das, S. and K. Aki, (1977). Fault plane with barriers: A versatile fault model, J. Geophys. Res., 82, 5658-5670.

Dubois, J., (1971). Propagation of P waves and Rayleigh waves in Melanesia: Structural implications, J. Geophys. Res., 76, 7217-7240.

Ebel, J. E., (1980). Source processes of the 1965 New Hebrides Islands earthquakes inferred from teleseismic waveforms, Geopys. J. R. astr. Soc., 63, in press.

Ebel, J. E., L. J. Burdick and G. S. Stewart, (1978). Source mechanism of the August 7, 1966 El Golfo earthquake, Bull. Seism. Soc. Am., 68, 1281-1292.

Everndon, J. F., (1970). Study of regional seismicity and associated problems, Bull. Seism. Soc. Am., 60, 393-446.

Evison, F. F., (1977a). Fluctuations of seismicity before major earthquakes, Nature, 266, 710-712.

Evison, F. F., (1977b). The precursory earthquake swarm, Phys. Earth Planet. Inter., 15, P19-P23.

Fuchs, K., (1966). The transfer function for P waves for a system consisting of a point source in a layered medium, Bull. Seism. Soc. Am., 56, 75-108.

Fukao, Y., (1979). Tsunami earthquakes and subduction processes in island arcs, J. Geophys. Res., 84, 2303-2314.

Fukao, Y. and M. Furumoto, (1975). Foreshocks and multiple shocks of large earthquakes, Phys. Earth Planet. Inter., 10, 355-368.

Futterman, W. I., (1962). Dispersive body waves, J. Geophys. Res., 67, 5279-5291.

Gardner, J. K. and L. Knopoff, (1974). Is the sequence of earthquakes in Southern California, with aftershocks removed, Poissonian?, Bull. Seism. Soc. Am., 5, 1363-1367.

Gutenberg, B. and C. F. Richter, (1954). Seismicity of the Earth, Princeton University Press.

Haicheng Earthquake Study Delegation, (1977). Prediction of the Haicheng earthquake, EOS, Trans. Am. Geophys. U., 58, 236-272.

Hamilton, R. M., (1970). Time-term analysis of explosion data from the vicinity of the Borrego Mountain, California, earthquake of 9 April 1968, Bull. Seism. Soc. Am., 60, 367-381.

Hamilton, R. M., (1972). Aftershocks of the Borrego Mountain earthquake from April 12 to June 12, 1968, U. S. Geological Survey Professional Paper 787, 31-54.

Hart, R. S., R. Butler and H. Kanamori, (1977). Surface wave constraints on the August 1, 1975 Oroville earthquake, Bull. Seism. Soc. Am., 67, 1-8.

Hartzell, S., (1980). Faulting process of the May 17, 1976 Gazli, U.S.S.R. earthquake, Bull. Seism. Soc. Am., 70, 1715-1736.

Haskell, N. A., (1967). Analytic approximation for the elastic radiation from a contained underground explosion, J. Geophys. Res., 72, 2583-2587.

Heaton, T. H., (1977). Generalized ray models of strong ground motion, Ph. D. thesis, Calif. Inst. Tech.

Heaton, T. H., and D. V. Helmberger, (1977). A study of the strong ground motion of the Borrego Mountain, California, earthquake, Bull. Seism. Soc. Am., 67, 315-330.

Helmberger, D. V. and L. J. Burdick, (1979). Synthetic seismograms. Ann. Rev. Earth Planet. Sci., 7, 417-442.

Helmberger, D. V. and S. D. Malone, (1975). Modeling local earthquakes as shear dislocations in a layered half space. J. Geophys. Res., 80, 4881-4888.

Husseini, M. I., D. B. Jovanovich, M. J. Randall and L. B. Freund, (1975). The fracture energy of earthquakes, Geophys. J. R. astr. Soc., 43, 367-385.

Ishida, M. and H. Kanamori, (1978). The spatio-temporal variation of seismicity before the 1971 San Fernando earthquake, California, Geophys. Res. Let., 8, 345-346.

Johnson, T. and P. Molnar, (1972). Focal mechanisms and plate tectonics of the southwest Pacific, J. Geophys. Res., 77, 5000-5031.

Jones, L. and P. Molnar, (1976). Frequency of foreshocks, Nature, 262, 677-679.

Jones, L. M. and P. Molnar, (1979). Some characteristics of foreshocks and their possible relationship to earthquake prediction and premonitory slip on faults, J. Geophys. Res., 84, 3596-3608.

Kagan, Y. and L. Knopoff, (1976). Statistical search for non-random features of the seismicity of strong earthquakes, Phys. Earth Planet. Inter., 12, 291-318.

Kagan, Y. and L. Knopoff, (1978). Statistical study of the occurrence of shallow earthquakes, Geophys. J. R. astr. Soc., 55, 67-86.

Kanamori, H., (1970a). Synthesis of long-period surface waves and its application to earthquake source studies--Kurile Islands earthquake of October 13, 1963, J. Geophys. Res., 75, 5011-5027.

Kanamori, H., (1970b). The Alaska earthquake of 1964: Radiation of long-period surface waves and source mechanism, J. Geophys. Res., 75, 5092-5040.

Kanamori, H., (1971). Seismological evidence for a lithospheric normal faulting--the Sanriku earthquake of 1933, Phys. Earth Planet. Inter., 4, 289-300.

Kanamori, H., (1977). Use of seismic radiation to infer source parameters, Proceedings of Conference IV: Fault mechanics and its relation to earthquake prediction, U. S. Geological Survey open-file report #78-380, 283-318.

Kanamori, H. and D. L. Anderson, (1975). Theoretical basis of some empirical relations in seismology, Bull. Seism. Soc. Am., 65, 1073-1095.

Kanamori, H. and G. S. Stewart, (1976). Mode of the strain release along the Gibbs fracture zone, mid-Atlantic ridge, Phys. Earth Planet. Inter., 11, 312-332.

Kanamori, H. and G. S. Stewart, (1978). Seismological aspects of the Guatamala earthquake of February 4, 1976, J. Geophys. Res., 83, 3427-3434.

Karig, D. E. and J. Mammerickx, (1972). Tectonic framework of the New Hebrides island arc, Mar. Geol., 12, 187-205.

Keilis-Borok, V. I., V. M. Podgaetskaya and A. G. Prozorov, (1972). Local statistics of earthquake catalogs, in Computational Seismology, Keilis-Borok, ed., Plenum Publishing, New York, 214-227.

Kelleher, J. and J. Savino, (1975). Distribution of seismicity before large strike slip and thrust-type earthquakes, J. Geophys. Res., 80, 260-271.

Kelleher, J., L. Sykes and J. Oliver, (1973). Possible criteria for predicting earthquake locations and their application to major plate boundaries of the Pacific and Carribean, J. Geophys. Res., 78, 2547-2585.

Langston, C. A., (1978a). The February 9, 1971 San Fernando earthquake, Bull. Seism. Soc. Am., 68, 1-30.

Langston, C. A., (1978b). Moments, corner frequencies and the free surface, J. Geophys. Res., 83, 3422-3426.

Langston, C. A. and D. V. Helmberger, (1975). A procedure for modeling shallow dislocation sources, Geophys. J. R. astr. Soc., 42, 117-130.

Luyendyk, B. P., W. B. Bryan and P. A. Jezek, (1974). Shallow structure of the New Hebrides island arc, Geol. Soc. Am. Bull., 85, 1287-1300.

Mallick, P. I. J., (1973). Some petrological and structural variations in the New Hebrides, in The Western Pacific: Islands Arcs, Marginal Seas, Geochemistry, J. Coleman, ed., Univ. of West. Aust. Press, Nederlands, 193-211.

Mansinha, L. and D. E. Smylie, (1971). The displacement fields of inclined faults, Bull. Seism. Soc. Am., 61, 1433-1440.

McNally, K. C., (1976). Spatial, temporal and mechanistic character in earthquake occurrence: A segment of the San Andreas fault in central California, Ph. D. thesis, University of California, Berkeley.

McNally, K. C., E. Chael and L. Ponce, (1979). The Oaxaca, Mexico earthquake (M_s = 7.8) of 29 Nov. 1978: New "pre-failure" observations, EOS, Trans. Am. Geophys. U., 60, 322.

Mogi, K., (1962). Study of elastic shocks caused by the fracture of heterogeneous materials and its relations to earthquake phenomena, Bull. Earthquake Res. Inst., 40, 125-173.

Mogi, K., (1963). Some discussions on aftershocks, foreshocks and earthquake swarms--the fracture of a semi-infinite body caused by an inner stress origin and its relation to the earthquake phenomena (third paper), Bull. Earthquake Res. Inst., 41, 615-658.

Mogi, K., (1968). Source locations of elastic shocks in the fracturing process (1), Bull. Earthquake Res. Inst., 46, 1103-1125.

Mogi, K., (1969). Some features of recent seismic activity in and near Japan (2)--activity before and after great earthquakes, Bull. Earthquake Res. Inst., 47, 395-417.

Mooney, W. D., and G. A. McMechan, (1980). Synthetic seismogram modeling of the laterally-varying structure in the central Imperial Valley, in The Imperial Valley earthquake of October 15, 1979: U. S. Geological Survey Professional Paper, in press.

Ohtake, M., T. Matumoto and G. V. Latham, (1977). Seismicity gap near Oaxaca, southern Mexico as a probable precursor to a large earthquake, Pageoph, 115, 375-385.

Papazachos, B. C., (1975). Foreshocks and earthquake prediction, Tectonophysics, 28, 213-226.

Pascal, G., B. Isacks, M. Barazangi and J. Dubois, (1978). Precise locations of earthquakes and seismotectonics of the New Hebrides island arc, J. Geophys. Res., 83, 4957-4974.

Rial, J. A., (1978). The Caracas, Venezuela, earthquake of July 1967: A multiple-source event, J. Geophys. Res., 83, 5405-5419.

Richter, C. F., (1958). Elementary Seismology, Freeman Press, San Francisco.

Rikitake, T., (1976). Earthquake Prediction, Elsevier Scientific Publishing Co, New York.

Rudnicki, J. W. and H. Kanamori, (1980). Effects of fault interaction on moment, stress drop and strain energy release, J. Geophys. Res., in press.

Santo, T., (1970). Regional study on the characteristic seismicity of the world, part III--New Hebrides islands region, Bull. Earthquake Res. Inst., 48, 1-48.

Savage, J. C., (1966). Radiation from a realistic model of faulting, Bull. Seism. Soc. Am., 56, 577-592.

Scholz, C. H. and J. T. Engelder, (1976). The role of asperity indentation and ploughing in rock friction, 1. Asperity creep and stick slip, Int. J. Rock Mech. Min. Sci, 13, 149-154.

Sharp, R. V., (1972). Tectonic setting of the Salton trough, U. S. Geological Survey Professional Paper 787, 3-15.

Suyehiro, S. and H. Sekiya, (1972). Foreshocks and earthquake prediction, Tectonophysics, 14, 219-225.

Shimazaki, K., (1973). Statistical method of detecting unusual seismic activities, Bull. Seism. Soc. Am., 63, 969-982.

Shlien, S. and M. N. Toksoz, (1970). A clustering model for earthquake occurrence, Bull. Seism. Soc. Am., 60, 1765-1787.

Shlien, S. and M. N. Toksoz, (1974). A statistical method of identifying dependent events and earthquake aftershocks, Earthquake Notes, 45, 3-16.

Stauder, W., (1968). Mechanism of the Rat Islands earthquake sequence of February 4, 1965, with relation to island arcs and sea floor spreading, J. Geophys. Res., 73, 3847-3858.

Stauder, W., (1973). Mechanism and spatial distribution of Chilean earthquakes with relation to subduction of the oceanic plate, J. Geophys. Res., 78, 5033-5061.

Stauder, W., (1975). Subduction of the Nazca plate under Peru as evidenced by focal mechanisms and by seismicity, J. Geophys. Res., 80, 1053-1064.

Stewart, G. S., (1978). Implications for plate tectonics of the August 19, 1977 Indonesian decoupling normal-fault earthquake, EOS, Trans. Am. Geophys. U., 59, 326.

Taylor, F. W., C. Jouannic, B. L. Isacks, A. L. Bloom and J. Dubois, (1978). Vertical motions associated with an earthquake sequence in the New Hebrides island arc, EOS, Trans. Am. Geophys. U., 59, 382.

Taylor, F. W., B. L. Isacks, C. Jouannic, A. L. Bloom and J. Dubois, (1980). Coseismic and quaternary vertical tectonic movements, Santo and Malekula islands, New Hebrides island arc, J. Geophys. Res., in press.

Tsai, Y. and K. Aki, (1970). Precise focal depth determination from amplitude spectra of surface waves, J. Geophys. Res., 75, 5729-5743.

U. S. Coast and Geodetic Survey, Seismological Field Survey, and California Institute of Technology, Earthquake Engineering Research Laboratory, (1968). Strong motion instrumental data on the Borrego Mountain earthquake of 9 April, 1968. No. 119.

Utsu, T., (1972). Aftershock and earthquake statistics IV, J. Fac. of Science, Hokkaido U., Geophys. Series 7, 4, 1-42.

Wesson, R. L. and W. L. Ellsworth, (1973). Seismicity preceding moderate earthquakes in California, J. Geophys. Res., 78, 8527-8546.

Wyss, M. and J. W. Brune, (1967). The Alaska earthquake of March 28, 1964: A complex multiple rupture, Bull. Seism. Soc. Am., 57, 1017-1023.

Yamakawa, N., M. Kishio and K. Abe, (1969). Spatial and time distributions of foreshocks and aftershocks of the earthquake near the southern Kuriles on October 13, 1963, Geophys. Mag., 34, 277-305.